UNIVERSIDAD AUTÓNOMA DE MADRID

DEPARTMENT OF MOLECULAR BIOLOGY

Molecular and Cellular Mechanisms of Hepatocarcinogenesis

Krishna Seshu Tummala

Madrid, September 2014

UNIVERSIDAD AUTÓNOMA DE MADRID

DEPARTMENT OF MOLECULAR BIOLOGY

Molecular and Cellular Mechanisms of Hepatocarcinogenesis

Doctoral thesis submitted to the Universidad Autónoma de Madrid for the degree of Doctor of Philosophy by M. Sci. in Molecular Biomedicine,

Krishna Seshu Tummala

Thesis Director

Dr. Nabil Djouder

Growth Factors, Nutrients and Cancer Group

BBVA Foundation-CNIO Cancer Cell Biology Programme

Spanish National Cancer Research Centre

Dr. Nabil Djouder, head of the Growth Factors, Nutrients and Cancer Group in the Spanish National Cancer Research Centre (CNIO),

CERTIFIES

That Mr Krishna Seshu Tummala, Master in Biotechnology from the Indian Institute of Technology Roorkee (IITR) – India, has completed his Doctoral Thesis **"Molecular and Cellular Mechanisms of Hepatocarcinogenesis"** and meets the necessary requirements to obtain the PhD Degree in Molecular Biosciences. To this purpose, he will defend his Doctoral Thesis at the Universidad Autónoma de Madrid. The Thesis has been carried out under my direction and hereby I authorize it to be defended to the appropriate Thesis Tribunal.

I hereby issue this certificate in Madrid on September 1st 2014.

Nabil Djouder — PhD Thesis Director

Josefa Predestinacion Garcia Ruiz — PhD Thesis Tutor

This thesis, submitted for the degree of Doctor of Philosophy at the Universidad Autónoma de Madrid, has been completed in the Growth Factors, Nutrients and Cancer Laboratory at the Spanish National Cancer Research Centre (CNIO), under the supervision of Dr. Nabil Djouder.

This work was supported by the following grants and fellowships:

- La Caxia/CNIO international Phd Fellowship. 2009 call – Krishna Seshu Tummala
- Proyecto SAF2010-18518, Ramón y Cajal, Ministry of Economy and Competitiveness, Spain – Dr. Nabil Djouder

Dedicated to all my mice

Acknowledgements

I would like to start this section by dedicating this piece of work to all the **scientists** that expanded our knowledge. I would like to thank **CNIO/LaCaxia** for considering me as the receipient of one of the best fellowship in one of the best institute. I cannot thank enough my **Mother**, who taught me how to be perseverant and independent and my **sister** who is always with me.

My sincere thanks will go to my mentor **Nabil**, which not only with me through all my crests and troughs but trained me how to face those situations. I believe, more than a good guide some of his qualities are worth keeping either being perseverant, not afraid to think out of the box and taking risks and "just do it" attitude. Thanks for that experience Nabil, I learnd a lot.

My PhD thesis committee members, **Erwin Wagner, Manuel Serrano and Romeo Ricci** played a very constructive and supportive role in shaping up the project, the paper and my science. I cannot thank enough these people.

One personality that inspired me more than I expected when I joined here was **Erwin**, either being outspoken for the right things and fighting for his people. He is always concerned about the success of the young students, and science in general, encouraging young people and those inspiring short talks during miriendas will always resonate in my mind.

Today, if I am here finishing this work it's because of some wonderful people from CCB, being not only a wonderful collegues but constitutes every brick of my personality. **Mohammad, Ljilljiana, Marta (Sr + Jr), Ozge, Stephanie, Mirco, Juan, Donatello, Helia, Mahmunt, Rainer, Hui, Eva, Alvaro, Martin, Almu, Ana (Sr +Jr), Maria (Sr + Jr), Karsten, Jochen, Holi, Santiago, Katja, Hugo, Stephan, Sebastian, Latifa, Mirna, Massimo, Barbara, Claudia, Carrolina (Sr + Jr) and Alberto**. Cannot repay you guys for all the kindness and help you showered me with.

A special hug goes to **Flor, Isa and Virginia** for making albondigas (NR) and looking out for all our mice. I would also like to thank some of the wonderful and most efficient people I worked with **Sagrario, Orlando, Latifa, Osvaldo, Pilar, Isabel, David, Santiago Ramon, Ximo, Manu, Diego, Lola, Marta Canemero, Mara, Jose, Steve** and **Stephanie** for helping me in different steps of the project.

Outside of CCB some wonderful personalities also helped me a lot, many thanks **Manu, Adres, Juanan, Gema, Paqi, Deago, Ximo, Iva, Mara, Chala, Virender, Bhabiji, Valencio, Sara (Sr+Jr), Mara, Fedrika, Charo, Alexandra, Tereza, Tribhu, Satish, Kranti, Marija, Marcos, Lucho, Luis, Victor, Mar Perez, Jorge, Juan Ramon** and many more.

My PhD thesis tutor **Josefa Predestinacion Garcia Ruiz** deserves a special mention for her support and great words.

Last but not the least, big thanks to "**Marta Brandt**" for being such a "patient" and perfect partner in crime.

Thanks to every one. Gracias a todos.

Abstract

Hepatocellular carcinoma (HCC) is the most common and frequently lethal, human primary liver neoplasm (GLOBOCAN 2008 v2.0). The early stage is characterized by low- to high-grade dysplastic nodules, “preneoplastic lesions”. These frequently develop in chronic inflammatory liver disease or hepatitis, which can contribute to fibrosis and cirrhosis followed by progression to HCC. Thus, precancerous lesions have clinical value for HCC prediction, but therapeutic options are limited.

In early stages of many cancers, including HCC, oncogene activation induces replicative stress, resulting in DNA damage leading to chromosomal instability (CIN), which accelerates tumour development from preneoplastic lesions. DNA damage elicits a key repair mechanism, the DNA damage response (DDR), initiated by phosphorylation and activation of checkpoint proteins Chk1 and Chk2. This induces p53-dependent responses, including cell cycle arrest, apoptosis and/or senescence, which limit preneoplastic lesions’ growth, but they become cancerous when p53 function is inactivated. However, the molecular basis of oncogene-induced DNA damage in sporadic cancers and in particular in hepatocarcinogenesis remains unclear.

Chronic mTORC1 activation in hepatocytes leads to HCC development via DNA damage at early stages of liver tumorigenesis. URI (Unconventional prefoldin RBP5 Interactor), an oncogene amplified in human ovarian carcinomas and part of the R2TP/URI-prefoldin (PFD)-like complex containing the co-chaperone protein HSP90, is a downstream target of the growth factor- and nutrient-regulated mTOR/S6K1 signalling cascade. URI promotes cell survival by binding PP1γ phosphatase, thereby increasing S6K1 activity-dependent survival signalling. Various mouse models to study cancer development were documented, but experimental models mimicking distinct stages of carcinogenesis are needed. Prompted by these observations, we generated several genetically engineered mouse models (GEMMs) for URI loss and gain of function. In particular a clinically relevant URI-tetOFF^{hep} mouse ectopically expressing human URI in hepatocytes recapitulates key molecular, cellular, and genomic events of human liver cancer, thus facilitating exploration of molecular mechanisms linking histopathological changes to hepatocarcinogenesis and oncogene-induced DNA damage. Our results reveal an unanticipated role of oncogene-induced NAD^+ depletion in DNA damage and subsequent tumorigenic processes.

.

Resumen

El carcinoma hepatocelular es el tumor del hígado más común en la población y de mayor letalidad (GLOBOCAN 2008 v2.0). Los estadios tempranos del desarrollo tumoral se caracterizan por la presencia de nódulos displásticos llamados lesiones preneoplásicas. Generalmente estas lesiones evolucionan dando lugar a la hepatitis, una enfermedad inflamatoria crónica del hígado que puede contribuir al desarrollo de la fibrosis y del carcinoma hepatocelular. Por lo tanto, las lesiones precancerosas tienen una gran importancia clínica para la predicción del posible desarrollo de carcinomas hepatocelulares. Sin embargo, las opciones terapéuticas son muy limitadas.

Los estadios tempranos del desarrollo tumoral se caracterizan por la presencia del estrés replicativo asociado a la activación de oncogenes. Dicho estrés replicativo genera daños en el ADN que conducen a la aparición de la inestabilidad cromosómica, la cual acelera el desarrollo tumoral en lesiones preneoplásicas. Los daños en el ADN activan mecanismos de reparación que se conocen globalmente como "la respuesta al daño en el ADN", y se inician con una cascada de fosforilaciones y la activación de las proteínas del ciclo celular Chk1 y Chk2. De forma dependiente de p53, la activación de estas kinasas induce la parada del ciclo celular, la entrada en senescencia o la apoptosis. Esta vía de señalización supone una barrera para el crecimiento de las lesiones preneoplásicas, pero las mutaciones en p53 conduces a la aparición de estadios cancerosos. Sin embargo, la base molecular de la activación de la respuesta al daño en el ADN mediada por oncogenes en tumores esporádicos, y en particular en carcinomas hepatocelulares, se desconoce.

En los estadios tempranos del desarrollo tumoral, la activación crónica de mTORC1 en los hepatocitos conduce al desarrollo de carcinomas hepatocelulares a través de la respuesta al daño en el ADN. URI (*Unconventional prefoldin RBP5 Interactor*) es un oncogén amplificado en los carcinomas de ovario humanos que forma parte del complejo R2TP/URI-prefoldin. Además, es una diana de la ruta de señalización de los factores de crecimiento y los nutrientes, la cual está regulada por las proteínas de señalización mTOR/S6K1. URI promueve la supervivencia celular al interaccionar con la fosfatasa PP1γ, lo cual aumenta la actividad de S6K1. Hasta la fecha se han generado una gran diversidad modelos murinos para estudiar el desarrollo tumoral; sin embargo, se necesitan modelos experimentales que reflejen los distintos estadios del proceso tumoral. Con este fin, hemos creado modelos de ratón modificados genéticamente para la proteína URI, tanto de pérdida como de ganancia de función. En concreto, hemos generado un modelo de relevancia clínica, en el cual la proteína humana URI se expresa ectópicamente en los hepatocitos murinos. Este modelo (URI-tetOFF^{hep}) recapitula los eventos moleculares, celulares y genómicos clave de la fisiopatología de los tumores de hígado humanos. Por lo tanto, nos ha posibilitado la identificación de los mecanismos moleculares responsables de los cambios histopatológicos que acontecen durante la carcinogénesis hepática y la activación de la respuesta al daño en el ADN. Nuestros resultados revelan que la ausencia de NAD^+ como consecuencia de la activación de oncogenes desempeña un papel inesperado en el daño al ADN y la consecuente exacerbación del proceso tumoral.

Table of contents

Abbreviations

αctn	α-catenin
bp	Base pairs
ES cell	Embryonic Stem Cell
f/f	flox/flox
FLP	Flippase
IP	Immunoprecipitation
Kbp	Kilo basepairs
mAb	Monoclonal antibody
qRT-PCR	Quantitative Real Time PCR
SB	Southern Blot
HCC	Hepato Cellular Carcinoma
WB	Western Blot
IHC	Immunohistochemistry
ICC	Immunocytochemistry
FGF	Fibroblast growth factor
MAPK	Mitogen activated protein kinase
PI3K	Phosphoinositol-3-kinase
FoxA	Forkhead box
HNF	Hepatocyte nuclear factor
TBx	T-box family
Hhex	Hematopoietically-expressed homeobox protein
HBV	Hepatitis-B virus
HCV	Hepatitis-C virus
AAF	2-Acetylaminofluorene
LPC	Liver progenitor cells
CDE diet	Cholin-deficient ethionine-supplemented diet
DDC diet	3,5-diethoxycarbonyl-1,4-dihydrocollidine diet
ALT	Alanine transaminase
AST	Aspartate aminotransferase
ALT	Alkaline phosphatase

MaFC Macrovesicular fatty change

MiFC Microvesicular fatty change

NFLAD Non-alcoholic fatty liver disease

NASH Non-alcoholic steatohepatitis

MS Metabolic syndrome

FCA Focus of cellular alteration

BDH Bileduct hyperplasia

OH Oval cell hyperplasia

HCA Hepatocellular adenoma

HCC Hepatocellular carcinoma

GEMM Gentically engineered mouse model

HGF Hepatocyte growth factor

Introduction

1 LIVER: A VITAL ORGAN

1.1 Embryonic liver development

Liver is the largest internal organ of the human body performing both endocrine and exocrine functions with extraordinary regenerative potential. It is composed of both parenchymal and non-parenchymal cells. All the parenchymal cells of embryonic-liver derive from the anterior portion of definitive endoderm, which is established during gastrulating embryo (Fig 1) (1). Three distinct hepatic progenitor cells are present in medial and bilateral regions of the foregut. Cardiac mesoderm plays crucial instructive role in hepatic cell fate at around 7-8 somite cell stage (2). This is mediated by the fibroblast growth factor (FGF) signaling, which further induce the expression of albumin. The FGF1/2 driven hepatic specification is mainly controlled by downstream MAPK pathway and independent of PI3K signaling (3).

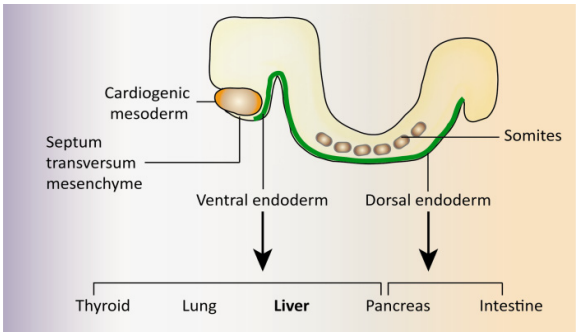

Figure 1. Schematic representation of a head-tail section of mouse embryonic (E 8.5) liver. Liver originates from the ventral endoderm of the foregut along with thyroid and lung.

1.2 Transcriptional factors regulating liver development

Liver development is orchestrated through a complex network of transcription factors that regulates specification, differentiation and cellular migration. For instance, although expressed in low levels in early hepatic progenitor, albumin is one of the best markers for hepatocyte lineage. In response to appropriate developmental cues, FoxA and GATA4 bind to the *albumin* enhancer elements and initiate specification(4). However, hepatocyte differentiation appear to be independent of FoxA1/A2 but dependent on HNF1β. Around 7 and 11 somite-stage, in response to the cardiac and mesenchymal cues, hepatic genes including *albumin, alphafetoprotein (Afp), transthyretin (Ttr), retinol binding protein (Rbp),* and *Hnf4a* are expressed. At around 21 somite cell stage in mouse, E-cadherin expression is down regulated in the hepatic cells and the cells invade the surrounding stroma as cords of hepatoblasts. Furthermore, *Hhex and TBx3 are* key regulator in the complete differentiation of hepatoblasts into hepatocytes. *Hhex* conditional ablation results in hepatic structures that lack a parenchymal cell component. However, *TBx3* regulates the hepatocyte differentiation, loss of which results in the loss of hepatocyte specific transcription

factors like Hnf4α and C/EBPα and increased expression of cholangiocyte markers like HNF6 and HNF1β. Hepatoblasts further migrates into septum transversum and differentiate to either hepatocytes or cholangiocytes with the orchestrated action of six transcription factors (HNF1α, HNF1β, FoxA2, HNF4α1, HNF6 and LRH-1). In adult stage, Embryonic HNF4β mediated hepatic specification is replaced by HNF4a, thus loss of HNF4α does not have an impact on hepatic specification but further differentiation of the hepatic progenitors is blocked. Wnt signaling in the posterior endoderm later inhibits *Hhex* activity. Antagonists for WNT in the anterior endoderm therefore are necessary to express *Hhex* and thus commit the endoderm to stem cell fate. Most of the embryonic signaling pathways gets silenced during development and reactivated during different steps of oncogenesis (AFP, H19 and Glypcan-3), thus having high clinical value.

1.3 Cellular composition and structure of the liver

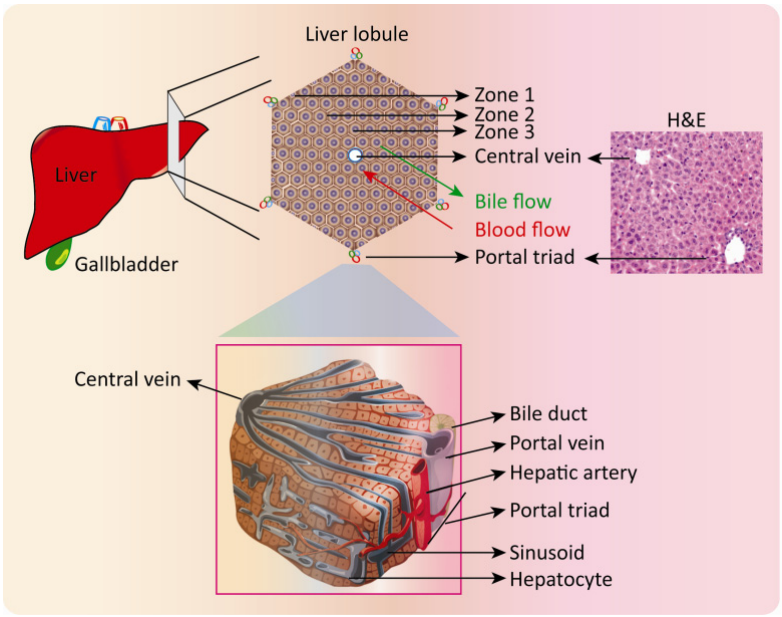

Figure 2. Schematic representation of liver architecture.

The basic architectural unit of liver is the liver lobule. Parenchymal hepatocytes are the major cell type constitutes 78% of liver volume. Other non-parenchymal cells that play a vital role in liver function are cholangiocytes (biliary epithelial cells), endothelial cells, sinusoidal endothelial cells, kupfer cells (resident liver macrophages), pit cells (natural killer cells), liver progenitor cells (LPCs)/oval cells and hepatic stellate cells (Fig 2). All the cells constitute the liver; perform specific patho-physiological functions as described in table 1. Hexagonal liver lobule is the functional unit of liver which is divided into three zones, zone 1 (periportal), zone 2 (transitional; midzonal), and zone 3 (centri-lobular) with portal triads on the six corners and central vein in the centre. Functionally, zone1 hepatocytes are specialized for oxidative liver functions such as gluconeogenesis, β-oxidation of fatty acids and cholesterol synthesis and zone 3 hepatocytes are specialized for glycolysis, lipogenesis and cytochrome P-450-based drug detoxification reactions (Fig 2).

Cell Type	Localisation	Function
Hepatocyte	Prenchyma	~70% of liver cells, Protein secretion, Bile secretion, Cholestrol metabolism, Detoxification, Urea metabolism, Glucose/glycogen metabolism, Acute phase response and Blood clotting.
Cholangiocyte/ Bile duct cell	Duct epithelium	~3% of liver cells, Bile transport, water secretion and bicarbonate levels and control pH of bile.
Liver progenitor cells (LPCs)/ Oval cells	Canals of Hearing	Rare, second line of regeneration, to differentiate into hepatocyte and cholangiocyte under special conditions.
Endothelial cell	Vasculature	Form veins, arteries, control blood flow, contribute toward parenchymal zonation.
Liver sinusoidal endothelial cell	Sinusoids	~2.5% of liver cells, Form sinusoidal plexus to facilitate blood circulation, Nutrient transfer from serum to hepatocytes, scavenging, cytokine secretion, antigen presentation and blood clotting.
Pit cell	Natural killer cell	Rare, cytotoxic activity
Kupffer cell	Sinusoids	~2% of liver, Scavengers of foreign material, secrete cytokines and proteases etc.
Stellate cell	Perisinusoidal	~1.4% of liver cells, maintenance of extracellular matrix, VitA and retinoid storage, regenerative response to injury and secretion of cytokines.

Table 1. Localization and function of the major liver cell types

Hexagonal shaped liver lobule contains central vein (drains the blood) in the centre and portal triad (portal vein, bile duct and hepatic artery) in the six corners of the hexagon supplying blood to the lobule, which flows through the network of sinusoidal capillaries (Fig 2). Bile flows from the centre of the hepatic lobule to the portal areas and on to the hepatic duct. Hepatocytes lined with sinusoidal capillaries (discontinuous epithelium) carry the oxygen-rich blood from the hepatic artery and nutrient rich blood drained from spleen, stomach, intestine and pancreas via portal vein (dual blood supply).

1.4 Regenerative capacity of the liver

Several endogenous metabolic alterations or exogenous factors induce liver regeneration. Viral infections like hepatitis-B virus (HBV) and hepatitis-C virus (HCV), alcohol consumption, xenobiotic compounds and high-caloric-food intake are some of the agents that induce liver damage and also predispose for liver diseases and cancer (5).

Partial hepatectomy (two-thirds of liver) mainly results in the activation and proliferation of hepatocytes to reconstitute the volume of the organ in a week (6). However, with the viral infections (HBV and HCV), hepatotoxic xenobiotics, choline-deficient ethionine-supplemented diet (CDE), 3,5-diethoxycarbonyl-1,4-dihydrocollidine (DDC), 2-Acetylaminofluorene (2-AAF) and D-galactosamine treatment, which render to inhibit hepatocyte proliferation, a second line of bi-potential adult stem cell pool called liver progenitor cells (LPCs)/oval cells undergo rapid proliferation and differentiate to hepatocytes to resume the liver function and have been shown to be strongly associated with human neoplastic liver disease with hepatocyte differentiation (7). LPCs are likely candidates for the potential HCC cell of origin. Several genetic fate-tracing experiments in the context of several liver injury models like partial hepatectomy (PH), CDE, DDC and carbon tetrachloride (CCl4) injections suggested that they do not contribute for the major hepatocyte pool

(8,9). The tumorigenic potential of these cells have also been showed to be above par with the adult hepatocytes, cholangiocytes and hepatoblasts, thus raising the prerequisite to study the role of these cells during tumor development (10).

2. LIVER DISEASES

2.1 Liver Function

Liver condition or disease	Bilirubin (0.1-1.0 mg/dL	ALT (7-56 U/L) and AST (0-35 U/L)	ALP (41-133 IU/L)	Albumin (3.4 - 5.4 g/dL)	PT (12-13 s)
Acute liver damage	Normal or increased after ALT and AST	Increased, ALT is usually higher than AST	Normal/moderately increased	Normal	Usually Normal
Chronic liver disease	Normal or increased	Mildly or moderately increased	Normal/moderately increased	Normal	Normal
Alcoholic Hepatitis	Normal or increased	AST moderately increased, AST/ALT=~2	Normal/moderately increased	Normal	Normal
Cirrhosis	May be increased but occours later in the disease	AST moderately increased, AST/ALT<~2	Normal or increased	Normal or increased	Usually prolonged
Bile duct obstruction, cholestasis	Normal or increased in compleete obstruction	Normal or moderately increased	Increased often greater than 4 times	Usually normal butchronic disease leads to decrease	Usually normal
Cancer metastasized to liver	Usually Normal	Normal or slighltly increased	Greatly increased	Normal	Normal
HCC	May be increased in advanced disease	AST is higher than ALT but lower than alcoholic disease	Normal or increased	Normal or increased	Prolonged
Autoimmune	Normal or increased	Moderately increased; ALT is usually higher than AST	Normal or slightly increased	Usually decreased	Normal

The Liver is a metabolic center that is characterized by the production of Hepatocyte-specific enzymes that are important for liver function and also used as markers for liver dysfunctions.

Table 2. Table representing different liver disease conditions and the corresponding liver functional parameters

2.1.1 Alanine Transaminase (ALT): ALT catalyzes the transamination reactions, higher concentrations of ALT are found in liver and lower levels are observed in kidney, heart and muscle. Liver injury often leads to the increase in serum ALT levels from the normal 7-56 U/L. However, the absolute peak of ALT elevation often does not correlate with the extent of liver damage (11).

2.1.2 Aspartate aminotransferase (AST): AST catalyze the inter-conversion of aspartate and a-ketoglutarate to oxaloacetate and glutamate. AST expression is observed in heart, liver, skeletal muscle and kidney. Extensive tissue necrosis, myocardial infarction, and chronic liver diseases like liver degeneration and necrosis shows elevated AST levels.

2.1.3 Alkaline phosphatase (ALP): ALP is found in mucosal part of intestine, kidney, bone, liver and placenta. Serum ALP levels normally lies between 41 to 133U/L, moderately elevated in acute viral hepatitis and drastically increased in cholestasis. The expression of different serum metabolites and enzymes specific for liver dysfunction has been described in table 2.

2.2 Fatty change

Without compromising the liver function often fatty change (Macrovesicular fatty change (MaFc) and Microvesicular fatty change (MiFC)) and associated changes in the inflammatory pathways constitute a major predisposing factor for HCC development through Non-Alcoholic Fatty Liver Disease (NFLAD). NFLAD is characterized by an excessive accumulation of fatty acids and triglycerides in the hepatocytes. Chronic NFLAD with cryptogenic cirrhosis and associated necroinflammatory activity characterize the Non-Alcoholic Steato-Hepatitis (NASH) state, which is one of the main non-viral factors to induce liver cancer. NASH is a progressive disease often accompanied by obesity and metabolic syndrome (MS), over a period of 10 years NASH develops into liver cirrhosis, 10% of the NASH affected patients suffer liver related mortality (12).

Perturbations in lipid metabolism and deposition, subtle liver injury often leads to lipodosis/fatty change. Two different kinds of fatty changes have been reported.

2.2.1 Macrovesicular fatty change (MaFC): MaFC arises when hepatocytes contain a large well-defined single rounded vacuole within each cell. Nucleus and cytoplasm often displayed to the periphery, hydrophobic degeneration-clear cytoplasm without nuclear displacement can be observed. This condition is predominant as an imbalance between lipid uptake from blood and secretion of lipoproteins by the hepatocyte (13).

2.2.2 Microvesicular fatty change (MiFC): MiFC arises when hepatocytes are partially or completely filled with numerous small lipid vacuoles, displaying foamy appearance. This condition often arises with more severe hepatic dysfunction as well as nutritional disturbances. Fatty change and necrosis may appear simultaneously as a response to xenobiotic exposure, chronic hepatic injury, diet, metabolic and hormonal status and fasting before the necropsy (13).

2.3 Pigmentation

Lipid peroxidation, hepatocyte/erythrocyte breakdown or altered heme metabolism often leads to pigmentation. Accumulation of lysosomal lipofuscin granules, iron storing complex

(Iron/hemosiderin) in a complex with ferritin, bile acids and bile acid derivative product porphyrin are often seen in different liver disorders.

2.4 Hepatocellular changes

2.4.1 Hepatocellular hypertrophy/ heapatocytomegaly: Activating metabolic enzymes causing increase in endoplasmic reticulum, peroxisomes and mitochondria result in hepatocytomegaly. Sinusoidal compression and loss of hepatic plate architecture is often observed. Persistent hypertrophy also results in degeneration and necrosis of hepatocytes, associated with increase in absolute liver weights (13).

2.4.2 Cell death (Necrosis, apoptosis): Direct or indirect cellular damage including anoxia leads to cell death. Apoptosis (single cell necrosis) is very rare in adult liver; however it can be exacerbated by treatment. Affected hepatoctes may present condensed chromatin, not associated with an inflammatory response unless there is simultaneous necrosis. Rounded apoptotic bodies are typically surrounded by a clear halo, and are phagocytosized by adjacent normal cells including hepatocytes and macrophages (5,13).

2.4.3 Karyocytomegaly and/or multinucleated heptocytes: Anisokaryosis (irregularly shaped nucleus) is randomly distributed in the hepatic lobule with more affected hepatocytes in the centrilobular region. This is a reflection of the hepatocyte polyploidy that occurs in the absence of cytokinesis. Eosinophilic cytoplasmic inclusions may be seen in affected hepatocyte nuclei because of cell membrane invaginations (13).

2.4.4 Inflammatory cell infiltrates (Hepatitis): A variety of focal, multifocal and diffused inflammatory cells are frequently present in liver tissue. Infiltrations of different inflammatory cells are typically a response to parenchymal cell death that causes ranging from infectious agents, exposure to toxins, xenobiotic metabolites and tissue anoxia. Neutrophyl infiltration is primarily a response to liver cell injury and necrosis before the infiltration of lymphocytes and macrophages. The extent of parenchymal cell death determines the kind of inflammatory reaction from microfocal lesions to large patches of coagulated necrotic cells (5).

2.4.5 Fibrosis: Fibrosis is a regenerative response by the activated stellate cells, portal fibroblasts and myofibroblasts in the liver by producing extracellular matrix proteins (mainly collagen) around the portal areas in response to fibrogenic cytokines like TGF-β1, angiotensin II, and leptin. Pericellular, peribiliary and postnecrotic are the three different fibrotic patterns commonly seen in mice. Oval cell proliferation often spreading from the periportal areas is commonly seen. Irreversible form of fibrosis is accompanied by a nodular or non-nodular regenerative response in

the liver represents cirrhosis. Fibrosis is detected by Masson trichrome, Van Gieson or Sirius red histological stainings combined with alpha smooth muscle actin (α-*SMA),* collagen, type1, alpha 1 (*col1a1)* and tissue inhibitor of metalloproteinase 1 *(Timp1)* (14).

2.5 Non-neoplastic, preneoplastic and neoplastic liver lesions.

2.5.1 Non-neoplastic lesions

A variety of non-neoplastic proliferative lesions occur spontaneously in rodents and humans, causes ranging from early growth, pregnancy to partial hepatectomy.

2.5.1.1 Focus of cellular alteration (FCA): FCA is commonly observed in mice older than 12 months of age or the mice treated with xenobiotics. FCA is defined by the predominant cell type present, if not as basophilic, vacuolated, esinophilic, and/or clear cell hepatocytes without a predominant cell type. Normally no or only minimal compression of surrounding liver tissue is observed. Pleomorphic cells with enlarged vesiculated nuclei and prominent nucleoli are observed. Eosinophilic foci are composed of usually enlarged hepatocytes with acidophilic cytoplasm. Increase in endoplasmic reticulin, peroxisome or mitochondria is observed in eosinophilic foci (13).

2.5.1.2 Ito cell hyperplasia: Focal or diffused proliferation of fat-storing perisinusoidal Ito cells is a rare condition occurs predominantly in mice (13).

2.5.2 Neoplastic lesions

2.5.2.1 Bile duct hyperplasia (BDH): BDH arises from the proliferating small bileducts in portal region; it might be focal and commonly associated with periductular fibrosis and peri-ductular cell infiltration (15). Biliary epithelium may show degenerative or atrophic changes. BDH often associated with evidence of hepatic injury and repair and obstruction of bile flow.

2.5.2.2 Cholangiofibrosis: Cholangiofibrosis originates from an initial oval cell hyperplasia in response to pronounced hepatic parenchymal necrosis. Dilated cystic bile ducts filled with mucus and cellular debris surrounded by inflammatory cell infiltrates and connective tissue is often observed. This lesion is inflammatory, proliferative and metaplastic reaction involving bile duct epithelium and is seen with hepatocellular toxicity caused by xenobiotics (16).

2.5.2.3 Oval cell hyperplasia (OH): Oval cell hyperplasia arises from terminal ductile epithelial cells (canal of Hearing cells) spontaneously, following liver infections and hepatotoxic injury. OH originates from portal areas and is often multifocal, resulting in few small ductules with streaming into hepatic parenchyma. Oval cells express keratin, have an oval shaped nucleus and pale

basophilic cytoplasm. Hepatocarinogenic treatment and hepatotoxic injury are often associated with oval cell proliferation. Chronic active hepatitis in mice often leads to oval cell expansion. OH suspected to be involved in the lineage of hepatocellular and cholangiocellular carcinomas and may serve as the hepatic cancer stem pool (17). HCA is broadly divided into telangiectatic, mixed hyperplastic/ adenomatous and leions with large cell hepatocellular atypia varients.

2.5.2.4 Hepatocellular adenoma (HCA): HCA arises spontaneously in old mice, accelerated after carcinogenic hepatotoxins and gene alterations in GEMMS (18). Histologically, HCA displays nodular lesions compressing the adjacent normal hepatocytes. Frequently HCA is observed in females using steroidal contraceptives or estrogen analogues. HCA is demarcated from surrounding parenchyma; liver plates often impinge obliquely on surrounding liver parenchyma. HCA presents, a fibrous encapsulated single nodules with an increased mitotic index. Cellular atypia may be present with signs of degenerative processes such as intracytoplasmic-inclusions, hyaline bodies or vacuoles. In mice hepatocellular carcinomas can be seen histologically arising within adenomas of both spontaneous and induced adenomas (19).

2.5.2.5 Cholangiocarcinoma (CC): Cholangiocarcinoma is the neoplasm of the cholangioytes (bile-duct cells), if originates with-in the part of bile ducts within the liver it's called intra-hepatic, if its originated in the bile-ducts outside of the liver it's called extrahepatic. The exact causes are unknown however; there are several predisposing conditions like chronic inflammatory bowl condition (ulcerative colitis), primary sclerosing cholangitis, choledochal cysts, liver fluke infection, and increase in age. This cancer is more commonly seen in women than in men.

2.5.2.6 Hepatocellular carcinoma (HCC): Hepatocellular carcinoma (HCC) is the most common, frequently lethal, primary liver malignant neoplasm, and also the third leading cause of cancer-related death in human population (GLOBOCAN 2008 v2.0). HCC follows a stepwise disease progression initiated by chronic liver damage/injury, inflammation, followed by activated regenerative response (fibrosis/cirrhosis) forming a hyperplastic nodule, which develop into dysplastic nodule and finally to HCC (Fig. 3) (5). NAFLD and NASH represent the major predisposing factors for HCC development in the western world (20,21). Absence of portal tracts, 2-3 cell thick hepatocelluar plates/cords, nuclear atypia are the key histologial features to identify HCC. A well-differentiated HCC with better prognosis display a clear pattern of hepatic plates separated with sinusoids, while an undifferentiated HCC with worse patient prognosis lack the hepatocyte shape and hepatic pates (Fig. 3). HCCs are also classified based on their architectural patterns like *Trabeular* type (plate-like, common in moderate to well differentiated HCC), *Pseudoglandular and acinar* type (glandular arrangement of tumor cells in single layer or dialation of bile canaliculus-like

structures) and *Scirrhous* type (a rare subtype with marked fibrosis along the sinusoids-like blood spaces). In spite of the detailed aetiology, antiviral strategies and histopathological evaluation the therapeutic options for HCC are very limited. High risk patients are often screend with serum alfa-fetoprotein (AFP), Alanine-transaminase (ALT) incombination with ultrasonography/CT scan and MRI (22). Standard of care often varies depend on the residual liver function, tumor stage and patient performance stats. Patients with more advanced HCC sorafenib is the only viable option with 3-months increased survival (23). The incidence of human HCC is 3 fold in males compared to females; this affect is attributed to the diminished IL6 secreted by macrophages in females by estrogens and estrogen dependent pitutay harmone prolactin (PRL) (24,25).

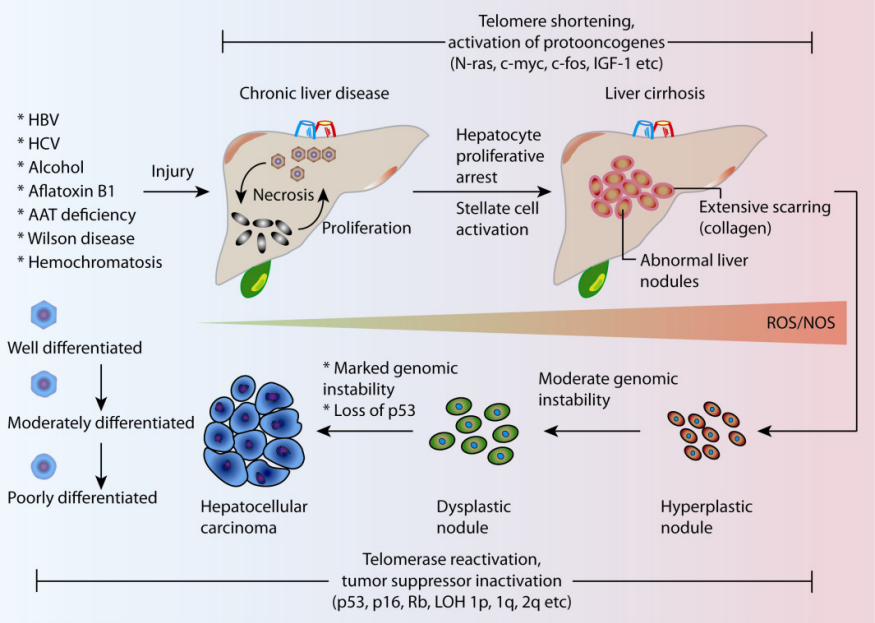

Technological advances in the field of gene targeting and gene manipulation in mouse models, allowed generating GEMMs mimicking human disease. GEMMs are critical to understand hepatocarcinogenesis, thus facilitating mechanism based intervention studies.

Figure 3. Schematic representation of HCC development.

3. Mouse models to study HCC development

Based on the predominant etiological factors several GEMMs and gene expression analysis have been performed to understand the oncogenic potential of viral proteins (HBV and HCV) (table X). HBV and HCV infections have different patho-physiological outcomes. HCV is a single stranded RNA virus that belongs to flavivirus family doesn't integrate into the genome unlike double stranded HBV genome. HCV infection often leads to cirrhosis (70% vs. 50%), and HCC formation (75% vs. 29%) compared to HBV infection.

HBV transgenic mice over expressing the viral protein HBV X protein (HBx) developed clear cell HCC by 11-15 months of age, recapitulating the gender bias observed in human HCC, but not the

inflammatory and fibrotic background often associated in human disease. This mouse model also put forward the "one-hit" theory, where a carcinogen both initiates and fuels the cancer progression. Expressing truncated HBx protein (X15) with the transactivating potential along with a mouse proto-oncogene *c-myc* accelerated HCC formation by 4 months (Table 3). c-Myc expression is predominantly cytoplasmic, more evident in the neoplastic nodules than the surrounding normal cells, supporting the "two-hit" hypothesis and synergism between HBx and c-Myc.

Mouse model	Transgene used	Characteristics
Mouse models of HCC development based on HBV infection		
CD1	*HBx* gene + enhancer	**Month 4**: High HBx expression **Month 8-10**: Adenoma + HBx and AFP **Month 11-15**: Male mice die of HCC
C57BL/6xDBA	*HBx* gene + enhancer + a portion of pre C-C sequence	**Month 4**: High HBx expression **Month 6**: Neoplastic nodules + HBx + PCNA **Month 11-18**: HCC + HBx + PCNA **Month 17**: Metastasis + HBx + PCNA
Tg. C57BL/6 (*p21-HBsAr* or *p21-HBx)*	*HBsAg* or *HBx* genes	**Month 5**: High serum glutamic-pyruvate transaminase in *p21-HBsAg* transgenic mice **Month 0-12**: Half of the mice had steatosis without inflammation **Month 15-24**: Male mice develop HCC in *p21-HBsAg* **Month 18-24**: Both male and female develop HCC in *p21-HBx* mice
Tg. C57BL/6 xSJL *HBx15-c-myc*	*HBx* gene encoding amino acids 58-154 + *c-myc)*	**Week 1**: Increased mitosis + nuclear pleomorphism + polykaryon hepatocytes **Month 2-3**: Focal necrosis + Kupffer cell proliferation **Month 4-5**: Adenomas + HCC + increase in liver size **Month 24-32**: Macroscopic HCC
Tg. Alb-1 HBV) Bri44	*Pre-S*, *HBsAg*, *HBx* genes	**Months 2-7**: Expression of HBV envolpe protein **Month 4**: Moderate to severe hepatitis **Month 6**: Regenerative nodules and oval cell hyperplasia **Month 8**: Adenomas + AFP **Month 12-20**: HCC + AFP
Mouse models of HCC development based on HCV infection		
Tg. HCV (E1-E2)	HCV envelope gene (E1-E2)	**Months 0-24**: No adenoma or HCC **Month 1-18**: Absence of envelope in the sera of mice
Tg. HCV (core)	HCV core gene	**Month 3**: Hepatic steatosis **Month >12**: Progression of steatosis, increase in oxidative stress **Month 16**: Male mice developed HCC (25-30 %) Female mice developed HCC (0-14 %)
Tg. C57BL/6 HCV FL-N, S-N)	HCV polyprotein (FL-N) or structural protein (S-N)	**Month >10**: Hepatic steatosis increased with age **Month >13**: HCC in FL-N/35 background + No fibrosis **Month >18**: HCC in S-N/863 background + No fibrosis
Tg. FVBXC57BL/6 HCV (E1-E2)	HCV core gene or core E1-E2 gene	**Months 0-21**: No HCC or adenoma **Week 20**: HCC after DEN **Week 32**: Both trangenic and nontransgenic mice developed HCC after DEN treatment

Table 3. Table representing different GEMMs and their characteristic features, based on HBV and HCV viral oncogenes

Similar to HBV and HCV viral proteins, Simian vacuolating virus 40 (SV40) has a potential to induce tumors. Mechanistically, it has been shown to suppress the transcriptional properties of the "guardian of genome" p53. p53 is the protein most frequently mutated protein in human hepatocellular carcinoma (30%) with 73% of them are missense substitutions. When the SV40 T-antigen is expressed under specific inducible promoters like albumin, α1-antitrypsin, serum amyloid P component or antithrombin III, liver tumors are induced as early as 1-3 months of age. The tumors displayed aggressive metastatic phenotype.

In addition to the viral oncogene GEMMs, several GEMMs have been generated to study the function of endogenous proto-oncogenes and their synergy (Table 4).

- The co-operation of Myc with other oncogenes and growth factors has been shown extensively to accelerate liver tumor formation. Myc alone induces HCC with a high latency (15-25 months), while it's combined ectopic expression with either E2F transcription factor-1 (E2F1), transforming growth factor alpha (TGF-α) or epidermal growth factor (EGF) markedly reduce the latency of tumor formation (3-6 months). Myc transgenic mice are genetically close to human HCC of good prognosis.

Genetically engineered mouse models for HCC

Mouse model	Latency	Characteristics
c-myc (Alb)	15-25 months	55% penetrance, hepatocyte specific (Albumin promoter used)
c-myc (WHV)	9 months	100% penetrance, woodchuck hepatitis virus regulatory sequences (WHV)
c-myc + E2F1 (Alb)	6-9 months	100% penetrance, hepatocyte specific, oncogne cooperativity
b-catenin + H-ras (Adeno virus)	6-8 months	100% penetrance, adenoviral cre, oncogne cooperativity
TGFa (Metallothionein 1)	10 -20 months	50% penetrance, Metallothionein 1 promoter + zinc
TGFa + c-myc (Alb)	10 months 4 months (+zinc)	100% penetrance, Albumin promoter, cooperativity of oncogenes
EGF + c-myc (Alb)	3-4 months	100% penetrance, Albumin promoter, cooperativity of oncogenes
FGF19	10-12 months	50% penetrance, not liver specific
SV40 T-antigen (Alb, a1 antitrypsin)	1-3 months	100% penetrance, rapid tumor incidence due to uncontrolled replication
AAT (a1 antitrypsin)	12-23 months	100% penetrance, effect of AAT-deficiency on the liver
PTEN (Alb-cre)	10-11 months	30-66% penetrance in females and males, effect of steatoepatitis
TGF-b1 (AAT)	+AAT: > 5 months	100 % penetrance, effect of steatoepatitis
GNMT	10 months	100 % penetrance, effect of steatoepatitis
Mdr-2 (whole body)	>12 months	100 % penetrance, cholangitis, strong inflammation

Chemically induced HCC mouse models

Mouse model	Latency	Characteristics
One shot DEN/ (DEN+Pheno barbital)	5-10 months	Genotoxic method inducing structural changes in DNA, 80-100 % of male mice develop HCC, No metastasis/fibrosis/chirrosis poorly recapitulates the human disease.
Long term DEN	5-8 months	Genotixic, 100% male and 30% in female, leads to very aggressive HCC with metastasis and H-ras mutations
Peroxisome proliferators	12-24 months (dose dependent)	Variable with the strain and the agonist used, metastasis is observed, no evidence in human disease
Aflatoxin	Early HCC in 12 months high grade HCC in 15-28 months	Considerable variation with the strain DBA/2J: 90%, C57BL/N: 25-66%, metastasis is observed, suitable model for AFB-inducede human HCC
CCl4	26 months	Dose dependent penetrance (50-94%) in both male and female, metastasis is observed
Choline defecient diet	10-12 months	100% peetrance, steatohepatitis driven tumorigenesis
Thioacetamide	10-22 months	70-100% penetrance

Table 4. Table representing different GEMMs and their characteristic features, based on different proto-oncogenes

- Activating mutations in β-Catenin have been observed in around 24% (missense mutations 68%) of the human hepatic tumors and have been considered as an early event in hepatocarcinogenesis. However, a Wnt activating β-Catenin mutation alone induces only hepatomegaly, secondary mutations are required for hepatocarcinogenesis. When both β-catenin and H-ras are mutated in a mouse model, HCC incidence is very rapid, by 2 months of age all the mice develop HCC and higher grade of HCC developed after 6 months of age.

- Hepatic mitogens like hepatocyte growth factor (HGF), EGF, TGF-α which play a vital role in hepatic development may also act as oncogenes. TGF-α is one of the potent hepatotrophic mitogen, synthesized by hepatocytes after partial hepatectomy, transgenic mice over expressing TGF-α, not only showed tumor development in liver but also in pancreas and mammary glands. These tumors are genetically more similar to the human counterpart with poor prognosis. Oncogenic cooperativeness has been demonstrated with c-Myc and TGF-α where 100% of the mice develops HCC after 40 weeks. EGF is another well-studied growth factor controlling different vital process such as, cell growth, proliferation and differentiation. Transgenic over expression of secreted form of EGF spontaneously induce HCC as early as 24 weeks.

Finally, some GEMMs have been demonstrated the role of tumor environment and mimicking the injury-fibrosis-HCC sequence. Non-cell autonomous affects of the fibroblast growth factor-19 (FGF-19) have been studied by ectopically expressing FGF19 in skeletal muscle cells. After 52 weeks around 50% of the transgenic mice succumb to HCC, these FGF-19 transgenic mice displayed more incidences in female mice with increased nuclear β-catenin expression.

4 Role of DNA damage response in HCC development

HCC frequently arises in the context of chronic injury thus lead to inflammation and promotes DNA damage and chromosomal aberrations. DNA damage in the hepatocytes often triggers a series of signaling events leads to DNA damage response (DDR) pathway. DDR often drive the cell fate into DNA repair, temporary/permanent cell cycle arrest or apoptosis, all of which have been implicated to play a major role in hepatocarcinogenesis (26). There are several modes of DNA damage and their corresponding DDR. Stalled replication forks (or single stranded nicks) are corrected by homologous recombination (HR), point mutations by mismatch repair (MMR) and double-strand break by non-homologous end joining (NHEJ). Aberrations in DDR has been showed to compromise genomic integrity and increasingly recognized as the common feature of human HCC. Additionally, in many sporadic cancers, activation of oncogenes, mainly downstream of growth factor signalling pathways, induces DNA replication stress, which results in DNA damage leading to CIN. Importantly, the implication of replicative stress in the generation of CIN is recently demonstrated to be responsible for intra-tumoral heterogeneity (27). Therefore oncogene-induced replicative stress is a well-defined model for cancer development. Interestingly, in premalignant lesions, oncogene-induced DNA damage elicits a p53-dependent response, including apoptosis and/or senescence which, limits growth of the lesions.

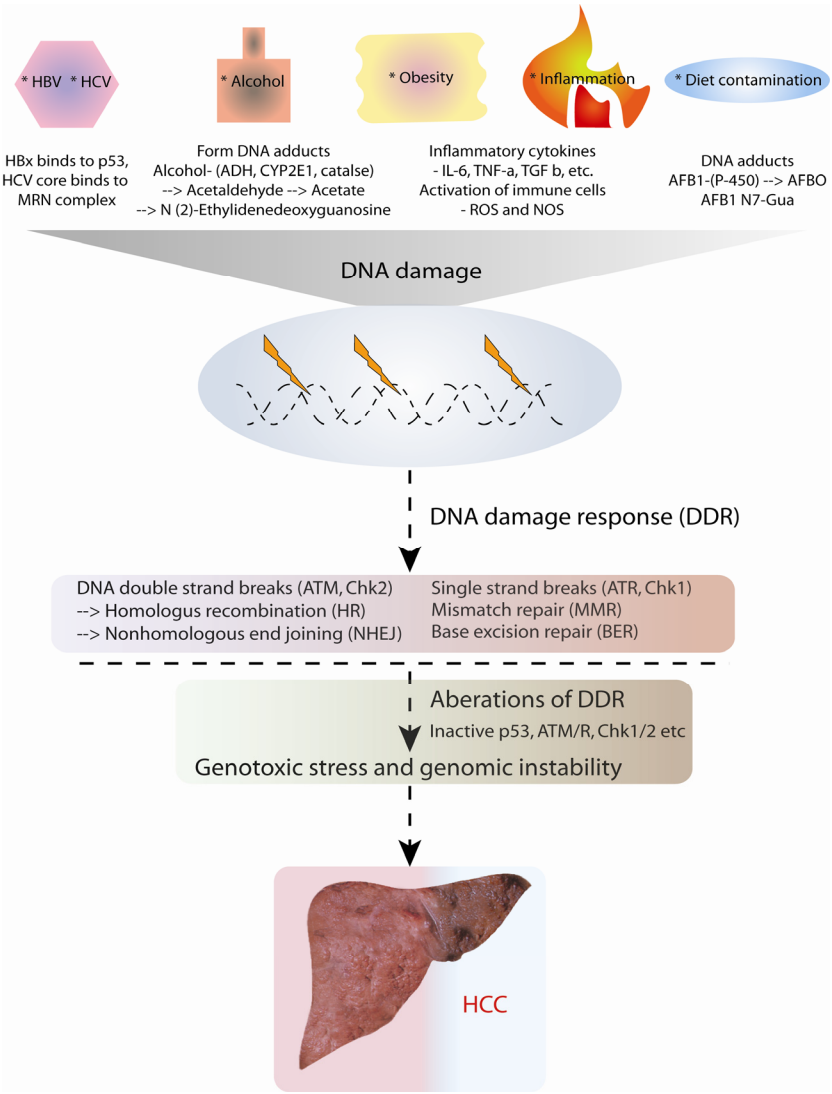

Figure 4. Schematic representation of HCC development through DNA damage induced by several etiologial factors of HCC.

When p53 function is lost preneoplastic lesions become cancerous (28). However, the molecular basis of oncogene-induced DNA damage in sporadic cancers remains largely unclear.

4.1 NAD+ as a metabolic adapter between DNA damage, oxidative stress and tumorigenesis

Given the devastating effects of genomic instability, cells have evolved a multiple series of interconnected mechanisms that maintains genomic integrity. The integrity of the DNA is continuously challenged by a variety of agents described above. For example, exposure to the sun

ultraviolet radiation alone induces 1 X 10^5 DNA lesions per day (predominantly pyrimidine dimmers). Likewise Ionizing radiation (as well as other factors described above) can induce single-stranded breaks and double stranded breaks, which elicits ATR or ATM dependent repair process. High levels of reactive oxygen/nitrogen species and inflammatory agents have been shown to elicit DDR pathway. Key molecular players of this pathway are different families of NAD+ consuming enzymes, poly (ADP-ribose) polymerases (PARPs) and sirtulins (SIRTs).

4.1.1 The PARP family

PARPs are a family of enzymes found in both eukaryotes and prokaryotes that generate ADP-ribose modifications onto the acceptor proteins. In human, 17 different PARPs have been identified based on the sequence homology studies. Based on the composition of functionally characterized domains PARP family is further divided into four sub families. *DNA-dependent PARPs,* require DNA binding for the enzymatic activity; *tankyrases,* with protein-binding ankyrin repeats; CCCH *zinc finger PARPs* shown to bind viral RNA; and *macro PARPs,* with ADP-ribosylating activity.

All DNA-dependent PARPs are nuclear during interphase, with PARP2 and 3 exhibiting additional cytosolic function. PARP-1 belongs to the DNA-dependent PARP sub-family is major nuclear enzyme, which detects DNA damage, binds to the single or double stranded DNA breaks, and then uses NAD+ as a substrate to form nicotinamide and ADP-ribose. Multiple ribosylation leads to the branched ADP-ribose polymers on the nuclear receptor proteins, which in turn modify the DNA repair proteins proximal to DNA. The major acceptors of poly (ADP-ribose) are PARP-1, histones, topoisomerase I and II, DNA polymerase α, and β, DNA ligase I and II, nuclear retinoid X receptor, nuclear factor (NF)-κB, and p53. PARP-1 has been reported to play a major role in nucleotide and base excision repair (NER and BER), by interacting with XRCC1 (X-ray repair cross complementing 1).

4.1.2 The Sirtulin family

The 7-member mammalian sirtulins (SIRT1-7) are most widely known for their life span extending activity. Sirtulins are activated by wide array of stress signals and, therapeutic targets in associated with metabolic syndrome (MS), neuro-degeneration, aging and cancer. The mammalian sirtulins display differential localization, predominantly nuclear (SIRT1, SIRT6 and SIRT7), cytosolic (SIRT2), or mitochondrial (SIRT3, SIRT4 and SIRT5) localization. Except SIRT4 and SIRT5 all the other members display lysine deacetylase activity.

SIRT1 expression is elevated in wide array of cancers (colon cancer, skin carcinomas, acute myeloid leukemia and prostate cancers) suggesting that it might work as a cancer promoter. However, other

cancer types like mutant breast cancer 1, early onset-mutant (BRACA1) breast cancer cells, contain significantly low SIRT1 levels, restoration of which inhibited the tumor cell growth. In GEMMs of cancer, SIRT1 protects against intestinal tumors in beta-catenin-driven cancer model, high fat diet (HFD) induced HCCs and age related spontaneous tumor development. SIRT1 have been shown to protect metabolic syndrome associated liver cancer and DNA damage induced by DEN (29).

Interestingly, not only competing at the substrate (NAD^+) levels, SIRT1 deacetylates and thus blocks the PARP1 activity (30), indicating that NAD^+ deficits impact on the SIRT1-PARP axis.

4.2 Fluctuating NAD^+ levels in cancer

Multiple *in vitro* studies have been reported the NAD+ status influencing the genomic stability and sensitivity to the cytotoxic and DNA-damaging agents. NAD+ precursors like nicotinamide (50-500 μm) increased intracellular NAD+ and enhanced the DNA repair when induced by N-methyl-N'-nitro-Nitrosoguanidine (MNNG) in primary human epithelial cells.

Dimethyl sulphite (DMS) induced DNA damage is also dependent on intracellular NAD+ levels. Moreover, even in the absence of DNA damaging agents, NAD+ depletion increased spontaneous DNA damage in human HaCaT keratinocytes, which is reversible with the addition of nicotinamide. Furthermore, NAD+ levels are often negatively correlated with malignant phenotype in human skin cancers and DEN induced HCCs. table x exemplifies the affect of NAD+ levels in different tumor models.

Animal model	Carcinogen	Nicotinamide dose	Organ	Effect on tumor
Mouse	None	Oral	All	None
Mouse	UV	Topical (200 mM)	Skin	Inhibition
Mouse	UVB	Oral(niacin-0.5;1% diet)	Skin	Inhibition
Mouse	TPA	Topical (150 mM)	Skin	Inhibition
Mouse	DMBA and Croton oil	Oral(0.2% diet)	Skin	None
Mouse	Urethane	Oral (0.25;0.4% diet) Oral (niacin)(0.25% diet)	Lung Lung	Inhibition None
Rat	ENU	Oral (niacin) (0.4% diet)	Bone marrow (haemopoetic cells)	Inhibition
Rat	Bracken fern	Oral (0.5% diet)	Intestine	Inhibition
Hamster	BOB	ip (30 mg/kg bw)	Pancreas	Inhibition
Rat	DEN	ip (350-500 mg/kg bw)	Kidney Liver	Increase Inhibition
Rat	Streptozotocin	ip (350 mg/kg bw)	Kidney	Inhibition
Rat	Heliotrine	ip (500 mg/kg bw)	Pancreas	Increase
Mouse	Transplanted murine breast adenocarcinoma	Oral (2.5; 5%)	Subcutaneous	Inhibition
Mouse	Transplanted murine breast adenocarcinoma	ip (1000 mg/kg bw)	Subcutaneous	Inhibition

BOB: N-nitrosobis(2-oxopropylamine) TPA: (12-O-tetradecanoylphorbol-13-acetate)
ENU: N-ethyl-N-nitrosourea DMBA: 9, 10-dimethyl-12-benzanthracene

Table 5. A table representing different tumor models and the corresponding affect of boosting NAD^+ levels.

4.3 Sources of NAD^+: *de novo* synthesis and salvage pathway

Although NAD^+ can be synthesized *de novo* from tryptophan, it is only assumed that perhaps the main source of NAD^+ is from salvage pathways, which require the uptake of other NAD^+ precursors (from other adenine nucleotide metabolites) from the diet (31). Among those natural compounds nicotinic acid (NA) (commonly called niacin) through the Preiss-Handler route is involved in generating NAD, and therefore converging with the synthesis of NAD^+ from tryptophan. Nicotinamide (NAM) and nicotinamide riboside (NR) are also implicated in NAD^+ synthesis through a completely independent pathway. NAM generates NAD^+ via the involvement of nicotinamide phosphoribosyltransferase (NAMPT), a homodimeric enzyme that controls the rate-limiting step in the resynthesis of NAD^+ through NAM (32,33). NAMPT transforms NAM into nicotinamide mononucleotide (NMN), which on its turn is converted into NAD^+ by the NMN adenylyltransferase (NMNAT). Finally, NR is phosphorylated upon its entry in the cell by the NR kinases (NRKs), generating NMN, which is then converted to NAD^+ by NMNAT (32-34).

Both NA and NAM can lead to higher NAD^+ levels, even though the effects might be tissue-specific (34). The cell/tissue-specific efficiencies of distinct NAD^+ precursors might be related to the differential expression of the rate-limiting enzymes in their respective metabolic pathways. In addition, salvage pathways seem to depend on *de novo* NAD^+ synthesis. This is supported by the fact that tissues that lack the complete *de novo* NAD^+ biosynthesis pathway, nicotinamide (NAM) is preferred over nicotinic acid (NA) via the Preiss Handler route, as the main precursor for NAD^+ biosynthesis (33,35). In this context, mice receiving an IP injection of NA showed a transient increase in NAD^+ concentration and a high excretion rate of nicotinuric acid in urine, accounting for almost half of the administered NA. In contrast, NAM injection raises NAD^+ levels which are more stable and with almost no nicotinuric acid excretion (33,35).

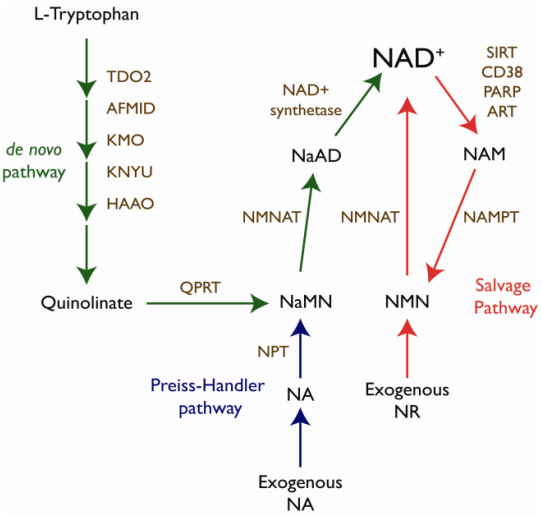

Figure 5. A scheme representing the pathways resulting in NAD^+ synthesis.

5. Other cell signaling pathways affected in human HCC

HCC develops on a predisposing liver disease that is highly prevalent, and develops into a treatment-resistant malignancy with multifaceted molecular pathogenesis. HCC is characterized by a phenotypic molecular heterogeneity hinting a diverse cellular origin, which makes its refractive to the current molecular targeting strategies. Telomerase, β-catenin and p53 are the most common

genetic alterations observed in human HCC, although no clear oncogene addiction has been reported. Current studies with GEMMs and cues from human disease suggest two possible pathogenic mechanisms. First being cirrhosis associated with hepatic regeneration right after the tissue damage by viral infections, alcohol abuse, toxins or change in metabolism (for e.g. Insulin resistance, obesity, type-II diabetes or NASH). Second line of mechanism is the classical view of mutations in single or multiple oncogenes and tumor suppressors induced by genomic instability. Both the mechanisms have been linked to the changes in several critical signaling pathways. These pathways include the RAF/MEK/ERK/AP1 pathway, WNT/β-catenin pathway, insulin-like growth factor pathway, hepatocyte growth factor/c-MET pathway, growth factor-regulated angiogenic signaling pathway and phosphatidylinosital-3 kinase (PI3K)/AKT/mechanistic target of rapamycin (mTOR) pathway.

5.1 The RAF/MEK/ERK/AP1 pathway

The Ras pathway represents a dominant signaling network promoting growth factor independent cell proliferation and cell survival. Binding of several growth factors (e.g. EGF and IGF-1) to their receptors induces the activation of intracellular Ras (via GRB2/SHC/SOS), which in-turn activates c-raf/b-raf, MEK and ERK. Activated ERK activates a hub of transcription factors (e.g. Elk-1, c-Jun/AP1) that regulates the genes involved in proliferative and survival functions.

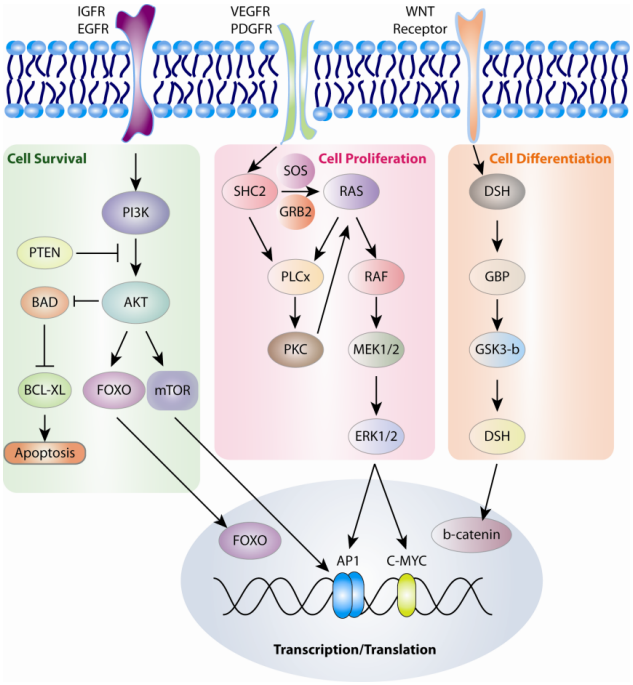

Figure 6. Major cell signaling pathways implicated in the pathogenesis of HCC.

Although aberrant Ras pathway activation occurs in different levels, the frequency of mutations in Ras gene is rare (*NRAS*: 4% and *KRAS*: 6%). Intermediate signaling is regulated by the mitogen/extracellular protein kinase kinases MEK1 and MEK2, which in-turn phosphorylate and activate the downstream signaling molecules extracellular-regulated protein kinases ERK1 and ERK2. HBx oncoprotein expressed from HBV has been shown to interact with PIN1 (over expressed

in HCC), which may enhance activation of the MAPK pathway by dephophorylating CRAF and thus promoting its activation by RAS. Downstream of the MAPK signaling is the transcription factor family activator protein 1 (AP-1). AP-1 functions as a dimeric complex containing members of the JUN, FOS, ATF (activating transcription factor) and MAF (Masculoapaneurotic fibrosarcoma) protein family members. Conditional inactivation of *c-Jun/AP1* in liver has been shown to decrease the tumor burden induced by chemical carcinogen (DEN). However, another members of the family, JUNB and JUND, counteract the inhibitory affect of c-Jun/AP1 on p53 (mediated apoptosis). Recently, the pro survival activity of c-Jun has been reported in the liver cancer initiation by suppressing c-Fos-mediated apoptosis independent of p53 (36,37).

5.2 The WNT/β-catenin pathway

An early carcinogenic event in the development of HCC seems to be the abnormal regulation of β-catenin, which is mutated in around 24% of human HCC (catalogue of somatic mutations in cancer: COSMIC). In the normal state, WNT ligands bind to the members of Frizzled family of surface receptors and activate the WNT signaling pathway. Receptor binding activates the downstream protein DSH (downstream of dishevelled), which consequently prevents the phosphorylation (and thus inactivation) of β-catenin by glycogen synthase kinase-3β. Once stabilized from the proteosomal degradation, β-catenin translocates to the nucleus and acts as a co-activator of the genes involved in proliferation (e.g. *MYC, MYB, CJUN and CYCD1)*, angiogenesis, survival and the extracellular matrix forming genes. Ectopic over expression of β-catenin alone is not able to induce tumorigenesis but rather it provides the growth advantage to the tumor cells. However, with the consecutive loss of a tumor suppressor *iqgap2* leads to the spontaneous HCC formation.

5.3 Receptor tyrosine kinases and growth factor-mediated angiogenic signaling

Liver is a highly vascularized organ, depends on the effective angiogenesis for cellular regeneration or regeneration during injury. Tumor growth, vascular invasion and metastasis of liver also depend on the efficient angiogenesis. A collaborative process between the activated endothelial cells and parenchymal cells leads to the effective vasculature. Normal angiogenesis is disturbed in tumor setting as the tumor cells, endothelial cells and pericytes secrete an excess of pro-angiogenic factors to the stroma. Several angiogenic factors like VEGF-A, angiopoietin-2 and PDGF have been shown to be up-regulated in human HCC. Commonly enriched angiogenic factors (e.g. VEGFs, PDGFs, placental growth factors, TGF-α and -β, fibroblast growth factor, EGFF, HGF, angiopoietin and

interleukin-4 and -8) leads to the activation of RAF/MEK/ERK/AP1, PI3K/AKT/mTOR and Janus kinase (JAK)/signal transducer and activator of transcription (STAT) pathways.

5.4 PI3K/AKT/mTOR growth factor and nutrient-signaling pathway

Constitutive activation of the PI3K/AKT/mTOR signaling pathway has been demonstrated as a major determinant of tumor cell growth and survival in different tumor types. Activated via a multitude of growth factors PI3K produce the lipid second messenger PIP3b (phosphoinositoltriphosphate), which in turn activates the serine/threonine kinase AKT/protein kinase B (PKB). AKT regulates different transcription factors like FOXO (control genes of glycolysis) and several cytoplasmic poteins like BCL-2 associated death promoter (BAD) and mTOR, thus increasing the survival and proliferation while keeping the apoptosis in check.

mTOR is a master regulator often activated in human HCC, coordinates the signals from the nutrients, growth factors, intracellular energy and oxygen levels to cell survival and proliferation. Different inhibitors (rapalogues) of mTOR are currently in clinical trials as individual therapies or in combination with other compounds for treating HCC.

5.4.1 URI a downstream player of mTOR/S6K1 pathway

5.4.1.1 Structure of URI

The evolutionarily conserved, Unconventional prefoldin RBP5 Interactor (URI) is a member of the R2TP/URI-prefoldin (PFD)-like complex containing the heat shock protein 90 (HSP90) (38).

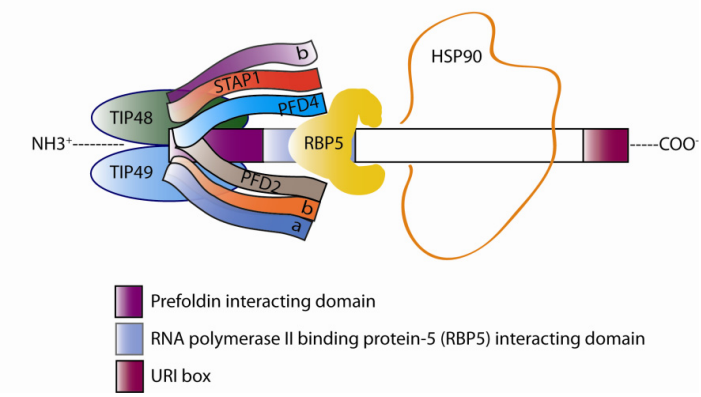

Expression of URI mRNA is ubiquitously detected in various tissues, but enriched in the testis, prostate, pancreas and skeletal muscle(39). Human URI protein is unconventional with 494 amino acids and 90kDa molecular weight in the prefoldin family.

Figure 7. Schematic representation of prefoldin-URI complex.

URI posses both nuclear and cytoplasmic localization signals, however, the protein are predominantly localized in the cytoplasm with diffused signals in the nucleus (40). In contrast to the other members of the prefoldin-family, URI has additionally highly conserved domains like an RPB5

interacting domain and URI box along with the conventional prefoldin domain. In humans, URI is a part of a 1 MDa multi-protein complex comprising a core subunit of RNA polymerase II RPB5, the ATPases TIP48 and TIP49 STAP1 (SKP2-associated alpha-PFD 1) and two prefoldins (PFD2 and PFD4-related)(39,41).

5.4.1.2 Function of URI

Biochemical analysis in yeast and human cells showed that URI is a target of nutrient sensitive mTOR transcriptional program (42). Amino acid limitations leads to the down regulation of URI protein in yeast and loss of URI resulted in elongated and agar penetrating yeast cells, as hallmarks of invasive growth (42,43). Moreover, URI is recently described as an oncogene amplified in human ovarian carcinomas downstream of the growth factor and nutrient-regulated mTOR/S6K1 signalling cascade (44). URI inhibits phosphatase PP1γ, thereby increasing S6K1 activity-dependent survival signalling. Growth factors stimulation induces disassembly of URI/PP1γ complexes, releasing PP1γ to enhance sensitivity of cancer cells to apoptosis. URI/PP1γ complexes maintain the mitochondrial threshold for apoptosis in accordance to nutrients availability. In this context, URI over expression promotes survival while its deletion enhances cancer cell death (44,45).

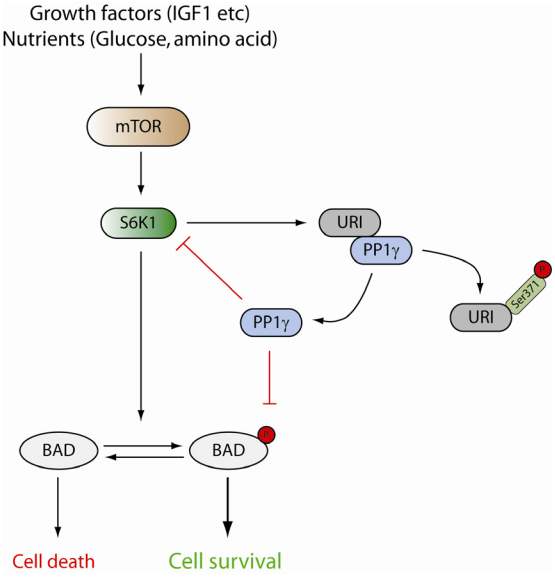

Figure 8. Mechanistic model of URI-PP1γ mediated feedback loop for mTOR signaling

Prompted by these observations, we generated genetically engineered mouse models (GEMMs) for loss- and gain-of-function of URI. In the URI gain-of-function mouse, human URI (hURI) is expressed specifically in hepatocytes, recapitulates key molecular, cellular, and genomic events of human liver cancer. hURI-tetOFF^{hep} mouse develops spontaneous liver tumors, while genetic URI reduction in hepatocytes protects against diethylnitrosamine (DEN)-induced HCC. Using quantitative transcriptomic and proteomic methodologies, we explore molecular mechanisms at early stages of tumorigenesis.

Objectives

Liver is the largest vital metabolic organ present in vertebrates that perform wide variety of functions like detoxfication, protein synthesis, glucose homeostasis and producing necessary enzymes for digestion etc. Hepatocellular carcinoma (HCC) represents the most common primary liver malignancy and third leading cause of cancer related death. State of the art diagnosis use ultrasonography (US) every 6-12 months with alpha-fetoprotein (AFP) every six months as the standard of care for screening. K-RAS/Raf/MEK/ERK, Wnt/β-catenin, Cytokine/growth factor/stress signals-JNK-AP1, telomerase/p53/apoptosis, PI3K-AKT-mTOR are the key signaling pathways altered.

Unconventional prefoldin RBP5 Interactor (URI) was previously reported to be part of the R2TP/URI-prefoldin (PFD)-like complex containing the heat shock protein 90 (HSP90) (38). It was also described as an oncogene amplified in human ovarian carcinomas downstream of the growth factor and nutrient-regulated mTOR/S6K1 signaling cascade (44). In this context, URI inhibits PP1γ phosphatase, thereby increasing S6K1 activity-dependent survival signaling (45). Of note, chronic mTORC1 activation in hepatocytes induces DNA damage in early hepatocarcinogenesis stages and finally HCC formation (46). Prompted by these observations we hypothesize that URI may act as an oncogene downstream of mTOR signalling with theurapeutic value.

The specific aims of this project are:

1. Generate hepatocyte specific URI GEMMS and study the patho-physiological roles of URI.
2. Decipher the mechanistic role of URI in liver homeostasis and carcinogenesis.
3. Investigate the therapeutic benefits of targeting URI in HCC development.
4. Determine the relevance of URI expression and its associated molecular mechanisms in human liver disease.
5. To address the identity of HCC cancer cell of origin.

Objetivos

El hígado es un órgano metabólico vital presente en los vertebrados, que desempeña múltiples funciones tales como: la detoxificación, la síntesis de proteínas, la homeostasis de la glucosa, la producción de enzimas necesarias para la digestión, etc. El carcinoma hepatocelular es el tumor de hígado más común en la población y representa la tercera causa de muertes por cáncer. Las técnicas de diagnóstico utilizadas actualmente son la ultrasonografía cada 6-12 meses y el análisis de la alfa-fetoproteína cada 6 meses. Las vías de señalización clave alteradas en los carcinomas hepatocelulares son: K-RAS/Raf/MEK/ERK, Wnt/β-catenin, citoquinas/factores de crecimiento/ señales de estrés-JNK-AP1, telomerasa/p53/apoptosis y PI3K-AKT-mTOR.

La proteína URI se identificó como parte del complejo R2TP/URI-prefoldin que contiene a la proteína de respuesta al choque térmico HSP90 (38). Es además un oncogén amplificado en los carcinomas de ovario humanos como diana de la ruta de señalización de factores de crecimiento y nutrientes regulada por las proteínas mTOR/S6K1 (44). En este contexto, URI inhibe a la fosfatasa PP1γ, aumentando la actividad de la proteína S6K1 y por lo tanto la supervivencia celular (45). De hecho, la activación crónica de mTORC1 en los hepatocitos induce daño en el ADN durante los estadios tempranos de la transformación celular, lo cual conduce al desarrollo de carcinomas hepatocelulares (46). Teniendo en cuenta estas observaciones, nuestra hipótesis es que URI es un oncogén en la ruta de señalización de mTOR con un valor terapéutico.

Los objetivos de esta tesis doctoral son:

1. Generar modelos murinos modificados genéticamente de forma específica en los hepatocitos, y estudiar el papel del URI en la patofisiología hepática.
2. Determinar el mecanismo molecular de actuación de URI en el mantenimiento de la homeostasis hepática y en la transformación tumoral.
3. Investigar la posible utilización de URI como diana terapéutica en los carcinomas hepatocelulares.
4. Determinar la relevancia de la expresión de URI (y los mecanismos moleculares asociados) en los carcinomas hepatocelulares humanos.
5. Determinar la célula de origen de los carcinomas hepatocelulares.

Materials and methods

1. Generation and handling of mice.

hURI knock-in mouse model (ColhURI) has been generated by flippase-mediated targeting and recombination of inducible human *URI* (hURI) cDNA tagged with the FLAG peptide in the 3' untranslated region of the homing locus of the collagen type I, alpha 1 locus (*Col1a1) Cola1* gene in KH2 embryonic stem cells (ESCs), having a tetracycline operator (Tet-op) (47).

In order to express hURI specifically in hepatocytes, ColhURI mouse has been crossed with a line containing the tetracycline-dependent transactivator (tTA) under the control of the liver activated protein (LAP) promoter to generate LAP-tTA/hURI*tetOFF* mouse, named hURI-tetOFF^{hep} mouse (48). Hepatocyte-specific ectopic hURI expression can be switched off by administration of doxycycline. hURI is expressed since conception and mice were off doxycycline, unless otherwise stated (Table 1). The URI conditional knockout mouse with *uri* floxed allele was generated by homologous recombination in embryonic stem (ES) cells (URI lox). In this allele, the exon 4 of *uri* was flanked by two LoxP sites. In addition, a neomycin resistance gene (Neo) flanked by two FRT sites was inserted before the second LoxP site for drug selection and was removed by expressing Flp recombinase. Expression of Cre recombinase would delete the targeted exon 4 and generate a delta allele (URI$^{D/D}$), leading of inactivation of the URI gene.

The germ line transmission of the founder mouse generated through an intercross between the chimeras and the Flp-deleter strain in order to remove the neomycin cassette was checked by Southern blot (5' and 3' arms were checked) and PCR analysis. Deletion of one allele by Cre recombinase in heterozygous ES cells was verified by reduced URI expression via WB analysis (Table 1). hURI-tetOFF^{hep} and URI lox mice have been backcrossed to C57BL/6 mice for at least 7 generations. All mice were housed in specific pathogen-free (SPF) animal facility Unit of CNIO. All experiments were approved by the CNIO-ISCIII Ethics Committee for Research and Animal Welfare (CEIyBA) and performed in accordance with the guidelines for ethical conduct in the care and use of animals as stated in the international guiding principles for biomedical research involving animals, developed by the Council for International Organizations of Medical Sciences (CIOMS).

Mice were kept in close observation and sacrificed when they displayed signs of sickness, in accordance to the Guidelines for humane endpoints for animals used in biomedical research. Littermates were always used as controls. Food (Harlan Laboratories) and water were provided *ad*

libitum. Same experiments have been performed by sacrifying mice at the same time and same lobes were used for the same experiment.

2. Antibodies.

Antibodies recognizing hURI and mURI have been described previously (45). Ki-67 (1:1) and Cyclin D1 (1:1000) were purchased from Dako. MAD2 (1:250), PCNA (1:1000), a-SMA (1:1000) and p65 (1:1000) were purchased from Santa Cruz. phospho-p44/42 ERK (Thr202/Tyr204) (1:1000), ERK (1:1000), S6K1 (1:1000), phospho-S6 (Ser240/244) (1:1000), S6 (1:1000), phospho-p38 (Thr180/Tyr182) (1:1000), p38 (1:1000), phospho-STAT3 (Tyr705) (1:1000), STAT3 (1:1000), phospho-AKT (Ser473) (1:1000), AKT (1:1000), BAX (1:1000), phospho-p53 (Ser18) (1:500), p53 (1:500), acetyl-p53 (Lys379) (1:500), cleaved caspase3 (1:500), phospho-Chk1 (Ser345) (1:500) and HSP90 (1:1000) were from Cell Signaling Technology. Phospho-H2AX (Ser139) (1:1000) was purchased from Merck Millipore. Phospho-Chk2 (Thr68) (1:500), Chk1 (1:500), Chk2 (1:500) were purchased from Upstate (Millipore). Phospho-S6K1 (Thr389) (1:1000), and GAPDH (1:2000) were from Abcam. Flag antibody (1:1000) was from Agilent. JNK1 (1:1000), p21 (1:1000) and PARP (1:500) was from BD-Pharmingen. Vinculin (1:1000) was purchased from Sigma. TDO2 (1:1000), AFMID (1:500), GCDH (1:500), CPS1 (1:1000), GNMT1 (1:1000) and NAMPT (1:1000) were purchased from Proteintech. AhR (1:1000) was from Enzo life sciences and ER (1:1000) was from Bethyl laboratories. AFP (1:500) was from R&D systems.

3. Cell culture and siRNA.

Knockdown experiments were performed using ON-TARGET plus SMART pool siRNA targeting human AhR, ER, TDO2, AFMID and URI as well as control siRNA, and were purchased from Dharmacon. HepG2, Huh-7, SNU398, SNU449 and HEK-293T Cells were grown in complete DMEM medium supplemented with 10% fetal calf serum and 100 units/ml penicillin and 0.1 mg/ml streptomycin purchased from Gibco. siRNA were transfected using Lipofectamine-RNAiMAX according to the manufacturer's instructions.

4. Immunoblotting and immunoprecipitation.

For immunoblotting, liquid N2 snap frozen liver tissues were used to prepare lysates. 50 to 100 mg of tissues were lysed using RIPA lysis buffer containing 10 mM Tris pH 7.5, 100 mM NaCl, 1 mM EDTA, 1 mM EGTA, 1 mM NaF, 20 mM $Na_4P_2O_7$, 2 mM Na_3VO_4, 0.1% SDS, 0.5% sodium deoxycholate, 1% Triton-X 100, 10% glycerol and supplemented with 10 mg/ml proteases inhibitor aprotinin and 1mM PMSF followed by homogenization using Precellys 24 Bead Mill homogenizer

(Bertin Technologies) (15 x 2 s, power set to 5500 w) and then clarified by centrifugation at 4ºC and 10.000 *g* for 10 min. Protein concentration was measured by using Bio-Rad Bradford reagent (Bio-Rad) and bovin serum albumin (BSA) as standard protein. 1mg/ml concentrated lysates were made by boiling the appropriate amount of protein lysates with 2X laemmli buffer (4% SDS, 20% glycerol, 10% 2-mercaptoethanol, 0.004% bromophenol blue in 0.2 M Tris-HCL of pH 7) at 70ºC, for 10 min. 10-30 mg of protein lysates were subjected into SDS-PAGE gels, and transferred to nitrocellulose membranes. The membranes were blocked with 5% nonfat milk in Tris-buffered saline containing 1% Tween 20 for 1h at room temperature. Blots were immune-stained with indicated antibodies. Immunoblots were processed by ECL (Amersham) according to the manufacturer's instructions. For immunoprecipitation, samples and assays were performed as described previously (45).

5. Chromatin immunoprecipitation (ChIP).

For Chomatin Immuno-precipitation, 6.10^7 SNU449 cells were cross-linked for 10 min at RT in 1% formaldehyde. Cross-linking reactions were stopped by adding 1.25 M glycine to a final concentration of 125 mM. Cells were centrifuged for 10 min at 4^0C and then washed in cold PBS. Cells were lysed with 1 mL of lysis buffer-1 (50 mM HEPES-KOH, pH 7.5, 140 mM NaCl, 1 mM EDTA, 10 % glycerol, 0.5 % NP-40, 0.25 % Triton X-100, 1 X protease inhibitor) followed by centrifugation at 4^0C and resuspension of the pellet in lysis buffer-2 (10 mM Tris-HCl, pH8.0, 200 mM NaCl, 1 mM EDTA, 0.5 mM EGTA, 1 X protease inhibitors. Finally the pellets were resuspended in 1 mL of lysis buffer-3 (10 mM Tris-HCl, pH8.0, 100 mM NaCl, 1 mM EDTA, 0.5 mM N-lauroylsarcosine, 1 X protease inhibitors), and 100 ml of 10 % Triton X-100 were added and sonicated for 20 min in a Covaris sonicator. The soluble fraction was quantified with Bradford, and 400 mg was used to immunoprecipitate the transcription factors and IgG's used as a control. Chromatin and antibody mixtures were incubated overnight at 4^0C in total volume of 500 ml. Immunoprecipitated mixture was washed with a low salt buffer (20 mM Tris-HCl, pH 8.0, 150 mM Nacl, 2 mM EDTA, 0.1 % SDS and 1 % Triton X-100), followed by high salt buffer (20 mM Tris-HCl, pH 8.0, 500 mM NaCl, 2 mM EDTA, 0.1% SDS and 1 % Triton X-100) and finally with LiCl wash buffer (10 mM Tris-HCl, pH 8.0, 250 mM LiCl, 1 mM EDTA, 1 % Na-Deoxycholate and 1 % NP-40). Samples were decross-linked by resuspending the beads in 210 ml of elution buffer (50 mM Tris-HCl, pH 8.0, 10 mM EDTA and 1 % SDS), incubating at 65^0C for 15 min and treating with 2.5 ul (from 32 mg/mL) of RNAse A for 2 hours. Next, 4 ml of (20 mg/ml of stock) of Proteinase K was added and incubated at 55^0C for 2 hrs. DNA was extracted by phenol/chloroform/isoamylalcohol mixtures, washed with 80% EtOH and resuspended in 200 ml of TE buffer. This was followed by quantitative real-time PCR. The specific primers used are listed below.P1-TDO2-F (AGGAGACTACACTACTGGGAGAAG); P1-TDO2-R-(CTTGTTTGCTAGCAGGGCGT); P4-TDO2-F(TTGTCTATGGGCAGGGTGAT); P4- TDO2-R

(GCCTGGTGCGAAAAACGAG); P5-TDO2-F (CTCCTGTAAGGACCTACCTAGC); P5-TDO2-R (ACCAAACTCCTCTGGCGTATC); P6-AFMID-F (CTAGAGGCTAGCAGCAGTGTG); P6-AFMID-R (CTTCCAGATCGCCCAGTACA); P7-AFMID-F (CAGGCACAGTTGGATCTCT); P7-AFMID-R (AGAGGACAGCCTCGGGTTAT); P8-AFMID-F (GCGGGTGTATGGTTACCTGT); P8-AFMID-R (ATGCCCGAGTGTTGTGTTGT); P9-AFMID-F (GCCTCAGTAAATGGGTTGAGAGA); P9-AFMID-R (CTGCACGCTACTTGCTTGTC); P10-AFMID-F (CACTGAGGCCAAGGCTAGAG); P10-AFMID-R (AGGAACACCATGGACGCATT); P11-AFMID-F (TAAAAGCAGCCCAATGCGGG); P11-AFMID-R (GTCGACCTCTGACCTCCACAT), Chr3-intron-F (CTTGGCCCTTCCTCTCCTAA); Chr3-intron-R (TGCAGTGGTCAGAAGATGTGT).

6. Immunohistochemistry, Immunoflouresence and histology.

Freshly harvested murine livers were fixed immediately in 10% buffered formalin solution overnight and embedded in paraffin. Sections of 3 mm were deparafinized, rehydrated and antigen retrieved by using 1M sodium citrate buffer (pH 6.5). After blocking endogenous peroxidase using 3% H2O2 (in methanol) for 5 min, sections were then blocked with 1:200 goat serum 5%BSA/PBST for 1h at RT. Furthermore, sections were incubated with primary antibodies overnight at 4ºC, after which Vectastain ABC kit (Vector Laboratories, Inc) was used, following manufacturer's instructions. Sections were then incubated with 33-diaminobenzidinetetracloride (DBA) and counterstained with hematoxylin. In the case of immunofluorescence, sections were incubated with PE-conjugated secondary antibodies (1:500) for 1h at RT, followed by DAPI staining. Quantification was performed either by counting the number of positive cells in a minimum of six 10X or 20X microscopic fields, or the percentage of positive area using Color Deconvolution plug-in in Image J.

7. Metabolic labelling.

Huh7, HepG2, SNU398 and SNU449 cells were transfected with siCtr or siAFMID, grown in 12 well plate until they reached 60% confluence. Cells were starved for 5 hours for tryptophan in tryptophan free media. 2.5 mM of [*benzene-ring-U-*^{14}C]-tryptophan was provided to the cells and incubated at 37^{0}C for 5 hours. Media was removed and the cells were washed 3 times with cold PBS. Metabolites were extracted in methanol and water (80:20) mixture, incubated for 10 mins at 4^{0}C. Metabolic lysates were centrifuged at maximum speed for 20 mins, at 4^{0}C. Radiolabelled samples were separated by thin layer chromatography (TLC) using ammonium acetate (1M, pH5) and ethanol (30:70). Cellulose F plates were used to separate the metabolites. Labelled NAD^{+}-[carbonyl-^{14}C] was used as positive control to calibrate the relative migration of labelled metabolites. After the migration was finished, TLC plates were dried and exposed to a radiosensitive PhosphorImager screen.

8. NAD^+ determination.

NAD^+ levels were determined using a commercial kit (Enzychrom, BioAssays Systems, CA), as previously described (49).

9. PARP activity assay.

PARP activity was measured from the liver lysates using TRIVIGEN colorimetric assay (4677-096-K). In brief, fresh livers were lysed in PARP buffer, and 10 mg of the protein from the supernatant was used. 96 well plate coated with histones were rehydrated and the sample mixtures were prepared using 10 ml of protein lysate, 15 ml of water and 25 ml of PARP cocktail (biotinylated NAD^+). Additionally, protein standards were also added to the wells by diluting 25 ml standards and 25 ml PARP cocktail. After washing with PBS and 0.1 % Triton X-100 followed by 2 washes of PBS, diluted strep-HRP was added and incubated for 60 min. Finally, color was developed by adding TACS-Sapphire colorimetric substrate and reading the absorbance at 450 nm.

10. Diethylnitrosamine (DEN) treatment.

14 days old mice were injected intraperitoneally with 25mg/kg of diethylnitrosamine (DEN) (Sigma) according to the previously described protocol (50). In experiments using genetic ablation of URI, consecutive to DEN injections, mice were fed with tamoxifen diet since weaning for the next 2 weeks, then changed to chow diet. Mice were sacrificed after 24 weeks of age and tumorigenesis was assessed macroscopically and quantified.

11. Ro-61-8048 treatment.

The compound was purchased from Sigma-Aldrich (SML0233), and dissolved in pure DMSO for a final concentration of 593 mM. 9 week old in house C57BL/6 mice were given DDC diet for 4 days and then shifted to chow diet. Mice were then injected with either RO-61-8048/Sunflower Seed Oil (25mg/Kg) or DMSO/Sunflower Seed Oil (1:100) intraperitoneally for 3 consecutive days.

12. Nicotinamide riboside treatment.

Nicotinamide riboside (97% purity) was purchased from Waterstonetech Pharma (Indianapolis, USA) and stored at -80^{o}C. 500 mg/kg/day of NR was dissolved in ice cold water and immediately mixed thoroughly with cold amorphous chow diet purchased from Harlan Laboratories. Pelleted NR food was stored at -20^{o}C. Mice were fed with NR diet *ad-libitum* as indicated in the experiment. Fresh food was prepared every week.

13. Genotyping and qRT-PCR.

For genotyping tail DNA was extracted by overnight incubation of tails with the following buffer (1% SDS, 0.1M NaCl, 0.1M EDTA and 0.05M Tris (pH8)). Extracted DNA was precipitated using ice-cold isopropanol which was further washed with 70% ethanol. The DNA pellet was further dried and resuspended in 400 ml of water. 1 ml of DNA was used for genotyping. For the *ColhURI* locus the following primers were used: P1-F: GCACAGCATTGCGGACATGC; P2-R: CCCTCCATGTGTGACCAAGG; P3-R: GCAGAAGCGCGGCCGTCTGG. For the *LaptTA* transactivator locus the following primers were used: P1-F: TCTGAGCATGGCCTCTAA; P2-R: GCTGGAGTAAATTTCACAGTG; P3-R: TCTCACTCGGAAGGACAT. For qRT-PCR, total RNA was extracted from 20-50 mg snap frozen liver tissue, using Trizol (Sigma). First strand cDNA synthesis was performed by using Ready-to-go first strand beads (GE Healthcare). qRT-PCR was performed using an ABI PRISM 7700 (Life Technologies), and GoTaq Real-Time qPCR mix (Promega). Fold changes have been determined by using $2^{-\Delta\Delta}$CT (51) and normalized to *b*-actin. Finally, the fold changes were obtained by converting the logarithmic scale to an exponential scale (2^DDCT). The following primers were used b-Actin-F: CACAGCTGAGAGGGAAATCG. β-Actin-R: AGTTTCATGGATGCCACAGG. Timp1-F: AGGTGGTCTCGTTGATTCGT. Timp1-R GTAAGGCCTGTAGCTGTGCC. α-SMA-F: CAATGGCTCTGGGCTCTGTA. α-SMA-R: TCATCCCCCACATAGCTGTC. Col1a-F: AGGGCCAGGGGGTCCAGCATTTC. Col1a1-R: GGTGCCCCCGGTCTTCAG. Bax-F: GTGAGCGGCTGCTTGTCT. Bax-R: GGTCCCGAAGTAGGAGAGGA. XIAP-F: GAGGCAGGAAGCTAACGTTTT. XIAP-R: GCAGCTCGTCTGAGATCAATG. PUMA-F: CTGTATCCTGCAGCCTTTGC PUMA-R: ACGGGCGACTCTAAGTGCT.

14. iTRAQ.

For protein extraction, 20 mouse livers (5 per group) were individually processed. Lysis solution (4% SDS, 10 mM DTT, 100 mM HEPES, pH=7.6) including 0.1% Benzonase Nuclease (Novagen) plus a cocktail of protease inhibitors was added to small pieces of tissue (1 mg tissue: 20 µL buffer). Samples were homogenized in a Precellys 24 Bead Mill Homogenizer (Bertin Technologies) (15 x 2 s, power set to 5500 w) and then clarified by centrifugation at 4ºC and 16000 rpm for 15 min. Recovered supernatants were cleaned-up by methanol-chloroform extraction (52) and pellets were dissolved in 7M urea 2M tiourea 0.1M TEAB by sonication and vortexing. The protein concentration of the samples was determined according to the Bradford assay using BSA as standard (Protein Assay Kit, Bio-Rad). Samples for each group were prepared by pooling an equal amount of protein from each individual.

Protein digestion and labelling with iTRAQ reagents. Samples were digested using the filter aided sample preparation (FASP) method (53) with some modifications. Briefly, 100 ug of each sample dissolved in 7M urea 2M tiourea was loaded on the filter, reduced with 10 mM DTT for 1 h at 37ºC and alkylated using 50 mM iodoacetamide for 20 min in the dark. The excess of reduction and alkylation reagents was washed. The proteins were digested overnight at RT using endoproteinase Lys-C from *Acromobacter lyticus* M497-1 (Wako Pure Chemical Industries) with 1:50 enzyme to protein ratio. Finally, trypsin (Promega) was added and samples were subjected to a second digestion for 6 h. Each tryptic digest was labeled according to the manufacturer's instructions (ABSciex) with one isobaric amine-reactive tag as follows: liver peptides from 1 week control mice were tagged with Tag114. Tag115 was used for 8 week control mice. Tag116 was used for 8 week mutant mice and Tag117 for 1 week mutant mice. After 1 h incubation, labeled samples were pooled, and evaporated to dryness in a vacuum centrifuge. The iTRAQ sample was cleaned up using a Sep-Pak C18 cartridge for SPE (Waters Corp) (54). Eluted peptides were vacuum-dried and reconstituted in OFFGEL solution (5% glycerol, 1% ampholytes pH 3-10) prior to electrofocusing.

OFFGEL fractionation. For pI-based peptide separation, we used the 3100 OFFGEL Fractionator system (Agilent Technologies) with a 24-well set-up. The IPG gel strips of 24 cm-long (GE Healthcare) with a 3–10 linear pH range were rehydrated for 15 min with the Peptide IPG Strip Rehydratation Solution according to the protocol of the manufacturer. Subsequently, 150 µL of sample was loaded in each well. Electrofocusing of the peptides was performed at 20°C and 50 µA until the 50 kVh level was reached. After focusing, the 24 peptide fractions were withdrawn and the wells rinsed with 100 µL of a solution of 0.1%TFA. Rinsing solutions were pooled with their corresponding peptide fraction. All fractions were evaporated by centrifugation under vacuum. Solid phase extraction and salt removal was performed with home–made columns based on Stage Tips with C8 Empore Disks (3M) (55) filled with Poros Oligo R3 resin (Life Technologies). Eluates were evaporated to dryness and maintained at 4°C. Just prior nano-LC, the fractions were resuspended in 0.1% formic acid (FA).

Peptide analysis by nanoLC-MS/MS. Digested samples were separated by on-line reversed-phase nanoscale capillary LC and analyzed by electrospray MS/MS. The experiments were performed on an Eksigent nano LC system (Eksigent technologies) coupled to an LTQ Orbitrap Velos mass spectrometer (Thermo Scientific) equipped with a nanoelectrospray ion source (Proxeon Biosystems). Peptides were loaded from a cooled nanoLC AS-2 autosampler (Eksigent). In order to pre-concentrate and desalt the samples before switching the pre-column in line with the separation column, 5 µL from each sample was loaded onto a reversed-phase ReproSil Pur C18-Aq 5 µm 0.3 x 10 mm trapping cartridge (SGE Analytical, Victoria, Australia), and washed for 10 min at 2.5 µL/min

with loading buffer (0.1% FA). The peptides were eluted from a RP ReproSil Pur C18-AQ 3 µm 200 x 0.075 mm (Dr. Maisch GmbH) by application of a binary gradient consisting of 2% ACN in 0.1% FA (buffer A) and 100% ACN in 0.1%FA (buffer B), with a flow rate of 300 nL/min. Peptides were separated using the following gradient: 0-5 min 2% B, 5-150 min 60% B and 150-165 min 98% B. The column was operated at a constant temperature of 30ºC. The LTQ Orbitrap Velos was operated in positive ionization mode. The MS survey scan was performed in the FT analyzer scanning a window between 250 and 1750 *m*/*z*. The resolution was set to 60 000 FWHM at *m/z* 400. The *m*/*z* values triggering MS/MS with a repeat count of 1 were put on an exclusion list for 60 s. The minimum MS signal for triggering MS/MS was set to 1000 counts. In all cases, one microscan was recorded. The lock mass option was enabled for both MS and MS/MS mode and the polydimethylcyclosiloxane ions (PDMS, protonated $(Si(CH_3)_2O))_6$; *m*/*z* 445.120025) were used for internal recalibration of the mass spectra (56). For the HCD, up to the 15 most abundant isotope patterns with charge ≥2 from the survey scan were selected with an isolation window of 2 *m*/*z* fragmented in the C-trap collision cell. Normalized collision energy was set to 42%, the Q value to 0.25 and an activation time to 0.10 ms. Waveform filter was activated. The resulting fragments were detected in the Orbitrap system with a resolution of 7500 FWHM at m/z 400. The maximum ion injection times for the survey scan and the MS/MS scans were 500 ms and 250 ms respectively and the ion target values were set to 1E6 and 5E4, respectively for each scan mode. The 24-fractions were run in duplicates.

iTRAQ Data analysis. The raw files were processed using the Proteome Discoverer 1.3.0.339 software suite (Thermo Scientific). The fragmentation spectra were searched against the UniProtKB/Swiss-Prot mouse database (released date: October 19, 2011; 16407 entries) using MASCOT (57) as the search engine (v 2.2) with the precursor and fragment mass tolerances set to 10 ppm and 0.075 Da, respectively, and with up to two missed cleavages. Lysine and peptide N-termini labeling with iTRAQ-4plex reagent as well as carbamidomethylation of cysteine were considered as fixed modifications, while oxidation of methionine was chosen as variable modification for database searching. Peptides identification was filtered at 1% false discovery rate (FDR) and thus not dependent on the peptide score. Only peptides with high confidence were considered. The results were then exported into Excel for manual data interpretation. Although relative quantification and some statistical data were provided by the Proteome Discoverer software, an additional 1.3-fold change cut-off for all iTRAQ ratios (ratio <0.77 or >1.3) was selected to classify proteins as up- or down-regulated (58-60). Proteins with iTRAQ ratios below the low range (0.77) were considered to be under-expressed, while those above the high range (1.3) were considered overexpressed. Only proteins identified with 2 or more unique peptides and at least 3

iTRAQ peptide counts were considered. Gene Ontology analyses of the identified proteins were performed.

15. RNA extraction and sequencing.

For RNA extraction, 20 livers (5 per group) were individually extracted. RNA Integrity Numbers were 8.3 on average (range 7.5 to 9.2) when assayed by Lab-chip technology on a 2100 Bioanalyzer (Agilent). Sequencing libraries were prepared as in "TruSeq RNA Sample Preparation Guide" (Part # 15008136 Rev. A) with final PCR amplification limited to 10 cycles. The resulting purified cDNA libraries were sequenced on a Genome Analyzer IIx, following manufacturer's protocols. Samples were analyzed in different paired end sequencing runs. In order to balance read length and adjust base calling quality within conditions, reads from 8-week samples were trimmed to 50 bases. Likewise, reads from 1-week samples were adjusted to 78 bases. Reads were aligned to the mouse genome (NCBI37/mm9) with Tophat (61) version 1.3.1 (including Bowtie 0.12.7 (62) and Samtools version 0.1.16 (63)) allowing a maximum of 2 mismatches and 5 multihits for each read. The RNA fragment length was 230bp on average. Transcripts were assembled and their abundances estimated with Cufflinks version 1.0.3 (64). After that, we performed a differential expression analysis with Cuffdiff 1.0.3.

16. Statistical analysis

Statistical analyses were performed using GraphPad Prism V5.0 software. Statistical significance (p) ($p < 0.05$ = *, $p < 0.001$= **, $p<0.0001$= ***) between the means of a minimum of three groups was determined using unpaired two-tailed Student's t test. Results are expressed as the mean value +/- Standard Deviations (SD). All results are representative of at least three independent experiments. Kaplan Meier curve for the survival analysis of mice was calculated using 17 control and 17 mutant mice. Statistical parameter false discovery rate (FDR) estimates the probability of a gene set with false positive finding. Normalized enrichment score (NES) allows to compare enrichment analysis results across gene sets.

Results

1 Generation and characterisation of mice ectopically expressing URI in Hepatocytes

1.1 Generation of hURI-tetOFF^{hep} mice – Mice expressing ectopic URI in switchable manner

To elucidate primary events in HCC development, we generated a *Col1a1* knock-in mouse by flippase-mediated targeting and recombination of inducible human *URI* (hURI) cDNA tagged with the FLAG peptide in the 3' untranslated region of the homing locus of the collagen type I, alpha 1 locus (*Col1a1)* in KH2 embryonic stem cells (ESCs), having a tetracycline operator (Tet-op) (47) (Fig. 9a). Proper integration of the Flag-hURI cassette was verified by southern blot analysis, using a 3' probe as described in (Fig. 9a). As shown in the southern blot using both wildtype and mutant tail DNA, a band of 4.1 kb specific for the proper integration was apparent in addition to the 6.7 kb band for the wildtype allele (Fig. 9b).

In order to express hURI specifically in hepatocytes, ColhURI mouse has been crossed with a line containing the tetracycline-dependent transactivator (tTA) under the control of the liver activated protein (LAP) promoter to generate LAP-tTA/hURI*tetOFF* mouse (48) (Fig. 9c). These mice (designated hURI-tetOFF^{hep}) and littermates lacking both alleles and thus hURI expression are referred as "mutants" and "controls", respectively.

These mice were never on doxycycline (otherwise stated) thus hURI was expressed specifically in hepatocytes from one allele from E10.5 (65). Ectopic hURI expression analysis was perfomed using qRT-PCR (Fig. 9d), western blot (WB) (Fig. 9e) and Immunohistochemistry (IHC) hURI and FLAG antibodies (Fig. 9f) using 1-week old livers. hURI expression was roughly twice as strongly as mouse URI, determined using an antibody detect both the endogenous and ectopic hURI (Fig. 9g and 9h), corresponding to the fold-increase of URI expression in human HCC (shown later in the study. hURI-tetOFF^{hep} mice have been backcrossed to C57BL/6 mice for at least 7 generations. All mice were housed in specific pathogen-free (SPF) animal facility Unit of CNIO. All experiments were approved by the CNIO-ISCIII Ethics Committee for Research and Animal Welfare (CEIyBA) and performed in accordance with the guidelines for ethical conduct in the care and use of animals as stated in the international guiding principles for biomedical research involving animals, developed by the Council for International Organizations of Medical Sciences (CIOMS).

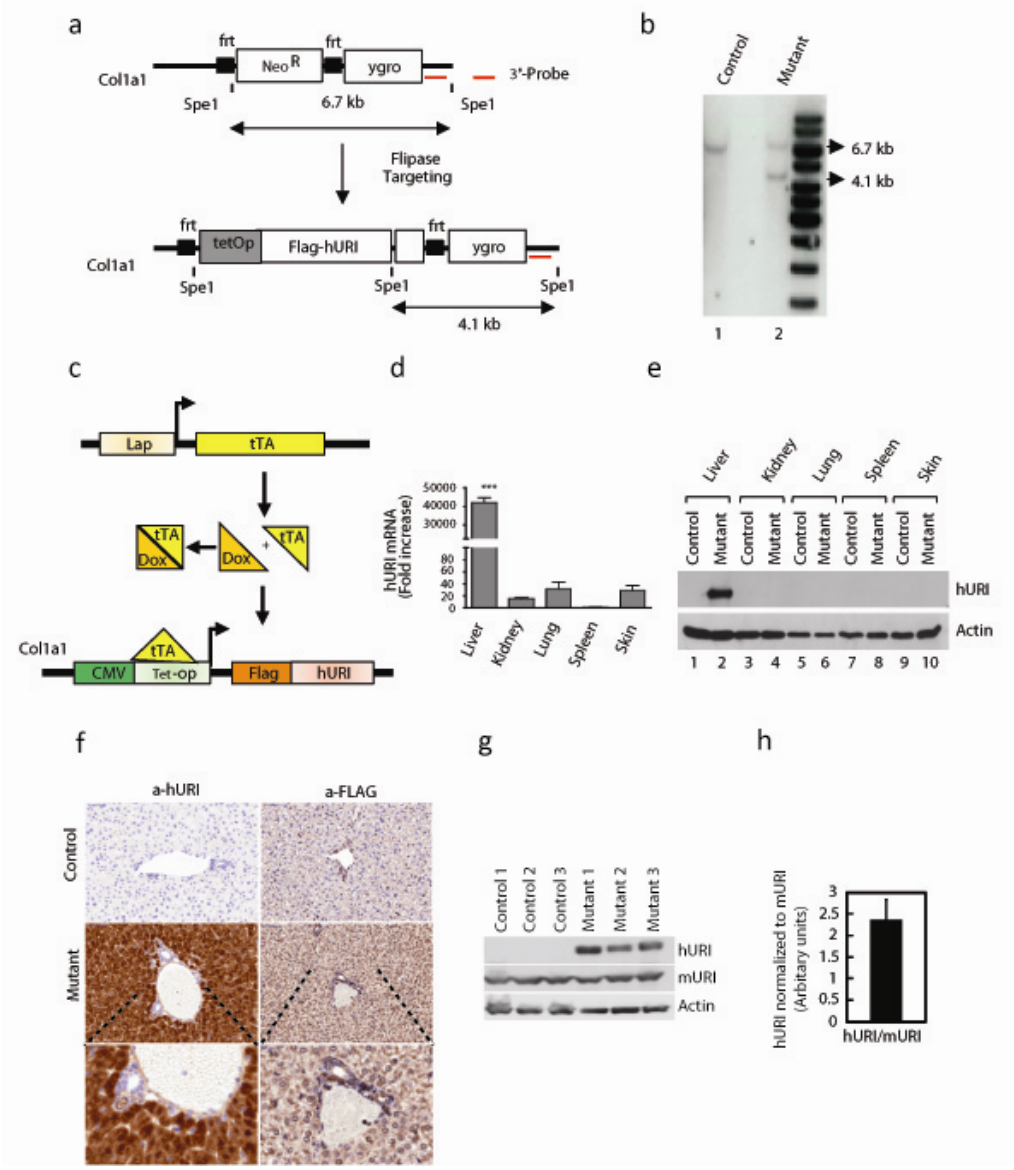

Figure 9 Generation and characterisation of hURI-tetOFF^{hep} mouse model. (a) Schematic representation of knock-in strategy of hURI in the *Col1a1* locus. Red line depicts 3' probe used. **(b)** Southern blot analysis using 3' probe showing correct targetting of hURI in the Col1a1 locus. **(c)** Schematic representation of the model hURI-tetOFF^{hep} mouse in which URI expression is under the control of the hepatocyte-specific LAP promoter. **(d)** Quantification of hURI mRNA expression in different organs derived from hURI- tetOFFhep mice. Denote hepatic specificity of the model. (***, $\rho \leq 0.001$). ($n \geq 5$). **(e)** WB analysis of hURI expression in different organs derived from hURI-tetOFFhep mice. **(f)** Representative pictures of IHC stained liver sections from control and mutant hURI-tetOFF^{hep} mice using hURI and FLAG antibodies. Insets represent the periportal area, showing hepatocyte specific hURI expression. n > 10. **(g)** WB analysis of control (controls 1 to 3) and mutant (mutants 1 to 3) hURI-tetOFF^{hep} mice. **(h)** Quantification of (g)**.** Scale bars represent 100 μm.

1.2 Mice expressing URI in hepatocytes induces spontaneous HCC development

We observed no pathological signs in 3-week-old mutants. In 8-week-old mutants we observed no tumours visually, but H&E staining revealed anisokaryotic clusters (Fig. 10a) resembling low-grade dysplastic nodules observed in human hepatitis (66,67). At 12 weeks the clusters developed into high-grade dysplastic nodules (Fig. 10a-c), reminiscent of human large liver cell dysplasia (66,67). Increasing signs of fibrosis (increases in Sirius Red staining and fibrotic markers detected by qRT-PCR) were observed in mutants' livers from 8 weeks (Fig. 10d-f).

Between 24-54 weeks macroscopic lesions including adenoma and early HCC emerged, between 54-65 weeks low-grade and differentiated HCC were fully apparent, and between 65-75 weeks 60% of mutants developed macroscopic high-grade tumours occupying 20-50% of their livers (Fig. 10a, g and h). The proliferation rate indicated that 25-50% of hepatocytes were Ki67-positive, suggesting aggressive tumours. According to World Health Organization criteria (WHO, 2008), all tumours were well/moderately differentiated: 20% glandular/acinar, indicative of telangiectatic variants, and 80% trabecular. No cholangiocarcinoma were detected (Fig. 10g).

Serum glucose, alanine aminotransferase, total bile acids and albumin levels indicated that the mutant livers were functionally damaged (Fig. 11a). All mutants died at around 85 weeks, before complete liver failure, when control mice were still apparently healthy (Fig. 11b). Immunohistochemistry (IHC) and pathological analysis also revealed hURI-positive cells in mutant lungs, morphologically resembling hepatocytes, indicative of aggressive micro-metastases in 30% of mutants with HCC (Fig. 11c and d). Histopathological characterization confirmed the presence of tumours, of various types and grade, with collapsed reticulin fibres suggesting increases in hepatocyte death and compensatory proliferation, as indicated by Ki67 (Fig. 11e). Increases in alpha fetoprotein levels, a clinical marker for human HCC, varied but all tumours displayed dramatic increases in p53 phosphorylation and abundance (Fig. 11f). Fully developed HCC appeared at 30 weeks in hURI-tetOFF^{hep} mice treated with the hepatocarcinogen diethylnitrosamine (DEN) (50) (Fig. 11g-j).

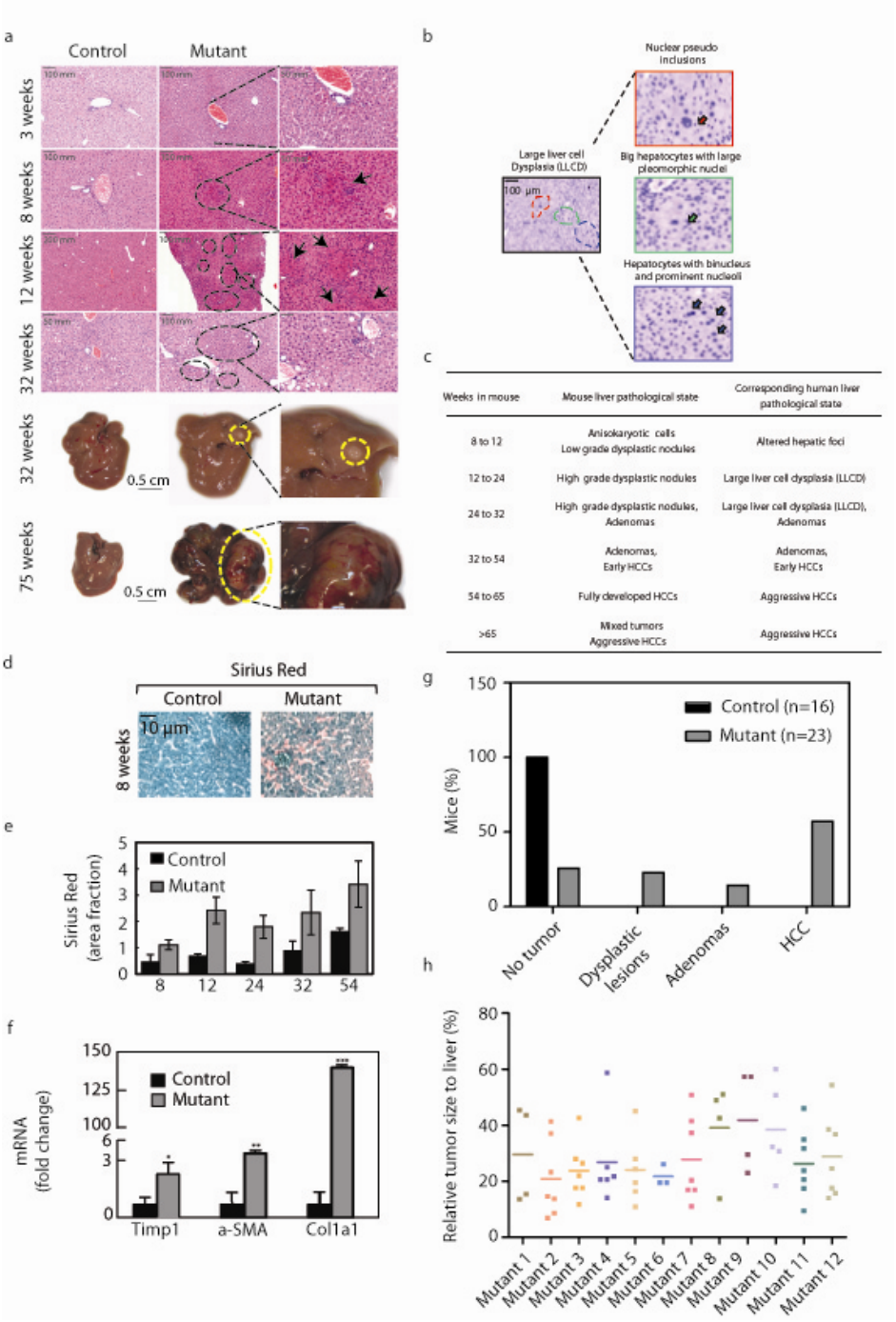

Figure 10 Characterisation of dysplastic lesions and liver damage in hURI-tetOFF^{hep} mouse model. (a) Representative pictures of H&E stained liver sections from 3 weeks (n > 6), 8 weeks (n > 19), 12 weeks (n > 11) and for 32 weeks (n > 7) control and mutant hURI-tetOFF^{hep} mice. Bottom pictures are representative images of whole livers from control and mutant hURI-tetOFF^{hep} mice at 32 and 75 weeks of age. Black dotted circles mark anisokaryotic clusters and LLCD-like lesions in mutant hURI-tetOFF^{hep} mice. Yellow dotted circles depict adenoma and HCC at 32 and 75 weeks of age, respectively. **(b)** Hematoxylin stained liver sections in 12-week-old mutant hURI-tetOFFhep mice. Image displays all characteristics of human Large Liver Cell Dysplasia (LLCD) like lesions. Insets show nuclear pseudo inclusions, large pleomorphic nuclei and hepatocytes with binucleus and prominent nucleoli. (n ≥ 5). **(c)** Table showing disease progression with age in mutant hURI-tetOFFhep mice, and the corresponding human pathological state. **(d)** Representative pictures of Sirius Red staining in 8-week liver section. **(e)** Quantification of Sirius Red positive area in 8, 12, 24, 32 and 54 week control and

mutant hURI-tetOFFhep mice. (*, ρ ≤ 0.05). (n ≥ 5). **(f)** qRT-PCR analysis of alpha smooth muscle actin (α-*SMA),* collagen, type1, alpha 1 (*col1a1)* and tissue inhibitor of metalloproteinase 1 *(Timp1)* transcripts expressed in livers of control and mutant mice at 8 weeks of age. β-Actin was used as housekeeping gene. (*, ρ ≤ 0.05; **, ρ ≤ 0.01). (n ≥ 5). **(g)** Percentage of control (n = 16) and mutant (n = 23) hURI-tetOFF^{hep} mice bearing liver abnormalities in 65 to 75 week old mice. **(h)** Tumor burden defined as tumor size relative to the total liver size and total number of tumors per liver in hURI-tetOFFhep mutant mice. (n = 12).

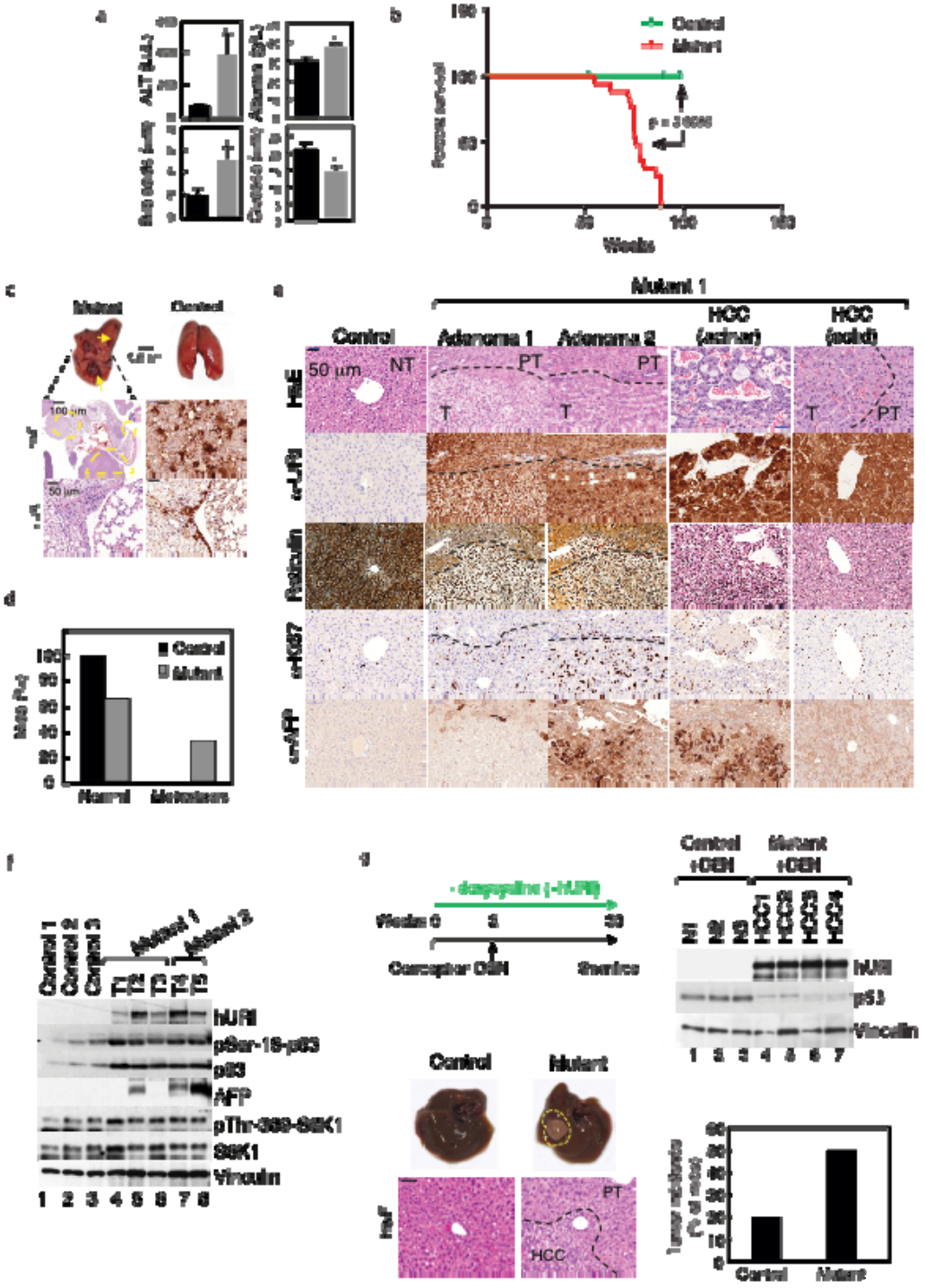

Figure 11 Characterisation of tumors induced with URI and DEN in hURI-tetOFF^{hep} mouse model. (a) Quantification of ALT, albumin, bile acids and glucose in serum from control and mutant hURI-tetOFFhep mice. (*, $\rho \leq 0.05$). ($n \geq 5$). **(b)** Kaplan Meier curve of control (n = 17) and mutant (n = 17) hURI-tetOFF^{hep} mice. $p < 0.0001$. **(c)** Representative pictures of lungs from control and mutant hURI-tetOFFhep mice at 75 weeks of age. Yellow arrows depict lung metastasis. Insets show H&E images with macro metastatic nodules in mutant lungs (dotted yellow circles). Lower images represent immunohostochemistry (IHC) for hURI in lung tissues. Hepatocyte-like cells are positively stained for hURI. **(d)** Histogram depicts percentage of mice presenting lung metastasis in control and mutant hURI-tetOFFhep mice. ($n \geq 5$). **(e)** Representative pictures of H&E and reticulin stained liver sections from control and 4 tumors derived from 1 mutant hURI-tetOFF^{hep}. IHC was performed using the indicated antibodies. n = 5. **(f)** WB analysis of control (controls 1 to 3) and mutant (mutants 1 and 2) hURI-tetOFF^{hep} mice. **(g)** Schematic representation of DEN treatment in control and mutant hURI-tetOFFhep mice. Right panel depicts WB analysis in control and mutant hURI-tetOFFhep mice treated with the carcinogen DEN. Bottom left panel represents pictures of full livers and H&E stained sections from control and mutant hURI-tetOFFhep mice treated with the carcinogen DEN. Dotted yellow circle denotes liver tumor. Dotted black line in the mutant H&E picture denotes border between HCC and peritumoral (PT) tissue. Bottom right panel represents histogram of tumor incidence observed in control and mutant hURI-tetOFFhep mice treated with DEN. ($n \geq 5$). Scale bars represent 20, 50, 100, 200 mm and 0.5 cm, as indicated.

When hURI was expressed from two alleles, increasing its expression to 6-fold compare to levels in heterozygous hURI-tetOFF^{hep} mice, HCC were consistently detected at 10 weeks (Fig. 12a-d), highlighting the importance of URI dosage. Embryonic development was not involved in HCC formation by hURI expression, because liver tumours (with similar incidence and features to those induced by hURI expression from E10.5) were detected in mice kept with doxycycline until 8 weeks then transferred to normal chow (Fig. 12e-h). Thus, hURI expression in mouse hepatocytes resembles many stages of human HCC development.

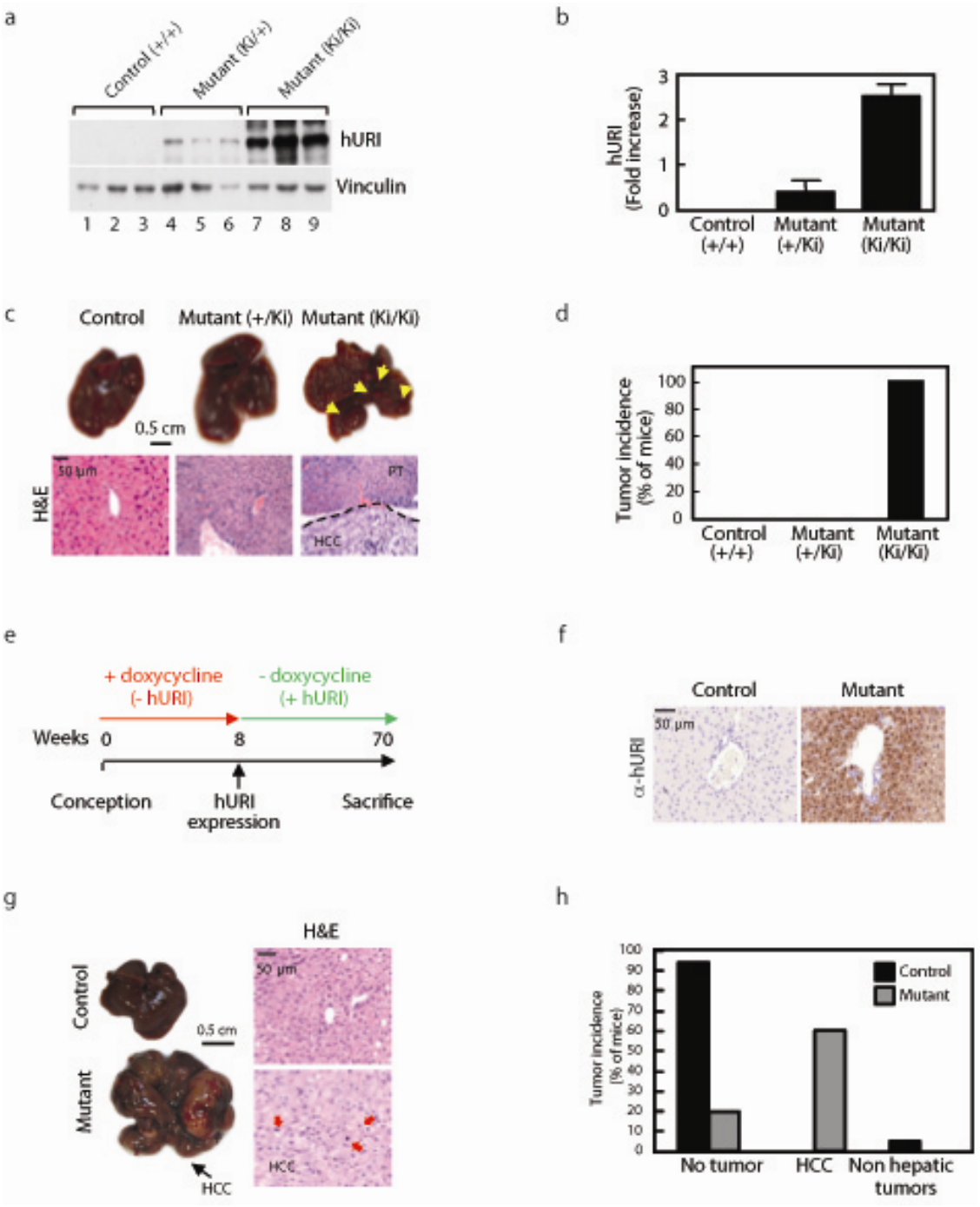

Figure 12 Hepatocarcinogenesis induced by URI expression is dependent on the dosage but not on the time of its expression. (a) WB analysis for hURI in livers derived from control and mutant hURI-tetOFF^{hep} mice. Denote increasing protein levels of hURI in the homozygous mice (Ki/Ki) compared to the heterozygous mice (Ki/+). **(b)** Right histogram represents quantification of hURI protein abundance. **(c)** Bottom left panel represents pictures of full livers and H&E stained sections from control and mutant hURI-tetOFFhep mice at 10 weeks of age. Denote that in (Ki/Ki) hURI-tetOFFhep mutant mice, HCC is already apparent at this early time point (10 weeks). Dotted black line in the mutant H&E picture denotes border between HCC and peritumoral (PT) tissue. **(d)** Bottom right histograms depict tumor incidence in control and mutant hURI-tetOFFhep mice of 10 weeks of age. (n ≥ 5). **(e)** Schematic representation of the doxycycline treatment used in control and mutant hURI- tetOFFhep mice as to take advantage of the switch-ability system. Mice were

kept in doxycycline containing diet until 8 weeks of age (+ doxycycline/ -hURI). From 8 weeks on, mice were fed chow diet for hURI expression in adult stage (- doxycycline/ +hURI), and sacrificed for analysis from 70 weeks of age. **(f)** IHC staining of hURI in the liver of 9-week-old control and mutant hURI-tetOFFhep mice. Denote that one week after doxycycline removal, hURI expression is already apparent and confined to hepatocytes. ($n \geq 5$). **(g)** Left panel represents pictures of full livers and H&E stained liver sections from control and mutant hURI-tetOFFhep mice. Red arrows in mutant H&E picture denote tumoral areas. **(h)** Bottom right histogram represents tumor incidence of mice described in (e).

1.3 URI is oncogenic and essential for hepatocarcinogenesis

Ceasing hURI expression in 8-week-old mutants displaying dysplastic lesions for 24 weeks did not affect liver-to-body weight ratios, but reduced signs of fibrosis (Sirius Red staining and a-SMA abundance) and abolished signs of dysplastic foci and tumours (Fig. 13a-e). S6K1 activity was increased in 24-week-old mice, but remained constant when hURI was switched off, indicating that mTOR/S6K1 activation was hURI-independent (Fig. 13b). Similarly, when hURI was expressed for 24 weeks, during which macroscopic high-grade dysplastic nodules and adenomas were apparent (see Fig. 9i), then switched off for 28 weeks some residual anisokaryotic clusters were still detected, but no adenomas or HCCs (Fig. 13f). Thus, maintenance of preneoplastic lesions and tumour development requires continuous hURI expression.

Next, we induced liver damage (which can initiate HCC) in URI loss-of-function GEMMs. Homozygous (lox/lox) and heterozygous (+/lox) mice carrying the URI lox allele were viable, fertile, and exhibited no overt abnormalities. Crossing URI (+/lox) heterozygous mice with a Mox-Cre line, to deplete URI ubiquitously, generated viable URI (+/Δ) mice (Δ/Δ homozygotes obtained from intercrosses were non-viable). To delete URI specifically in hepatocytes, we crossed URI (lox/lox) and serum albumin (SA)-CreERT2 (68) mice, obtaining pups in expected Mendelian ratios. URI deletion in hepatocytes after tamoxifen treatment to obtain $URI^{(\Delta/\Delta)hep}$, $URI^{(\Delta/\Delta)hep}$ or $URI^{(\Delta/\Delta)hep}$ mice was confirmed by IHC and (Western blot) WB (Fig. 13g and h).

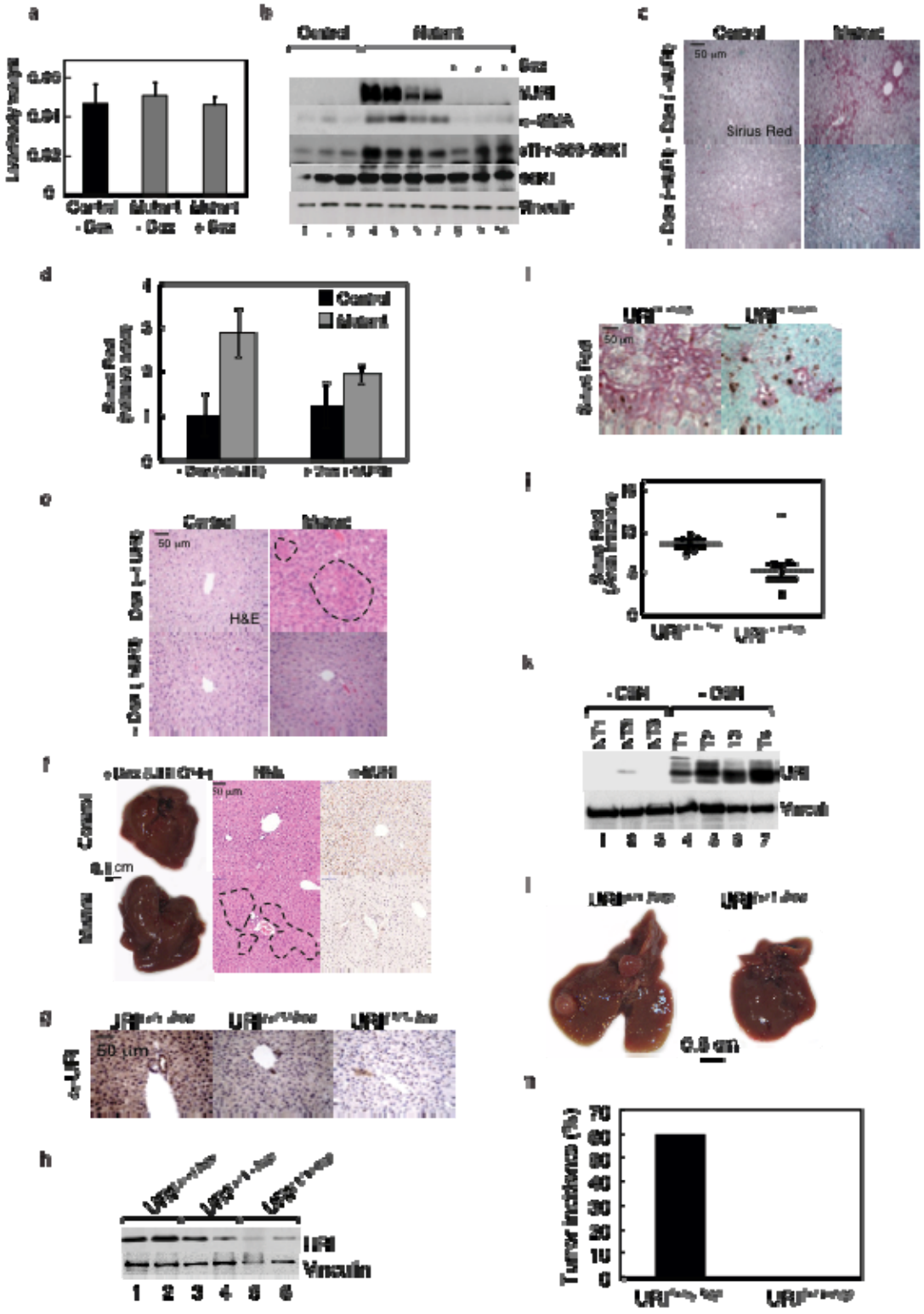

Figure 13 Liver tumorigenesis depend on URI expression (a) Liver to body weight ratio of control and mutant hURI-tetOFFhep mice treated with doxycycline for 24 weeks. Treatment started at 8 weeks of age, after the appearance of anisokaryotic hepatocytes. (n ≥ 5). **(b)** WB analysis from 32-week old control and mutant hURI-tetOFF^{hep} mice fed with either chow or doxycycline (Dox) containing-diet. (n ≥ 5). **(c)** Representative pictures

of Sirius Red stained liver sections from hURI-tetOFF^{hep} mice described in (b). Switching off hURI expression with Dox recues the formation of fibrotic areas. (n ≥ 5). **(d)** Quantification of (C). (*, ρ ≤ 0.05). **(e)** Representative pictures of H&E stained liver sections described in (a). **(f)** Representative pictures of full livers and H&E stained liver sections from hURI-tetOFF^{hep} mice treated with Dox for 28 weeks. Treatment started at 24 weeks of age, after the appearance of dysplastic lesions, adenomas and early HCC. Dotted black circles denote reminiscent anisokaryotic areas. (n ≥ 5). **(g)** Representative pictures of IHC for endogenous URI stained liver sections from URI$^{(+/+)hep}$ and URI$^{(+/\Delta)hep}$ mice. (n ≥ 5). **(h)** WB liver analysis for endogenous URI in URI$^{(+/+)hep}$, URI$^{(+/\Delta)hep}$ and URI$^{(\Delta/\Delta)hep}$ livers, confirming reduction of URI expression in URI$^{(+/\Delta)hep}$ and URI$^{(\Delta/\Delta)hep}$ mice. Denote reminiscent URI signal is due to inflammatory cell infiltration. **(i)** Representative pictures of Sirius Red and Reticulin stained liver sections from URI$^{(+/+)hep}$ and URI$^{(+/\Delta)hep}$ mice treated with DDC for 1 month. (n ≥ 5). **(j)** Quantification of fibrotic area. Denote decreased fibrotic area with reduction of URI protein levels. (**, ρ ≤ 0.01). (n ≥ 5). **(k)** WB analysis for URI in liver tumors from C57Bl/6 mice treated with the carcinogen DEN. Denote increased URI expression specifically in the tumors of DEN-treated mice but not in normal tissue (NT). (n = 3 without DEN and n = 4 with DEN). **(l)** Representative images of whole livers from URI$^{(+/+)hep}$ and URI$^{(+/\Delta)hep}$ mice treated with the carcinogen diethylnitrosamine (DEN)-induced HCC and sacrificed at 24 weeks of age. **(m)** Tumor burden of mice described in (i).

Because homozygous deletion in URI$^{(\Delta/\Delta)hep}$ mice led to organ failure and death after 10 days, URI$^{(+/+)hep}$ and heterozygous URI$^{(+/D)hep}$ mice, in which URI expression was approximately halved (Fig. 13g and h), were supplied a liver damage-inducing 3,5-diethoxycarbonyl-1,4-dihydrocollidine (DDC)-supplemented diet. URI$^{(+/\Delta)hep}$ mice presented significantly less liver damage and fibrosis than URI$^{(+/+)hep}$ mice (Fig. 13i and j), suggesting that URI reduction inhibits progression to HCC. Similarly, DEN-treatment increased URI in HCC derived from C57BL/6 mice (Fig. 13K) and induced early (24 weeks) tumour development in 60% of URI$^{(+/+)hep}$ mice, but no HCC in heterozygous URI$^{(+/D)hep}$ mice (Fig. 13l and m), indicating that HCC development requires URI.

1.4 URI expression induces DNA damage prior to premalignant lesions

Phosphorylation of histone H2AX (γH2AX), a DNA damage marker, and p53 phosphorylation and abundance, did not differ between 1-week-old mutant and control livers (Fig. 14a). At 3 weeks, a non-pathological stage with no dysplastic lesions, both γH2AX-positive nuclei abundance and phosphorylation of the 32 kDa subunit of replication protein A at Ser-4 and Ser-8 were substantially higher in mutants (Fig. 14b, 14c and 14d), indicating replicative stress and a DDR manifested by increases in p53 abundance and phosphorylation (Fig. 14d). Thus, hURI expression induces replication stress-dependent DDR before precancerous lesion formation and then p53-dependent apoptosis occurs in cells that unsuccessfully repair DNA (detected by cleaved caspase 3; Fig. 14d).

At this stage the hepatocyte proliferation rate was reduced in mutants (Fig. 14e and 14f) so DNA damage is not due to high oncogene-induced proliferation andcompensatory proliferation of neighbouring cells, which maintains tissue homeostasis and promotes HCC development (69), may not be an initiating tumorigenic event and not an immediate consequence of apoptosis.

γH2AX-positive nuclei were also more abundant in older mutant livers (8- and 12-weeks-old) with obvious dysplastic lesions. Furthermore, Ser-345 phosphorylation (and hence activation) of Chk1 was enhanced in mutants, but not Thr-68 phosphorylation of Chk2, confirming presence of SSB(70) (Fig. 14g-14i). We also detected accumulation of the Chk1 target p53 in 8-week-old mutants and several p53-stabilising changes: increased p53 phosphorylation at Ser-18 and acetylation at Ac-lys379 (Fig. 14i), and enhanced expression of p19ARF (Fig. 14j).

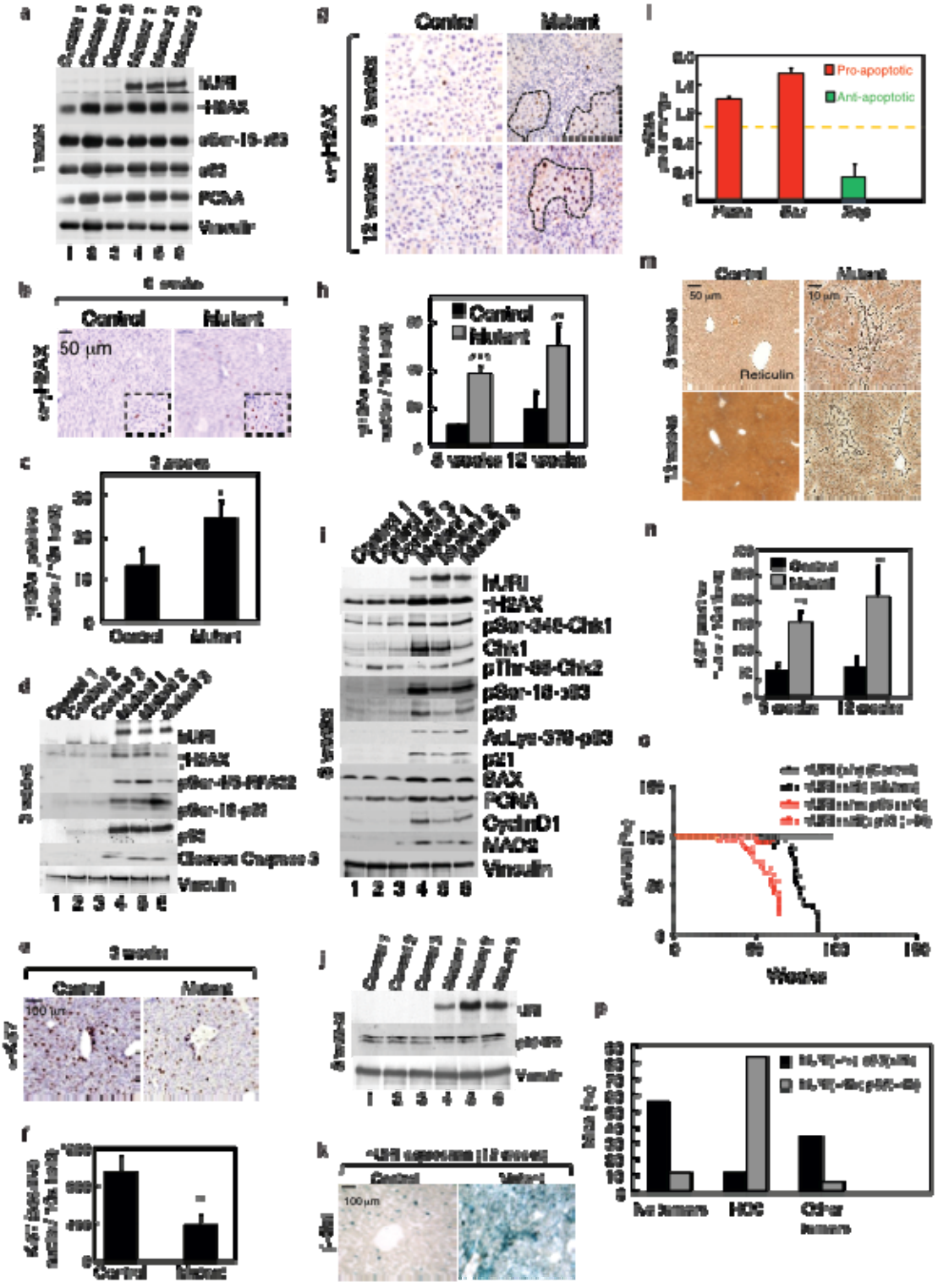

Figure 14 URI induces DNA damage (a) WB liver analysis of 1 week control and mutant hURI-tetOFFhep mice. Denote no differences in the phosphorylation levels of γH2AX or of p53 in the mutant hURI-tetOFFhep. **(b)** Representative pictures of γH2AX IHC stained liver sections from 3 week control and mutant hURI-tetOFF^{hep} mice. Insets denote γH2AX positive nuclei. n = 5. **(c)** Quantification of (b). (*, ρ ≤ 0.05). **(d)** WB analysis of 3

week hURI-tetOFF^{hep} livers. **(e)** Representative pictures of Ki67 stained liver sections of 3-week-old control and mutant hURI-tetOFFhep mice. (n ≥ 5). **(f)** Quantification of (e). **(g)** Representative pictures of γH2AX IHC stained liver sections from 8 week and 12 week control and mutant hURI-tetOFF^{hep} mice. Dotted black shapes depict anisokaryotic clusters positive for γH2AX. n = 6. **(h)** Quantification of (g). **(i)** WB analysis of 8 week control and mutant hURI-tetOFF^{hep} mice. **(j)** WB liver analysis of control and mutant hURI-tetOFFhep mice depicting increased levels of p19ARF in the mutant mice. **(k)** Representative picture of β-gal stained liver sections in 12 week control and mutant hURI-tetOFFhep mice. Denote increased β -gal staining (senescence) in the mutant mice. (n ≥ 5). **(l)** qRT-PCR analysis of pro-apoptotic p53 upregulated modulator of apoptosis (*Puma)* and Bcl-2-associated X protein *(Bax)* and anti-apoptotic X-linked inhibitor of apoptosis protein (*Xiap)* transcripts expressed in livers from 8 week control and mutant hURI-tetOFFhep mice. β-Actin was used as housekeeping gene. (n ≥ 5). **(m)** Representative pictures of reticulin stained liver sections in 8 and 12 week control and mutant hURI-tetOFFhep mice. Denote presence of collapsed reticulin fibers in the mutant hURI-tetOFFhep mice. (n ≥ 5). **(n)** Quantification of Ki67 positive nuclei in the liver, detected by IHC in 8 and 12 week control and mutant hURI-tetOFFhep mice. (**, ρ ≤ 0.01; ***, ρ ≤ 0.001). (n ≥ 5). **(o)** Kaplan-Meier survival curve of control (full line) and mutant (dotted line) hURI-tetOFF^{hep} mice with (red) and without (black) p53 inactivation. Denote that p53 inactivation decreases overall survival in mutant hURI-tetOFF^{hep} mice (dotted red line). (***, ρ ≤ 0.001). **(p)** Tumor incidence of control and mutant mice with and with out p53 inactivation.

Senescence-associated β-galactosidase activity, expression of several p53 target genes (*p21* and the pro-apoptotic genes Bcl-2–associated X protein *Bax* and *p53*-upregulated modulator of apoptosis *Puma*) and protein abundance of BAX were also higher in 8- and 12-week-old mutants than in controls, while expression of X-linked inhibitor of apoptosis was decreased (Fig. 14i, 14k and 14l). Accordingly, increases in hepatocyte death, manifested by collapsed reticulin fibres was detected followed byactivation of compensatory proliferation mechanisms, demonstrated by increased abundance of proliferating cell nuclear antigen (PCNA), cyclin D1 and Ki67-positive nuclei; and abundance of mitotic arrest deficient 2 (MAD2), a CIN marker and downstream effector of cyclin D1 (71) (Fig.14i, 14m and 14n), suggesting that hURI expression impaired genome integrity

We next tested whether p53 inactivation in the URI mouse model accelerates tumorigenesis, by crossing hURI-tetOFF^{hep} mice with p53ER^{TAM} mice, in which p53 activation requires ectopic 4-hydroxytamoxifen provision (72). Inactivation of p53 in hURI-tetOFF^{hep} mice significantly reduced survival and accelerated liver tumorigenesis (Fig. 14o). 80% of the mice displayed aggressive HCC (Fig. 14p), but deletion of *p19ARF* did not modify their survival or tumour burden (data not shown).

1.5 URI inhibits *de novo* NAD$^+$ synthesis to cause DNA damage

To identify initial hepatocarcinogenetic events, we first examined mTOR activation. We detected no increases in S6K1 activity at 1-week (Fig. 15a). In sequential immunoprecipitation experiments, using 1-week-old liver extracts, free hURI molecules were detected by WB after complete depletion of PP1γ (Fig. 15b and 15c), and vice versa (not shown). Furthermore, when 3-week-old mice were supplied a rapamycin-containing diet, progression to preneoplastic abnormalities continued (not

shown). Thus, although a fraction of hURI binds PP1γ, hURI apparently has a PP1γ-independent role in early hepatocarcinogenesis and precancerous lesion formation

We next assessed unbiased global transcriptomic and proteomic profiles during a very early non-pathological stage with no signs of DNA damage or dysplastic foci and an early premalignant lesion stage, using 1 and 8-week-old livers, respectively. Transcript sequencing revealed that small fractions of genes were differentially expressed upon hURI expression: 303 out of 12,295 genes at 1 week and 740 out of 11,133 (FDR<0.05) at 8 weeks (Fig. 15d and 15e). Similarly, isobaric Tags for Relative and Absolute Quantification (iTRAQ) identified 2394 proteins: 122 and 597 of which were differentially expressed in 1- and 8-week livers, respectively (Fig. 15f to 15i). There were also significant overlaps in the differentially expressed transcripts and proteins at 1 and 8 weeks (Fig. 15j and 15k), suggesting hURI's role as a transcriptional repressor. Heatmapping revealed that most differentially expressed proteins were downregulated, indicating hURI-dependent repression (Fig. 15l).

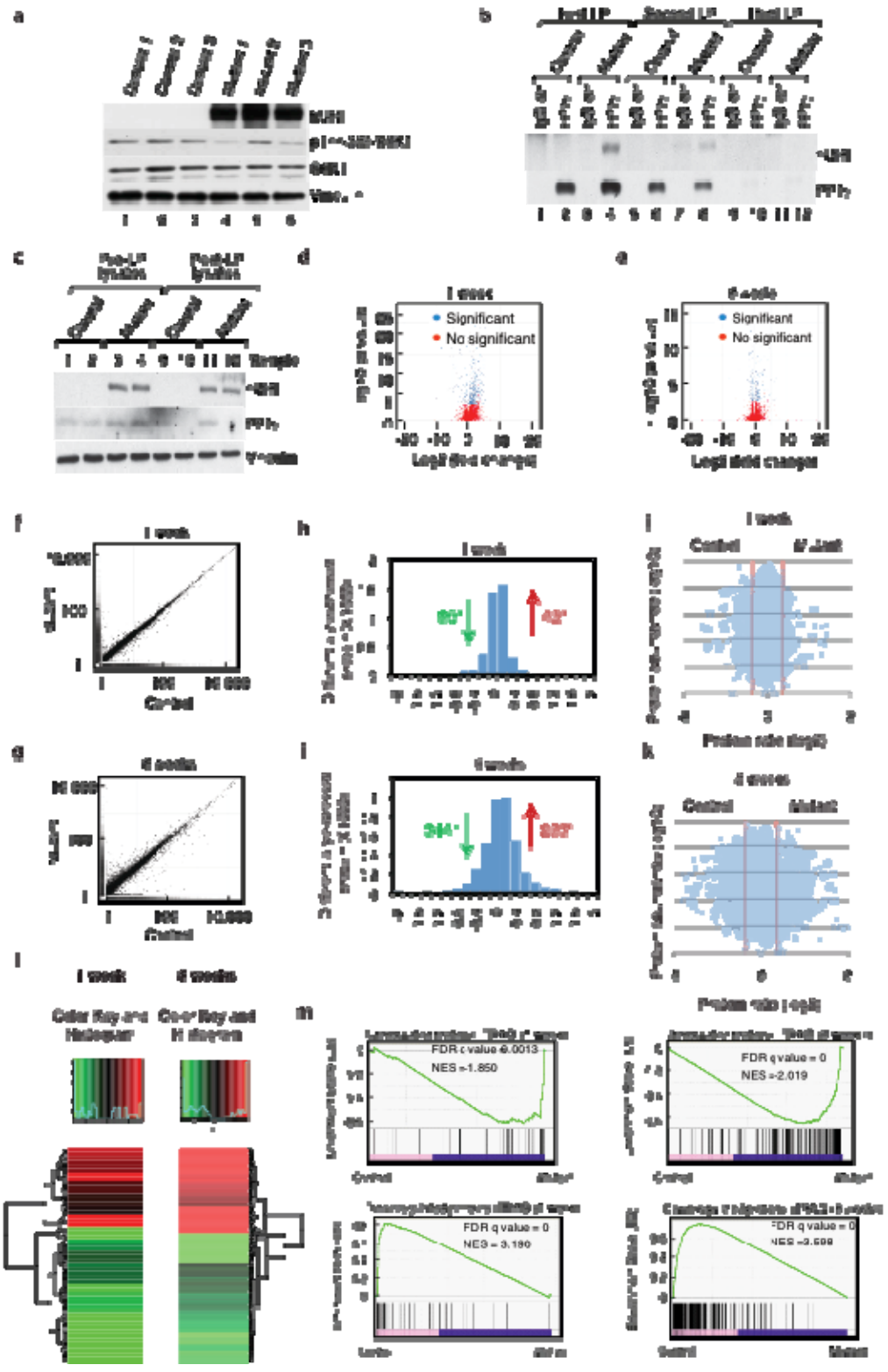

Figure 15 Mechanisms of URI induced DNA damage (a) WB analysis of livers derived from 1-week-old control and mutant hURI-tetOFF^{hep} mice. Denote
that hURI expression is unrelated to the S6K1 activation status. **(b)** Sequential immunoprecipitation (I.P) of

PP1γ in livers from 1 week control and mutant hURI-tetOFFhep mice. **(c)** WB analysis of inputs before the first I.P and output after the last I.P performed in (Y). Denote the presence of hURI after complete depletion of PP1γ (samples 11, 12). **(d and e)** Volcano plots from RNA sequencing representing significant differentially expressed (blue) and unchanged (red) mRNA species in livers from 1 (A) and 8 (B) week old hURI-tetOFFhep mice. n > 3. **(f and g)** Scatter plots representing liver transcripts from RNA sequencing from 1 (f) and 8 week (g) control and mutant hURI-tetOFFhep mice. **(h and i)** Dot plots of differentially expressed liver proteins found in iTRAQ of 1 (h) and 8 (i) week control and mutant hURI-tetOFFhep mice. **(j)** Heatmaps of downregulated (green) and upregulated (red) liver proteins found in iTRAQ of 1 and 8 week control and mutant hURI-tetOFFhep mice. **(k)** GSEA between upregulated and downregulated proteins found in iTRAQ and upregulated transcripts found in RNA sequencing in livers from 1 and 8 week control and mutant hURI-tetOFFhep mice.

Ingenuity Pathway Analysis (IPA) showed that enzymes implicated in the L-tryptophan/kynurenine pathway leading to *de novo* NAD^+ synthesis such as tryptophan 2,3-dioxygenase (TDO2) and arylformamidase (AFMID) catalyzing the initial rate-limiting step of tryptophan degradation, kynurenine 3-monooxygenase (KMO), kynureninase (KNYU) and 3-hydroxyanthranilate 3,4-dioxygenase (HAAO) were strikingly downregulated in 1- and 8-week-old mutant livers (Fig. 16a and 16b). Gene Set Enrichment Analysis (GSEA) (73) using the RNA sequencing data and Kyoto Encyclopedia of Genes and Genomes database corroborated these defects (not shown). WB confirmed that TDO2 and AFMID expression was reduced >50% in 1-week, 8-week-old mutant livers as well as mice expressing hURI from adult stage (8weeks) for 12 weeks confirming an effect independent of embryonic liver development (Fig. 16c-16f). Moreover, NAD^+ concentrations were reduced in 3- and 6-week mutant livers, compared to controls (Fig. 16g and 16h). Furthermore, small interference RNA (siRNA) knockdown of TDO2 and AFMID in HCC cell lines significantly reduced NAD^+ levels (Fig. 16i and 16j). In contrast, simultaneous increases in TDO2, AFMID and NAD^+ levels were detected in $URI^{(+/D)hep}$ livers, indicating that URI reduction or deletion increases *de novo* NAD^+ biosynthesis (Fig. 16k and 16l). Finally, thin layer chromatography of metabolites after [^{14}C]-tryptophan labelling (74) in four human HCC cell lines (Huh7, HepG2, SNU398 and SNU449 highlighted the importance of *de novo* NAD^+ synthesis in maintaining cellular NAD^+ pools. Labelling in NAD^+ was detected in all HCC cells, but markedly reduced following AFMID depletion (Fig. 16m).

Expression of key enzymes of three other pathways implicated in oncogenesis was unaffected by hURI expression: SHMT1, G6PD and GOT1 of the glycine/serine/threonine, pentose phosphate and glutamine/aspartate pathways, respectively (75,76) (Fig. 16b). Downregulation of enzymes involved in lipids synthesis was also predicted due to the fact that NAD^+ is an important cofactor in their synthesis (33). As shown later, we demonstrated that hURI controlled activities of aryl hydrocarbon and estrogen receptors (AhR and ER), transcribing enzymes of most of the top IPA-predicted downregulated metabolic pathways.

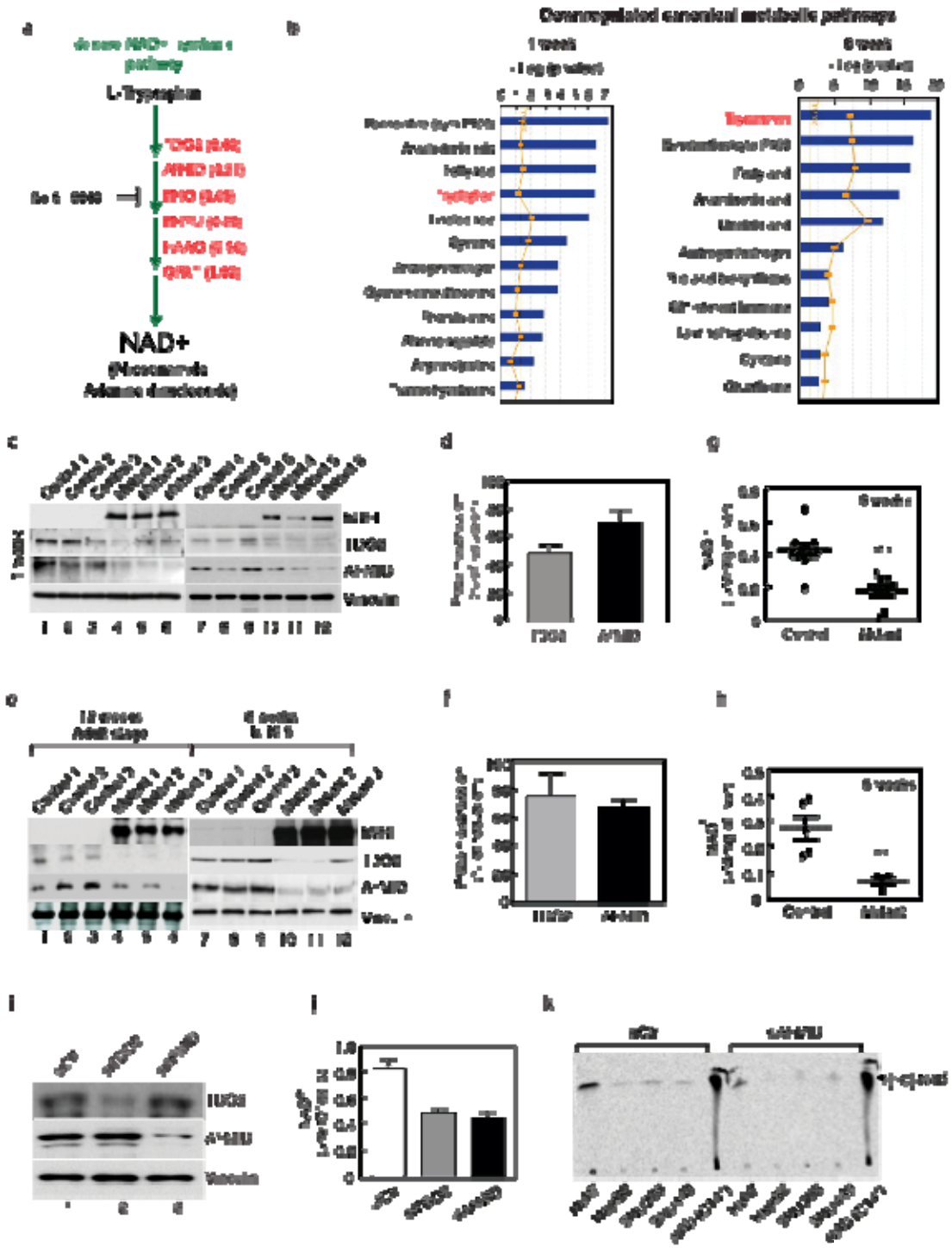

Figure 16 URI inhibits denovo NAD+ synthesis pathway from tryptophan (a) Schematic representation of de novo NAD+ synthesis. Fold change of protein detected in iTRAQ (mutant over control) are represented within the brackets. Ro-61-8048 is a compound known to block this pathway by inhibiting the activity of kynurenine 3-monooxygenase (KMO). **(b)** Top downregulated canonical metabolic pathways in 1 and 8 weeks iTRAQ data. Data were analyzed using Ingenuity Pathway Analysis (IPA) software. Denote tryptophan pathway (in red) as one of the most downregulated pathways. **(c)** WB analysis of 1 week control and mutant hURI-tetOFFhep mice**. (d)** Quantification of (c). **(e)** WB analysis of 8 week control and mutant hURI-tetOFF^{hep} mice and 20

weeks old hURI-tetOFF^{hep} mice expressing URI from 8 weeks**. (f)** Qunatification of proteins levels from 8 weeks WB shown in (e). **(g and h)** NAD+ levels in 3 and 6 week old hURI-tetOFF^{hep} livers. **(i)** WB analysis in SNU449 cell line treated with siCtr, siTDO2 or siAFMID, depecting the reduction of the protein levels. **(j)** Quantification of NAD+ levels in the HCC cell line described in (i). (**, $\rho \leq 0.01$). **(k)** Representative picture of Thin Layer Chromatography (TLC) analysis of tryptophan incorporation into NAD+ via de novo NAD+ synthesis, in 4 different HCC cell lines. Silencing of Afmid (siAFMID) impairs labeled tryptophan incorporation into NAD+, thus reducing total cellular NAD+ levels. Labeled [14C]-NAD+ was used as TLC migration control.

Furthermore, expression of nicotinamide phosphoribosyltransferase (NAMPT) (implicated in NAD^+ biosynthesis through salvage reactions) and activity of poly (ADP-ribose) polymerase (PARP), (the major NAD^+-consuming enzyme) were not affected at early time of 1 week and levels of both NADH and several dehydrogenases that reduce NAD^+ to NADH were all decreased (Fig.17b to 17d). All these data suggest that reduction in NAD^+ levels are solely due to downregulation of L-tryptophan/kynurenine catabolism.

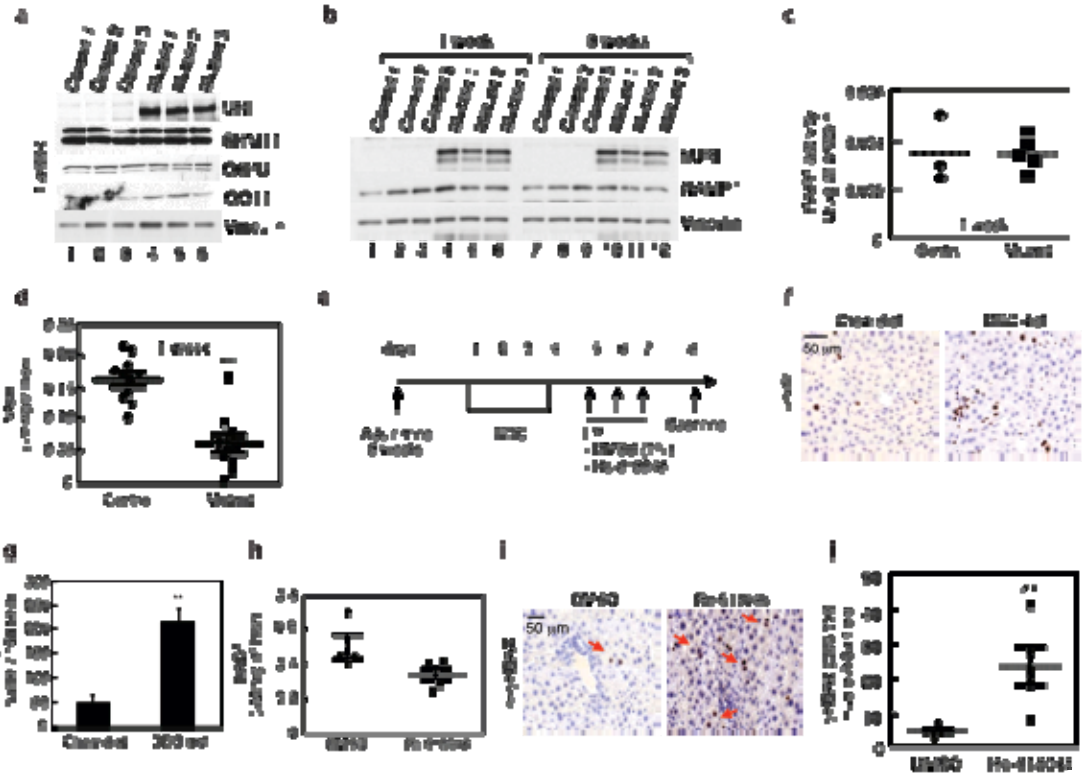

Figure 17 Inhibiting *de novo* NAD^+ synthesis pathway (a) WB liver analysis of important enzymes of other pathways IPA-predicted to be affected in 1 week old control and mutant hURI-tetOFF mice. Denote no changes in protein levels of these enzymes in the hURI expressing mutant hURI-tetOFF^{hep}. **(b)** WB analysis of NAMPT enzyme in 1 and 3 week old hURI-tetOFF^{hep} liver lysates. **(c)** PARP activity in 1 week liver extracts. **(d)** NADH levels in 1 week liver extracts. **(e)** Schematic representation of DDC followed by Ro-61-8048 treatment in C57BL/6 mice. **(f)** Representative Ki67 stained liver sections from C57BL/6 mice treated with DDC containing diet. (n>5). **(g)** Quantification of (f). **(h)** Liver NAD^+ levels in C57BL/6 mice described in (e). **(i)** γH2Ax staining of the liver sections described in (e). **(j)** Quantification of (i).

To validate the contribution of NAD^+ to DNA integrity we used a chemical inhibitor, Ro-61-8048, of KMO (77), a key L-tryptophan catabolism enzyme (Fig. 16a and 17e). We first induced liver injury and hepatocyte proliferation (manifested by increases in Ki67-positive nuclei; Fig. 17f and 17o) by supplying C57BL/6 mice for 4 days with a DDC-supplemented diet. DMSO (1%) or Ro-61-8048 (25 mg/kg) was intra-peritoneally injected during the next 3 days and mice were sacrificed on day 8. As expected, NAD^+ concentrations were reduced and DNA damage foci significantly elevated in Ro-61-8048-treated livers (Fig. 17h-17j). Thus, L-tryptophan/kynurenine pathway inhibition leads to reduced NAD^+ concentrations and DNA damage, recapitulating effects of hURI expression.

1.6 Restoring NAD^+ pools protects from DNA damage and aberrant *de novo* NAD^+ synthesis is a feature of oncogenesis

In further experiments, we supplied 3-week-old hURI-tetOFF^{hep} mice a nicotinamide riboside (NR)-supplemented diet (49). Without affecting their liver-to-body weight ratio, this significantly increased hepatic NAD^+ concentrations relative to controls on chow (Fig. 18a and 18b).

We detected dysplastic lesions and DNA damage foci in all mutants on chow, but no dysplastic lesions and very few DNA damage foci, with reductions in fibrotic area and both p53 abundance and Ser-18 phosphorylation, in NR-supplemented mutants (Fig. 18c-h). Prolonged NR treatment also prevented tumour development in 30-week-old mice expressing hURI, which developed tumours when fed chow (Fig. 18i and 18j). Thus, restoring NAD^+ pools protects from hURI-induced DNA damage, preneoplastic lesion formation-associated liver damage and tumour formation.

Furthermore, ceasing hURI expression in 8-week-old mice for 24 weeks restored AFMID levels, suppressed DNA damage, abolished the DDR (manifested by reductions in γH2AX foci and abolition of both p53 phosphorylation and accumulation) and activated NAD^+-dependent SIRT1 (manifested by reduced acetylation of p53 at Lys-379) (Fig. 18k and 18l). Thus, continuous hURI expression and consequent inhibition of *de novo* NAD^+ synthesis is essential for abolishing DNA repair and accelerating tumor formation.

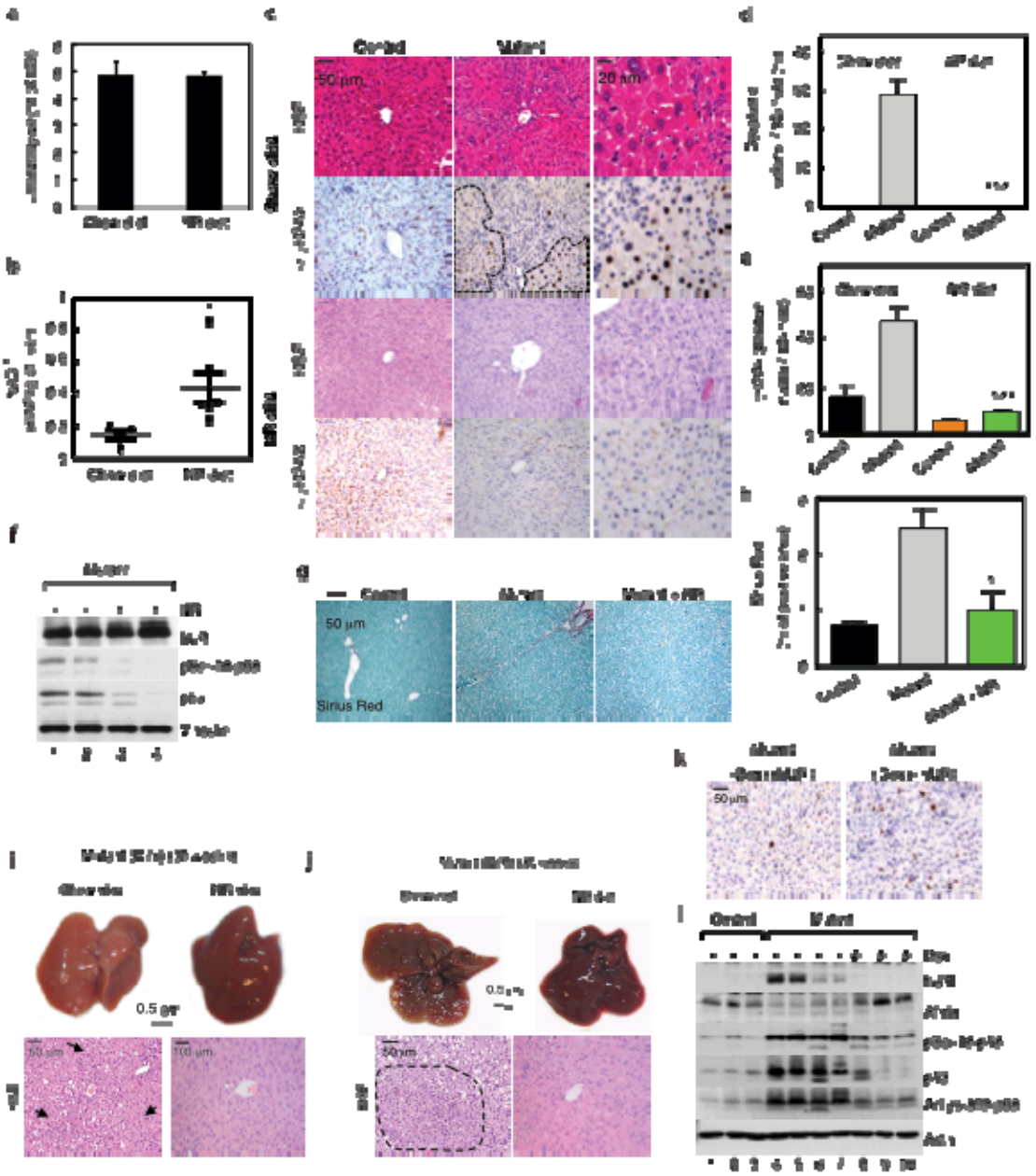

Figure 18 Metabolic rescue of URI induced phenotype by NR diet (a) Liver to body weight ratio of mutant hURI-tetOFF^{hep} mice fed either chow or NR diet. (n≥5). **(b)** Liver NAD^{+} levels in mutant hURI-tetOFF^{hep} mice fed either chow or NR diet. (*, p≤ 0.005). (n≥5). **(c)** Representative pictures of H&E and γH2AX IHC stained liver sections from 12 week old control and mutant hURI-tetOFFhep mice fed with chow (n = 5) or nicotinamide riboside (NR) diets (n = 7). Dotted black shapes depict anisokaryotic clusters present in mutant hURI-tetOFFhep mice under chow diet. These clusters are no longer present when these mutant hURI-tetOFFhep mice are fed NR diet (lower panels). **(d)** Quantification of total dysplastic area per slide in the hURI-tetOFFhep mice described in (A). (***, ρ ≤ 0.001). **(e)** Quantification of γH2AX positive nuclei in the hURI-tetOFFhep mice described in (A). (***, ρ ≤ 0.001). **(f)** WB analysis of mutant hURI-tetOFFhep mice fed with chow or NR diets. **(g)** Representative pictures of Sirius Red stained liver sections from hURI-tetOFFhep mice fed with chow or NR diets. n = 6. **(h)** Quantification of (g). **(i)** Representative pictures of whole livers and H&E stained liver sections from 30-week old mutant (+/Ki) hURI-tetOFF^{hep} mice fed either chow or NR diet. Dotted yellow circles depict tumor area and black arrows depict dysplastic foci present in the mutant (+/Ki) hURI-tetOFF^{hep} mice under

chow diet. n = 10 for controls/mutants fed with chow diet and n = 9 for controls/mutants fed with NR diet. **(j)** Representative pictures of whole livers and H&E stained liver sections from 30 week old mutant (Ki/Ki) hURI-tetOFFhep mice fed either chow or NR diet. Dotted black circles depict tumor area and black arrows depict tumor present in the mutant (Ki/Ki) hURI-tetOFFhep mice under chow diet. NR treatment in these mice prevents the appearance tumor formation. (n ≥ 5). **(k)** Representative pictures of γH2AX IHC stained liver sections from 32 week old mutant hURI-tetOFFhep mice fed with either chow or doxycycline (Dox) diets. n = 5. **(l)** WB analysis of hURI-tetOFF^{hep} mice described in (k).

Next, we explored whether other oncogenes had similar effects. *Ela-1-myc* mice, unlike *K-RAS^{G12V}* mice, develop pancreatic adenocarcinomas with high levels of DNA damage while pancreatic tumors initiated by K-RAS^{G12V} show no signs of replicative stress (78). We found that in early stages of tumorigenesis ectopic c-Myc expression induced DNA damage, but observed no γH2AX foci in pancreas from K-Ras^{G12V} mice (Figures 19a and 19b). The L-tryptophan/kynurenine pathway enzymes TOD2 and AFMID were clearly downregulated in *Ela-1-myc* but not K-*Ras^{G12V}* murine pancreas (Figure 19c). Short NR supplementation to 3-week-old *Ela-1-myc* mice did not effect on the incidence of preneoplastic lesions acinar-to-ductal metaplasia (ADM) formation, but ADMs observed in NR-fed mutants were less developed at this age. While chow fed 15-week-old mice developed carcinoma and increased ADM formation, *Ela-1-myc* mice under long term NR regimen decreased ADM and prevented carcinomas formation (Figures 19d-19g). Importantly pancreatic NAD^+ levels were significantly reduced in chow diet-supplied *Ela-1-myc* mutants but replenished to almost control levels when mutants were NR diet-supplemented (Figure 19h). These findings suggest that oncogene-induced DNA damage have a common bearing on NAD^+ levels.

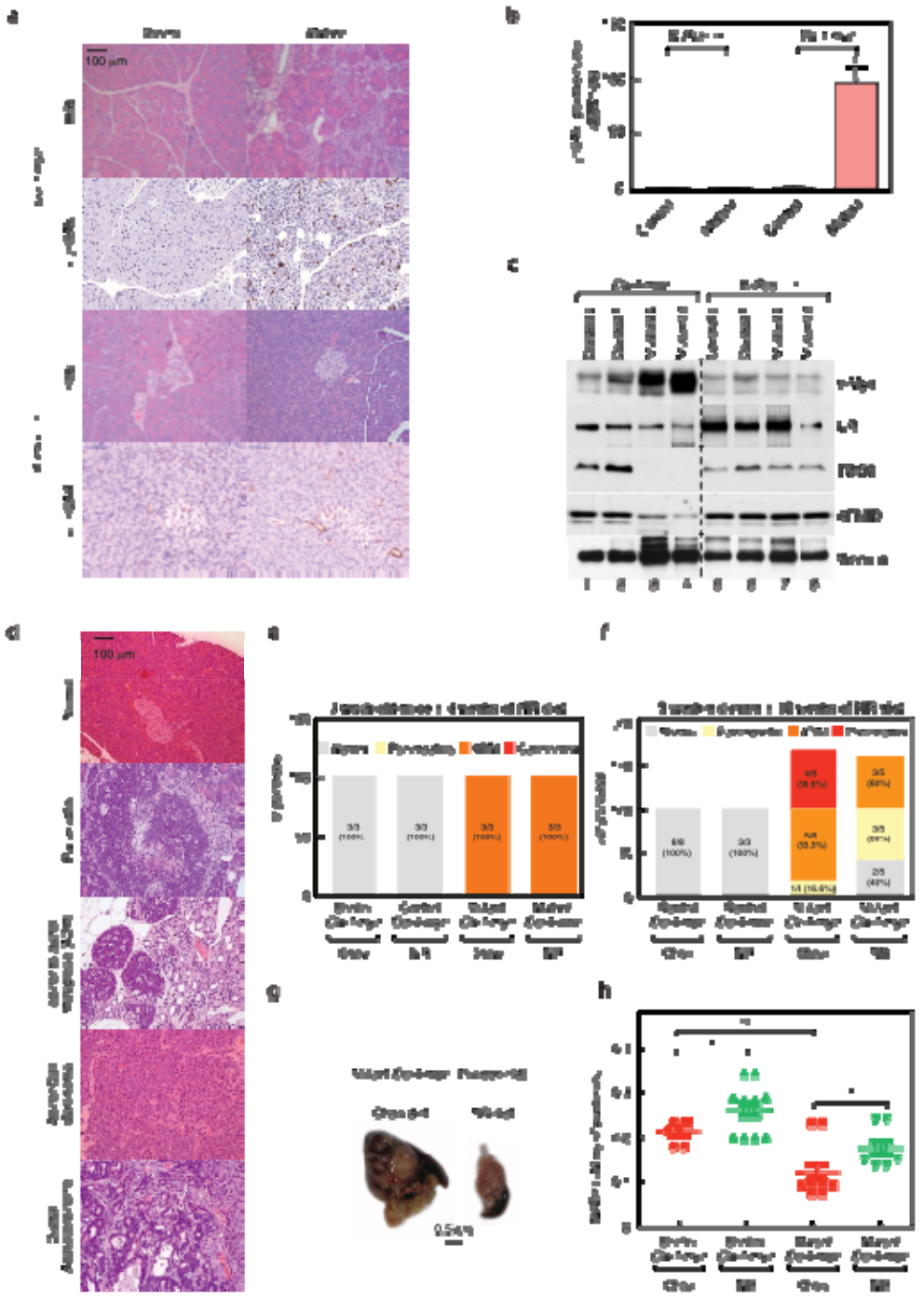

Figure 19 Affect of de novo NAD+ synthesis pathway on c-myc tumorigenesis (a) Representative pictures of H&E and gH2AX stained pancreas sections from control and mutant Ela-1-myc and K-RAS^{G12V} mice. (n ≥ 5). **(b)** Quantification of γH2AX positive nuclei in control and mutant Ela-1-myc and K-RAS^{G12V} mice. (*, ρ ≤ 0.05). **(c)** WB analysis of control and mutant Ela-1-myc and K-RASG12V mice. Denote that TDO2, c-Myc, URIand AFMID protein levels decrease only in the model known to induce carcinogenesis viaDNA damage pathway (Ela-1-myc) (compare lanes 3-4 to lanes 7-8). **(d)** Representative H&E pictures of normal, acinar-to-ductal metaplasia (ADM), Acinar cell carcinomas and ductal adenocarcinomas from 15-week-old *Ela-1-myc* mice. **(e)** Percentage of normal pancreas or pancreas with pancreatitis and ADM in 7- week-old mice under chow or NR regimen for 4 weeks. **(f)** Percentage of normal pancreas or pancreas with pancreatitis, ADM and carcinomas in 15-week-

old mice under chow or NR regimen for 12 weeks. **(g)** Representative pictures of pancreas from 15-week-old mutants *Ela-1-myc* supplemented with either chow or NR diets. **(h)** Pancreatic NAD^+ levels in 15-week-old *Ela-1-myc* mice fed either chow or NR diet for 12 weeks. Denote a significant decrease in *Ela-1-myc* mutant mice and an increase in mice fed with NR diet. (*, $\rho \leq 0.05$, **, $\rho \leq 0.01$). ($n \geq 5$). Scale bars 100 mm and 0.5 cm, as indicated.

1.7 URI regulates kynurenine metabolism by modulating AhR and ER activity

We found significant overlaps in differentially expressed transcripts between our RNA sequencing and available microarray datasets for livers from $AhR^{-/-}$ and $ER^{-/-}$ mice (79,80) (Fig. 20a to 20d) confirming our findings that AhR and ER mediate hURI-induced transcriptional repression of L-tryptophan/kynurenine catabolism. Furthermore, the enriched $ER^{-/-}$ sets included TDO2, corroborating reports that TDO2 is positively regulated by ER (81). Accordingly, siRNA depletion of AhR and ER in HepG2 cells reduced expression of TDO2 (and AFMID), while URI downregulation increased their abundance (Fig. 20e and 20f). Furthermore, cytoplasmic fractions of mutant livers were enriched with both nuclear receptors (Fig. 20g), indicating that hURI expression abolishes AhR and ER activity by inhibiting their cytoplasm-to-nucleus translocation. ALGGEN-PROMO v3.0 software predicted several AhR and ER binding sites in genomic sequences 5 kb upstream of the transcriptional start sites of TDO2 and AFMID promoters. Chromatin immunoprecipitation assays using SNU449 cell extracts and PCR revealed that both AhR and ER bound to these promoters, at different sites (Fig. 20h and 20i), indicating that they are direct transcription factors of TDO2 and AFMID. We also verified (by WB) the hURI-induced downregulation of other AhR and ER target genes detected in the RNA sequencing and iTRAQ analyses, including carbomyl-phosphate synthase 1 (CPS1), glutayl-CoA dehydrogenase GCDH) and glycine N-methyltransferase 1 (GNMT1) (Fig. 20j and 20k). Interestingly, $gnmt1^{-/-}$ mice develop chronic hepatitis and spontaneous HCC (82). These data confirm that hURI is a repressor of AhR and ER transcriptional factors.

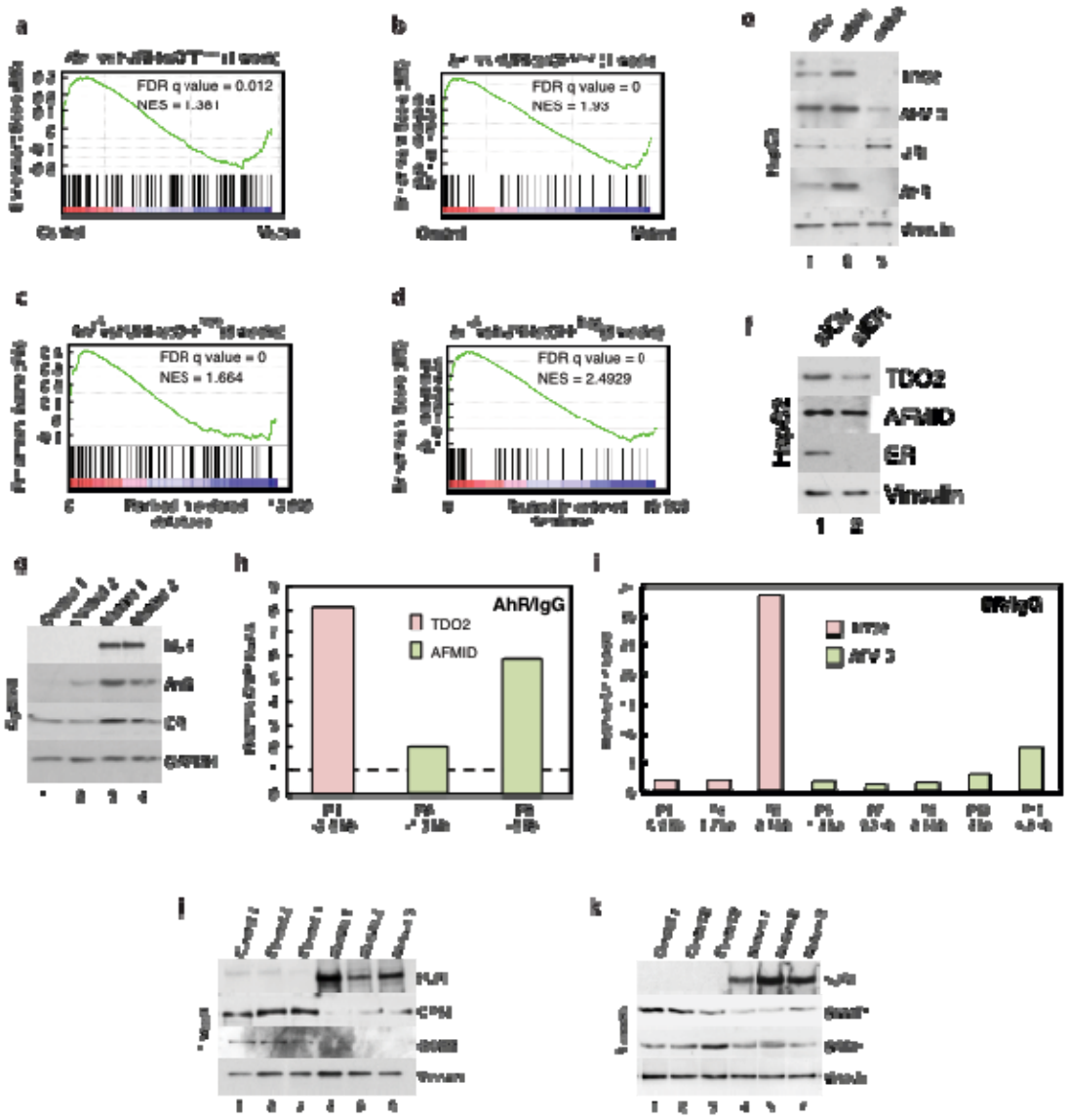

Figure 20 URI regulates AhR and ER transcriptional activity (a to d) GSEA analysis between liver gene arrays of *Ahr*$^{-/-}$ (a) *and Er*$^{-/-}$ (b) mice and liver RNA sequencing data from 1 week mutant hURI-tetOFF^{hep} mice and *Ahr*$^{-/-}$ (c) *and Er*$^{-/-}$ (d) mice and liver RNA sequencing data from 8 week mutant hURI-tetOFF^{hep} mice. **(e and f)** WB analysis of human HepG2 cells transfected with either scramble (siCtr) or siRNA against URI (siURI), AhR (siAhR) and ER (siER)**. (g)** WB analysis of cytosolic fractions from 1-week old hURI-tetOFFhep mice with the indicated antibodies. **(h and i)** ChIP assays showing association of AhR and ER with promoters of TDO2 and AFMID in SNU-449 cells. Semi-quantitative PCR of the intragenic region of chromosome 3 was used for normalization. **(j and k)** WB analysis of 1 (j) and 8 (k) week hURI-tetOFFhep mice liver extracts. Denote decreased protein levels of AhR and ER target genes in the mutant hURI-tetOFFhep mice.

AhR and ER may form inactive cytoplasmic complexes with HSP90, a member of the URI prefoldin complex (38,83,84). Reciprocal co-immunoprecipitation experiments confirmed that hURI and HSP90 interact with AhR or ER in cytosolic extracts of 1-week-old mutant livers (Fig. 21a and 21b).

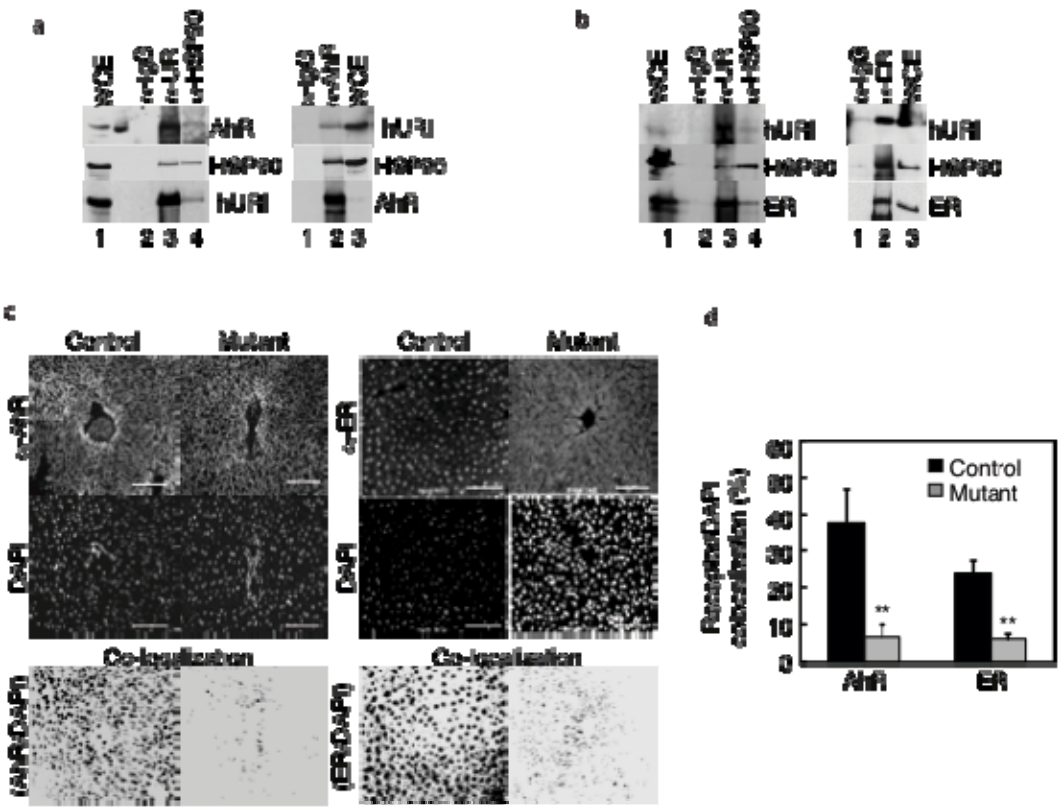

Figure 21 Co-immunoflouresence and immunoprecipitation analysis of URI/HSP90/AhR and ER complexes (a and b) Immunoprecipitation using liver cytosolic fraction extracts followed by WB analysis from 1 week hURI-tetOFFhep mice with the indicated antibodies. **(c)** AhR and ER liver immunofluorescence of 1 week old control and mutant hURI- tetOFFhep mice. DAPI was used for nuclear staining. Lower panels depict nuclear co- localization done using ImageJ. n = 5 for controls and mutants. **(d)** Quantification of nuclear co-localization of AhR and ER shown in (h). (**, $\rho \leq 0.01$). Scale bars represent 100 μm.

Confirmatory immunofluorescence analysis detected significant reductions in nuclear AhR and ER in hepatocytes of 1-week-old mutants (Fig. 21c and 21d). Thus, AhR and ER are apparently trapped in an inhibitory cytoplasmic protein complex containing hURI and HSP90, preventing their trafficking to the nucleus and thereby inhibiting transcription of L-tryptophan/kynurenine catabolic enzymes.

1.8 URI Expression Is Enhanced in Human HCC, Is Associated with Poor Survival and Correlates with *De Novo* NAD^+ Synthesis Inhibition

To evaluate URI's relevance in human hepatocarcinogenesis, we examined its expression in a tissue-microarray of 49 human liver samples (36 HCC, 4 peritumoral and 9 normal). Using a highly specific anti-URI antibody we detected no, weak and strong URI expression in normal livers, peritumoral areas of HCC patients and 60% of HCCs, respectively (Fig. 22a to 22e). Increased URI levels in 20 tumoral human samples, relative to paired peritumoral samples, were also detected by real-time PCR (not shown) and WB, with a positive correlation between URI expression and tumour

aggressiveness, detected by Ki67 staining (Fig. 22e). URI expression was expressed approximately twice as strongly in 70% of the tumoral tissues than in peritumoral counterparts (Fig. 22f and 22g), corresponding to the level of hURI expression in the hURI-tetOFF^{hep} mouse. We also detected significant correlations between URI expression and HBV- or HCV-associated HCC (and hence hepatitis, an early HCC stage), and increased URI expression in human hepatitis samples (Fig. 22f, 22g and 22h).

Furthermore, GSEA detected significant overlaps between transcriptomic signatures of our hURI GEMM and HBV-associated human HCC (85) (Fig. 23a, 23b). Importantly, URI expression was associated with poor prognosis in human HCC patients (Fig. 23c). Next, we checked for antagonism between URI expression and L-tryptophan/kynurenine pathway enzymes in human HCC. Comparative analysis using a gene array dataset from human HCC (86) detected inverse correlations between URI expression and TDO2, KMO and HAAO expression (Fig. 23d) WB analysis of the paired peritumoral and tumoral (HCC) samples revealed that AFMID and NAD^+ levels were positively correlated, and both negatively correlated with URI expression (Fig. 23e-h).

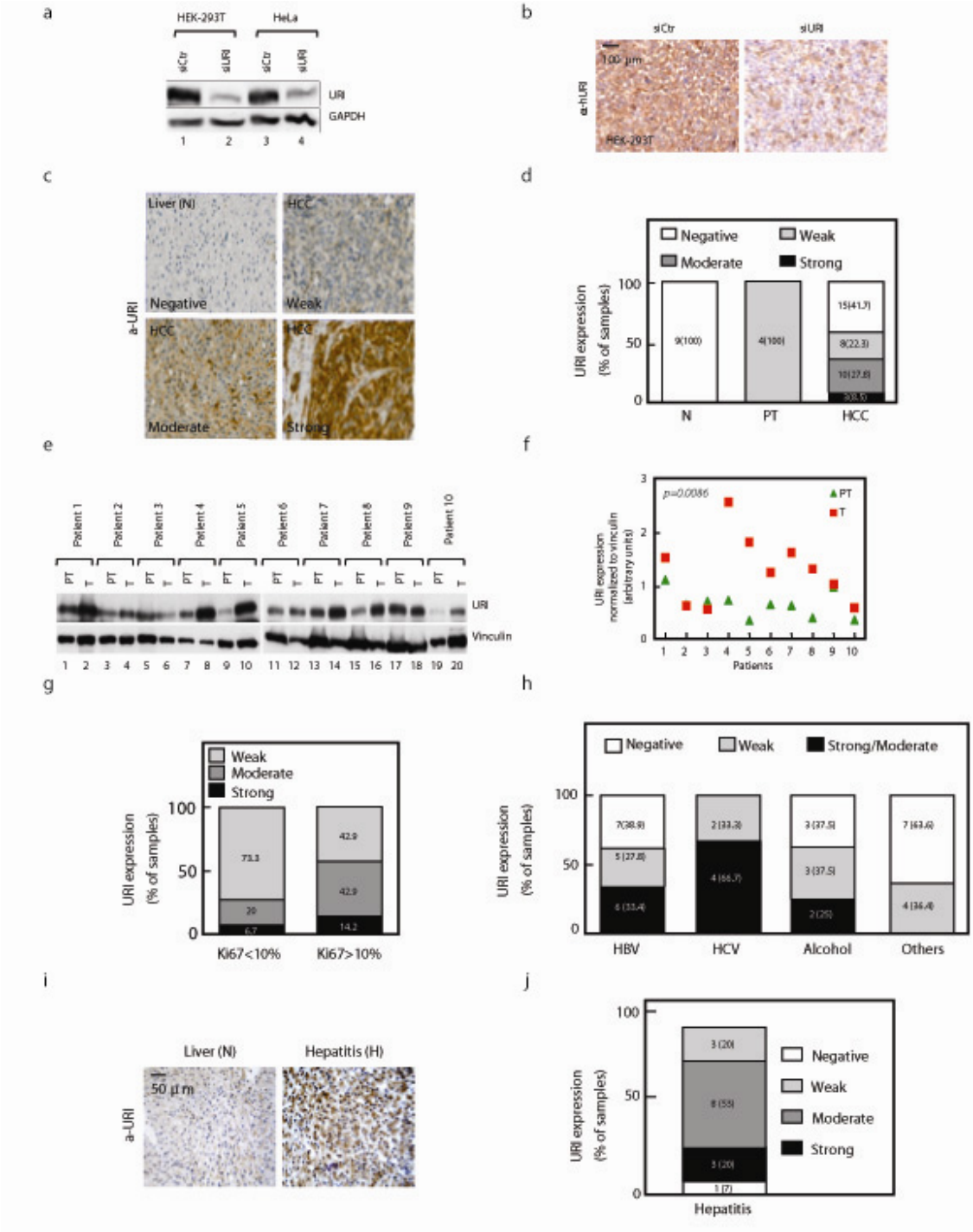

Figure 22 URI expression in human livers (a and b) Characterization of URI mouse monoclonal antibody by WB (a) and ICC (b). Endogenous URI was knock-downed in HEK-293T and in HeLa cells using siRNA against *URI* mRNA.

Moreover, using a database for 221 patients (87) (GEO ID: GSE14520), Cox regression analysis of TDO2, KMO, HAOO and quinolinate phosphoribosyltransferase (QPRT) expression indicated that

their overall survival was significantly associated (*P*, 0.025) with our tryptophan catabolism signature (Fig. 14j) Downregulation of TDO2 or HAAO also predicted poor prognosis for HCC patients (Fig. 23j, 23k and 23i). Thus, URI-mediated inhibition of *de novo* NAD^+ synthesis has apparent relevance in human HCC development.

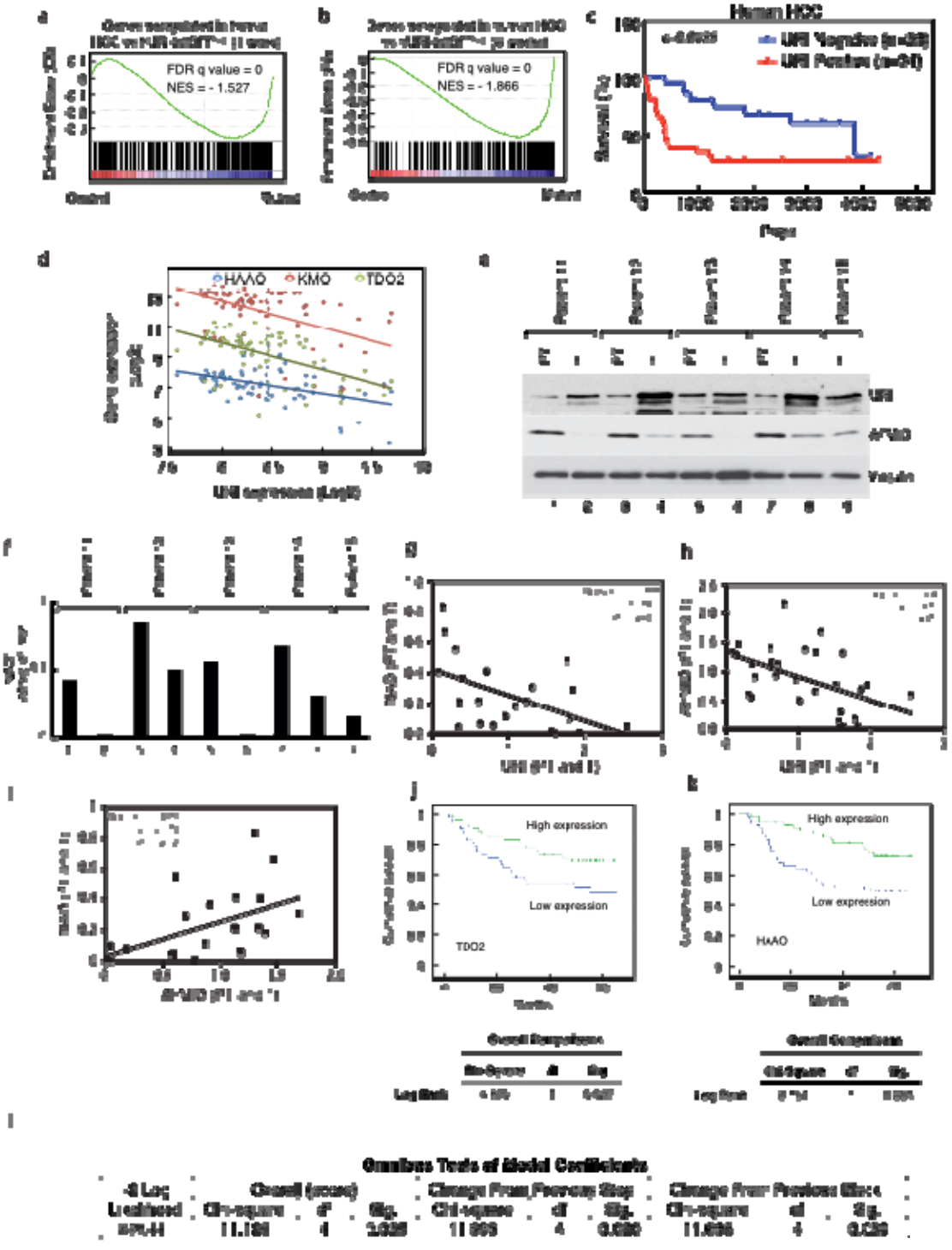

Figure 23 URI expression in human HCC and the correlation with *de novo* NAD+ pathway (a and b) GSEA between differentially expressed genes in human HCC and RNA sequencing datasets from 1 (a) and 8 week (b) old hURI-tetOFF^{hep} mice. **(c)** Kaplan Meier curve analysis of human HCC samples classified by IHC as positive (n=29) and negative (n=34) for URI expression. (Log-rank test p = 0.0035; hazard ratio = 0.3163; 95% confidence interval of ratio 0.1460 to 0.68). **(d)** Linear regression analysis of hURI and TDO2, KMO and HAAO expressions in a human HCC microarray dataset, showing inverse correlation between URI and TDO2, KMO, HAAO expression. **(e)** WB analysis of paired peritumoral (PT) and tumoral (T) liver samples from human patients. Denote decreased AFMID protein levels in the tumoral paired samples compared to the peritumoral. **(f)** Quantification of liver NAD+ levels in the peritumoral (PT) and tumoral (T) paired samples used in (B). (n ≥ 5). **(g)** Pearson correlation analysis between URI protein and NAD+ levels in peritumoral (PT) and tumoral (T) human liver samples. Denote a significant inverse correlation between URI and NAD+ levels. (p = 0.0136). **(h)** Pearson correlation analysis between URI and AFMID protein levels in peritumoral (PT) and tumoral (T) human liver sample. Denote a significant inverse correlation between URI and AFMID levels. (p = 0.0047). **(i)** Pearson correlation analysis of AFMID protein and NAD+ levels in peritumoral (PT) and tumoral (T) human liver samples. Denote a significant direct correlation between AFMID and NAD+ levels. (p = 0.0173). **(j and k)** Kaplan Meier curve analysis of human HCC patients based on gene expression of TDO2 and HAAO. **(l)** Multivariate Cox regression analysis for TDO2, KMO, HAAO and QPRT, in a cohort of 221 HCC patients. Overall patient survival was significantly associated with the tryptophan catabolism enzyme signature (p = 0.025). Scale bars represent 50 μm.

2 Characterizing the HCC cell of origin

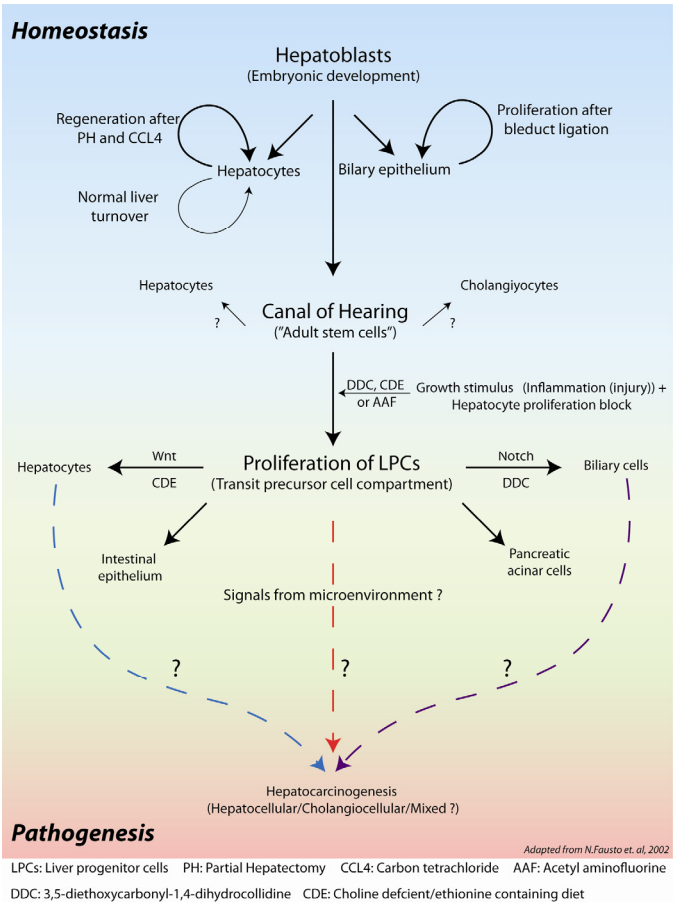

Figure 24 Scheme representing the role of different cell types in liver during development, stress and disease conditions.

During early murine embryonic liver development from endoderm around E8-E10, liver bud develops into a fully functional liver (E15) after hepatic and biliary differentiation. An embryonic bi-potential progenitor called “hepatoblast” residing next to the portal veins become cholangiocytes and the majority of hepatoblasts in the parenchyma differentiate into hepatocytes. Adult bi-potential liver progenitor population derived from the hepatoblast resides near the “canal of Hearing” around the portal triad, hence named as ductal/liver progenitor cells (LPCs) or oval cells in rodents. Proliferating small epithelial cells, named oval cells, have been observed at the earliest stages of liver carcinogenesis induced by different chemical carcinogens.

The differentiation of this adult stem cell population to either hepatocytes by Wnt, and cholangiocytes by notch signaling respectively is shown in different human diseases and chemical mouse models. The existence and responsiveness of facultative liver progenitor cells (LPCs) in rodents has been demonstrated convincingly in rat 2-AAF (2-acetylaminoflourene) and PHx (partial hepatectomy) model. By blocking the hepatocyte proliferation AAF facilitate the proliferation of LPCs prior to PHx induced liver regeneration (88). Similarly DDC (89) and CDE (90) are two extensively used models to study LPCs in the context of murine biology. Although, DDC and CDE recapitulate the expansion of LPCs, the blockade in hepatocyte proliferation is not complete unlike AAF model in rats (Fig. 16). These models are also of limited use to study the physiological relevance of LPC expansion, as the mice constantly lose weight, thus making the long-term follow-up not feasible. Many human studies provided the strong association between LPCs activation with liver damage, HCC development and poor patient survival.

In spite of the clinical relevance, functional studies to verify the role of LPCs in hepatocarcinogenesis more specifically, in HCC cell of origin have not been addressed.

2.1 Expression of hURI in hepatocytes leads to expansion of Sox9 positive ductal cells

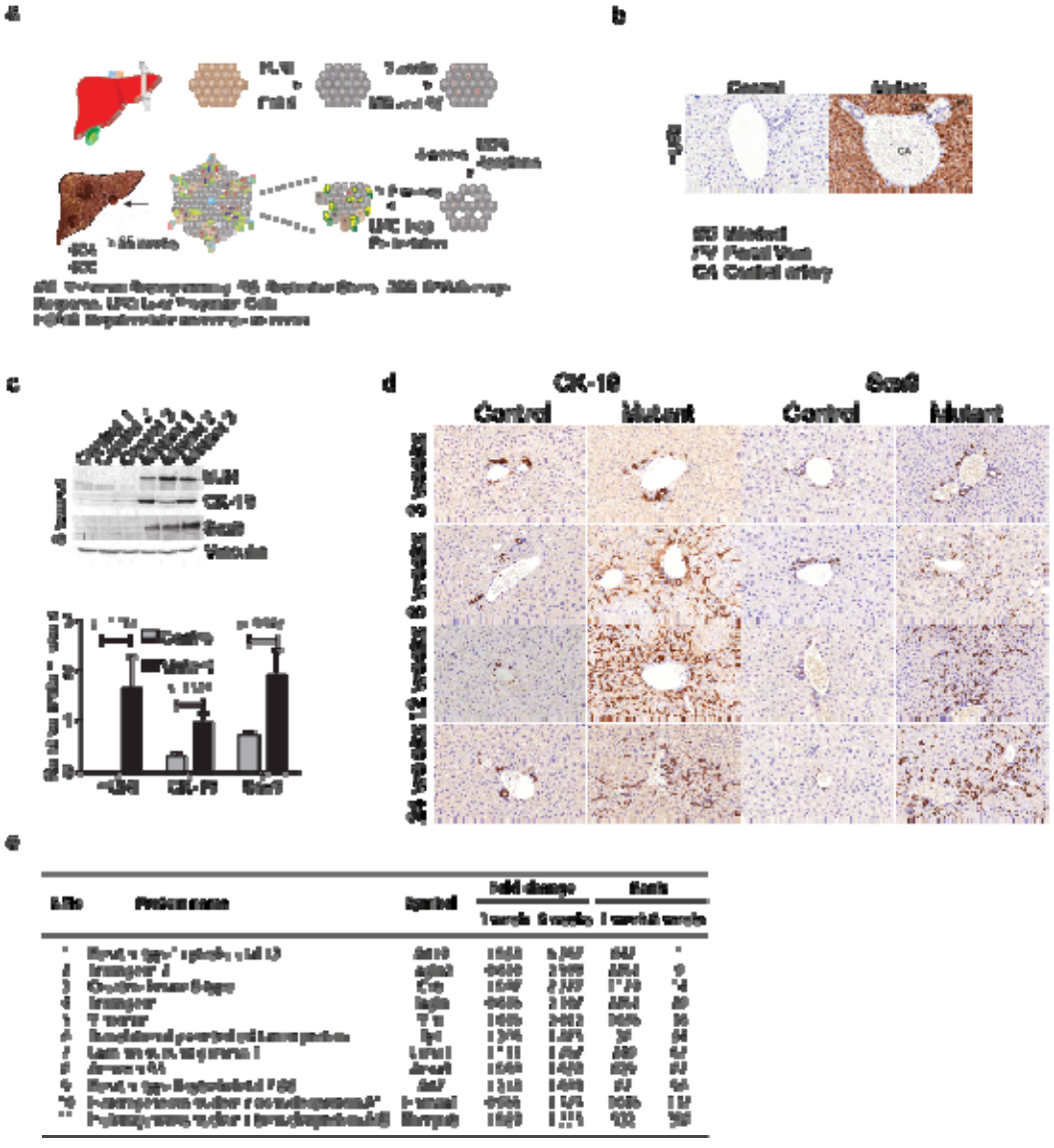

S.No	Protein name	Symbol	Fold change		Rank	
			1 week	8 weeks	1 week	8 weeks
1						
2						
3						
4						
5						
6						
7						
8						
9						
10						

Figure 25 Hepatocyte specific ectopic URI expression evoke ductal/LPC activation. (a) Scheme representing the different stages of HCC development by hURI in hURI-tetOFF^{hep} mouse model. **(b)** IHC analysis of 1-week old liver sections with ectopic URI specific antibody, cells lining the central artery (CA), bileduct (BA) and portal vein (PV) stained negative for URI expression. **(c)** WB analysis of 8-week old liver lysates for ectopic URI, Sox9 and CK19. Vinculin used as the loading control. Lower histogram depicts the relative levels of proteins. **(d)** Timecourse analysis of Sox9 and Ck19 positive cells in hURI-tetOFF^{hep} mouse model using IHC. **(e)** Table representing the Ductal/LPCs protein markers differentially expressed in 1 and 8 weeks iTRAQ analysis. Rank indicates the position in the list of top upregulated proteins and fold change indicates the fold increase of the protein in mutant with respect to control littermates.

Ectopically expressing oncogenic hURI, specifically in hepatocytes leads to spontaneous, heterogeneous HCC and HCA formation (Fig 25a). URI expression is hepatocyte specific, as shown by hURI negative ductal/LPC cells in the mutant liver (Fig 25b). The increase in ductal/progenitor cell expansion has been confirmed by immunoblotting with CK-19 and Sox9 (bonafide ductal/LPCs markers) in 8 weeks old hURI-tetOFF^{hep} liver lysates (Fig 25c). Moreover, there is a time dependent increase in cells stained positive for CK19 and Sox9, in hURI-tetOFF^{hep} model (Fig 25d). The above scenario suggests a microenvironment mediated LPCs expansion in a non-cell autonomous manner.

Signs of ductal/progenitor expansion during early asymptomatic stage of hURI expression (3 weeks) haven't been observed. However a marked expansion into the parenchyma was observed as early as 8 weeks and continued untill 24 weeks of hURI expression. Consistent with the increase in ductal/LPCs cell proliferation around 8 weeks, quantitative proteomic analysis (iTRAQ) revealed many ductal/LPCs cell specific proteins as top up-regulated proteins in 8 week, but not in 1-week-old livers (Fig 25e).

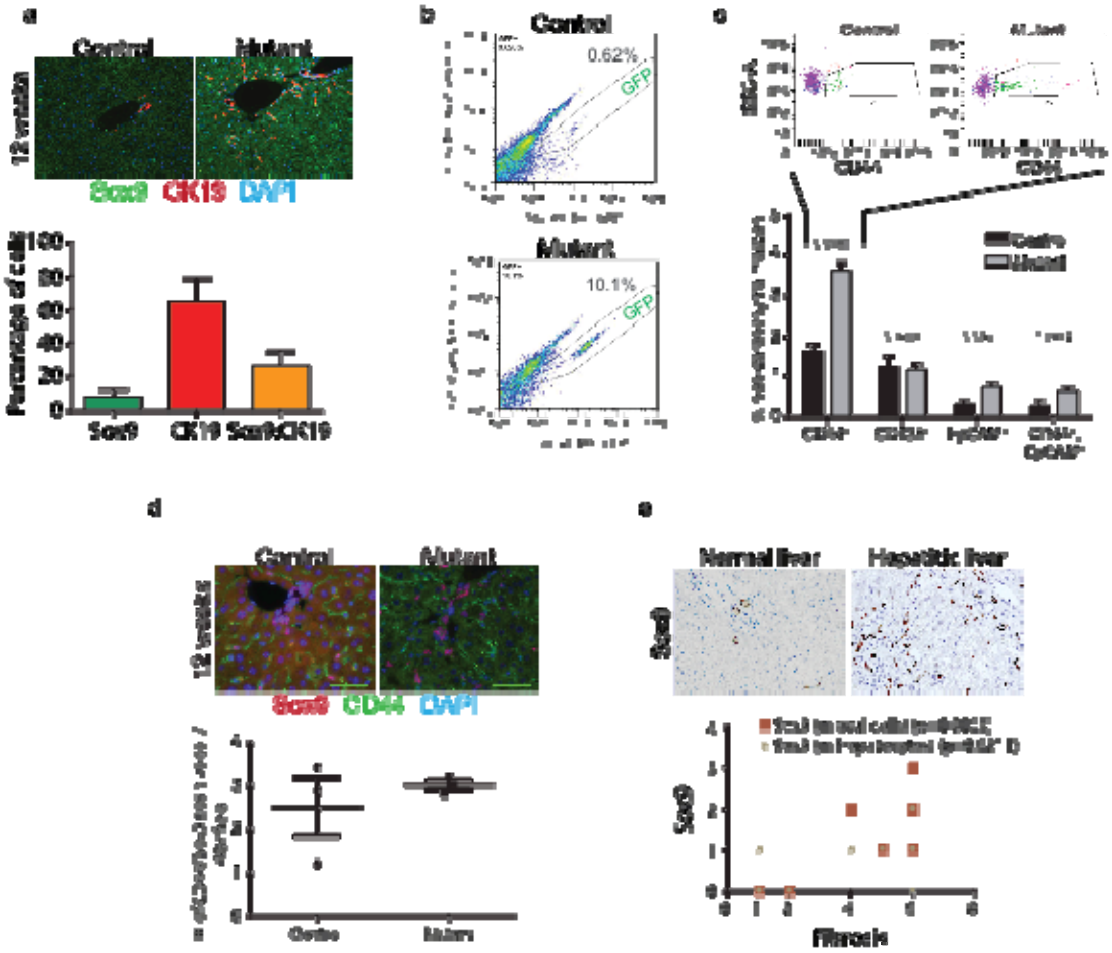

Figure 26 Chracterising the ductal/LPC population and their relevance in human liver disease. (a) Co-immunofluorescence staining of Sox9 (green) and CK-19 (red) in 12 weeks old hURI-tetOFF^{hep} liver sections. Below histogram represents the quantification of the staining. DAPI (in blue) used to stain nucleus. **(b)** FACS quantification of the percentage of ductal/LPC population in 12-week old hURI-tetOFF^{hep} mice non-praenchymal fractions. **(c)** FACS assisted charecterisation of ductal/LPCs for expressing different cancer stem cell markers. Below histogram represents the quantification as percentage of non-parenchymal fraction. **(d)** Co-immunofluorescence staining of Sox9 (red) and CD44 (green) in 12-weeks old hURI-tetOFF^{hep} liver sections. Dot plot below represents the quantification of cells expressing both markers. **(e)** IHC staining for Sox9 in normal and fibrotic human liver sections. Below dotplot represent the correlation of Sox9 expression in ductal and hepatocytes with the degree of fibrosis.

Co-immunofluorescence analysis was performed to characterize the proportion of ductal cells positive for Sox9, CK19 or both in 12 weeks old liver sections. Quantification of the percentage of positive cells revealed that around 30% of cells expressed both Sox9 and CK19 while around 10% and 60% of the ductal cells expressed either Sox9 or CK19, respectively (Fig 26a).

The number of ductal progenitors in hURI-tetOFF^{hep} mouse model was quantified by genetically labelling Sox9 positive cells with EYFP using previously described Sox9$^{IRES\text{-}eGFP}$ mouse model (91). FACS sorting of EYFP positive cells from the non-parenchymal liver fraction of 12 week old mice showed an increase in the ductal/LPCs population from 0,62% to 10.1% in hURI-tetOFF^{hep} mice compared to their control littermates (Fig 26b). Many cancer stem cells markers like CD44, CD133 and EpCAM have been described to be closely associated with the ductal/LPCs cells in human liver pathologies. In order to characterize the presence of different CSC markers expressing cells, the non-parenchymal fractions of 12-week-old control and mutant hURI-tetOFF^{hep} were isolated and stained for the respective markers followed by FACS analysis. A significant increase of CD44 and EpCAM population, but not in CD133 cells, in hURI-tetOFF^{hep} livers was observed (Fig 26c). Co-immuno fluorescence of CD44 and Sox9 in 12 weeks old mice showed weak enrichment of CD44 and Sox9 double positive cells in hURI-tetOFF^{hep} mice (Fig 26d).

In order to understand the relevance of the ductal expansion in human liver disease progression, 15 human hepatitis samples were stained with Sox9 and correlated with the liver damage associated fibrotic reaction (Fig 26e). A significant correlation of the Sox9 positive ductal cells with the degree of fibrosis (Fig 26e) has been observed, suggesting the association of liver damage with the activation of LPCs.

2.2 Sox9 positive ductal cells contribute to liver tumorigenesis *in vivo*

To understand the specific contribution of Sox9 positive cells to liver tumorigenesis, a previously described inducible Sox9$^{IRES\text{-}CreERT2}$ model (91) was used to specifically label and track the fate of Sox9 positive cells *in-vivo*. The efficiency of Sox9$^{IRES\text{-}CreERT2}$ mediated recombination was determined by crossing the mice with Rosa26R (92) and activating the Cre recombinase by supplying tamoxifen diet for 2 weeks starting from 5 weeks of age (Fig 19a).

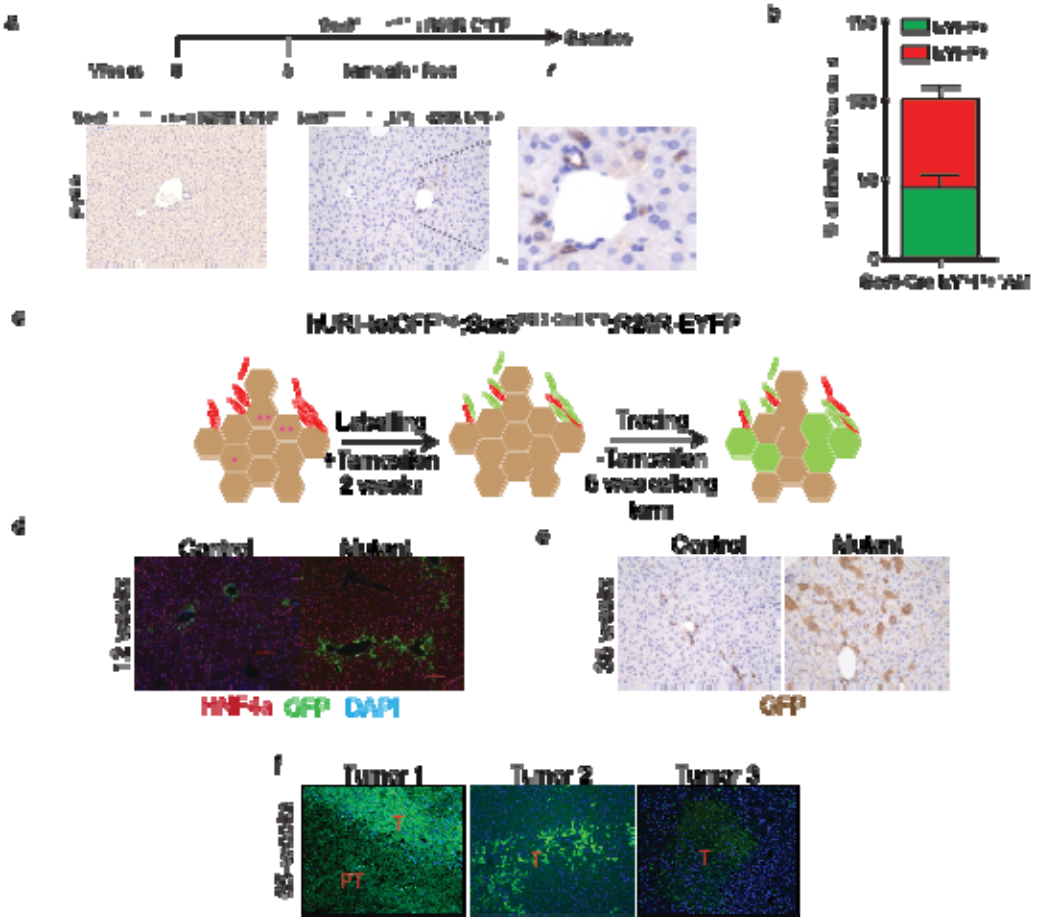

Figure 27 Sox9 positive ductal/LPC population contributes to HCC formation *in vivo.* **(a)** Schematic representation of the time scale of Sox9CreERT2 activation. IHC pictures stained for EYFP after labelling for 2-weeks. **(b)** Histogram representing the percentage of Sox9 positive cells stained positive or negative for EYFP. **(c)** Schematic representation of the labelling and analysis of Sox9 positive cells in hURI-tetOFF^{hep} model. **(d)** Immunofluorescence analysis of EYFP positive (green) Sox9 derived cells and hepatocytes (HNF4a (red)) after 12-week short term tracing experiment showing the double positive cells confined to periportal region in controls, while cells migrated well into parenchyma in mutants. **(e)** IHC analysis of EYFP positive cells derived from Sox9 positive cells after 30 weeks of tracing in 35 weeks old mice. Dysplastic anisokaryotic clusters display a positive signal for EYFP derived from Sox9 positive cells. **(f)** Immunofluorescence images representing the three tumor types identified after long-term tracing (60 weeks) in hURI-tetOFF^{hep} mice. EYFP stained in green represents the cells derived from Sox9 positive cells. DAPI was used to stain the nucleus.

IHC analysis revealed specific labeling with EYFP of few ductal/LPCs near the canal of hearing (Fig 27a). To estimate the efficiency of recombination, after the tamoxifen treatment the livers were co-immunostained for Sox9 and EYFP. Analysis of percentage of positive cells labeled with both Sox9 and EYFP was around 40%, while no cells were labeled double positive without tamoxifen diet (Fig 27b).

In order to analyze the relevance of Sox9 positive cells in our hURI-tetOFF^{hep} model, we crossed hURI-tetOFF^{hep} mice with Sox9$^{IRES\text{-}CreERT2}$; Rosa26R mouse model. Mice were treated with tamoxifen

diet for 2 weeks starting at the age of 5 weeks and transferred to normal chow diet to trace the labeled cells (Fig 27c).

Short term tracing for 5 weeks revealed GFP positive hepatocytes originating from Sox9 positive ductal cells in the mutant mice (Fig 27d). Tracing Sox9 positive cells for a longer time (30 weeks) revealed GFP positive clusters of anisokaryotic hepatocytes in parenchyma (Fig 27e). To see the contribution of Sox9 positive cells to tumor formation, we also performed tracing for 60 weeks. This tracing revealed three different scenarios where: the first tumor type didn't display any GFP positive hepatocytes, the second showed the contribution of few GFP positive hepatocytes to the tumor mass and the third type where the whole tumor was composed of GFP positive hepatocytes originating from Sox9 positive cells (Fig 27f).

2.3 Albumin positive hepatocytes contribute to liver tumorigenesis *in vivo*

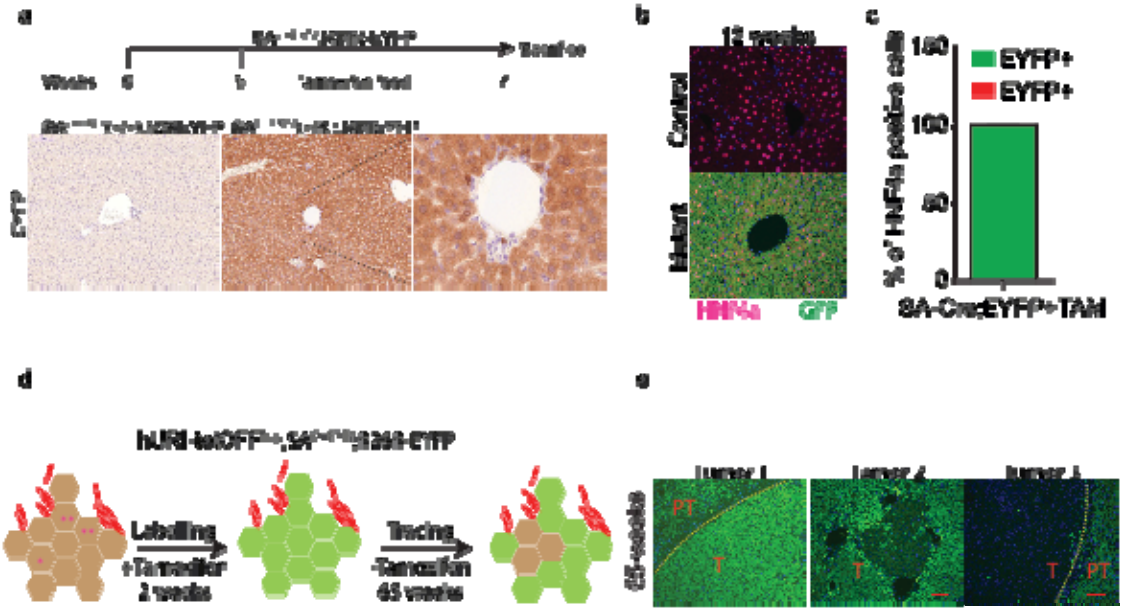

Figure 28 Hepatocyte tracing experiment using serum-albumin CreERT2 (a) H&E staining of hURI-tetOFF^{hep} mice with or without p53 or p19ARF inactivation. Bottom IHC pictures represent Sox9 positive ductal/LPC cells in all the models. **(b and c)** WB analysis for Sox9 levels in hURI-tetOFF^{hep} mice with or with out p53 and p19ARF inactivation. **(d)** WB analysis for Sox9 levels in hURI-tetOFF^{hep} model with continuous URI expression for 24 weeks and URI expression switched off after 8-weeks. **(e)** WB analysis for Sox9 levels in hURI-tetOFF^{hep} model with continuous URI expression for 24 weeks and mice fed with either chow or NR diet. **(f)** IHC staining for Sox9 and γH2Ax in 24-week hURI-tetOFF^{hep} mice fed with either chow or NR diet. **(g)** Number of Sox9 positive cells from the mice described in (f).

To verify the contribution of hepatocytes to tumorigenesis, we also performed lineage tracing using SA-CreERT2. To estimate the efficiency of SA-CreERT2 mediated deletion, we crossed the SA-CreERT2 line with a Rosa26R reporter mouse. Mice were treated with tamoxifen diet for 2 weeks

starting from 5 weeks of age (Fig 28a). IHC analysis of the tamoxifen treated livers revealed hepatocyte specific EYFP signal indicating SA-CreERT2 is active only in the hepatic compartment (Fig 28a). However, to estimate the efficiency of recombination, we calculated the percentage of HNF4a and GFP double-positive cells in mice carrying both SA-CreERT2 as well as Rosa26R alleles. IF analysis and further quantification revealed that all HNF4a positive mature heapatocytes are GFP positive indicating that the recombination efficiency was around 100% (Fig 28b and 28c).

Long-term (60 weeks) hepatocyte tracing experiment was performed in hURI-tetOFF^{hep} mice with SA-CreERT2; Rosa26R alleles. Consistent with the above results, three differential staining patterns for GFP have been observed. Scenarios where the whole tumor was formed by GFP positive hepatocytes, tumors partially composed of GFP negative hepatocytes and finally tumors composed entirely of GFP negative hepatocytes (Fig 28d), suggesting the possibility of non-hepatocyte cells contributed to tumorigenesis.

Altogether the above two tracing experiments using SA-CreERT2 and Sox9$^{IRES\text{-}CreERT2}$ suggested the significant contribution of bile-duct/progenitor cells in tumorigenesis and the potential tumor cell of origin in the liver.

2.4 hURI induced DNA damage response (p53 and p19ARF) is dispensable for ductal/LPCs expansion.

As previously described, we asked whether the hepatocyte proliferation arrest mediated by p19ARF/P53/p21 pathway was essential for LPC expansion in hURI-tetOFF^{hep} model.

To address this, we used hURI-tetOFF^{hep}; p53ER^{TAM} and hURI-tetOFF^{hep}; p19ARF$^{-/-}$mouse models with either cytoplasmic restricted p53 strain (p53ER^{TAM}) or complete loss of p19ARF expression (p19ARF$^{-/-}$) respectively. In both, mouse models, after 12 weeks of URI expression the expansion of Sox9 positive LPCs was still observed by IHC (Fig. 29a) and WB (Fig. 29b and 29c) analysis. However, the LPC expansion is completely abolished by switching-off hURI expression with doxycycline, as evident from IHC (Fig. 29a) and WB (Fig. 29d) analysis.

Moreover supplementation of mice with NR, also rescued the DNA damage and expansion of progenitors as described before, suggesting changes in metabolism and DNA damage induced by URI expression might play a role in LPCs proliferation (Fig. 29f and 29g).

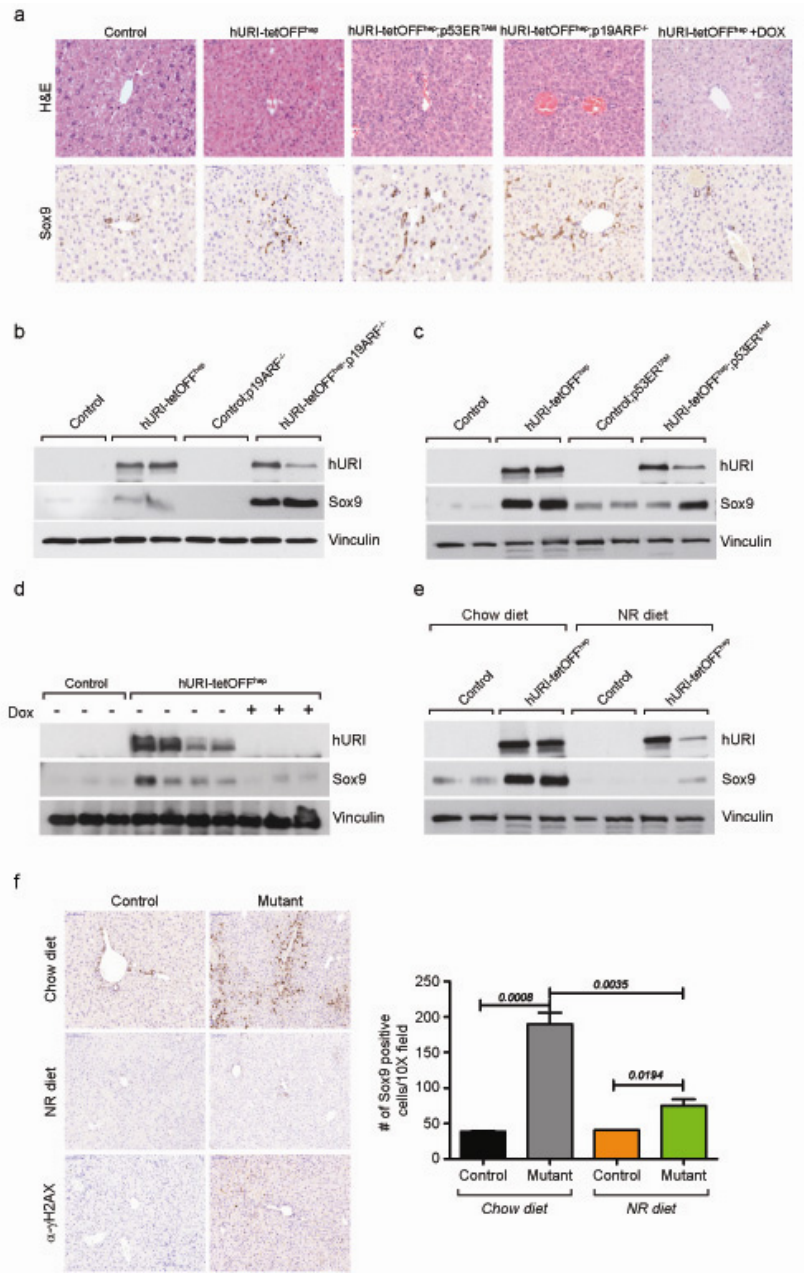

Figure 29 p53/p19ARF mediated DDR is dispensable for LPC/ductal cell expansion in hURI-tetOFF^{hep} mouse model (a) Histologial H&E analysis of mice expressing URI with or with out p53 and p19ARF inactivation **(b)** WB analysis of tissue lysates from hURI-tetOFF^{hep} model, with and with out p19ARF inactivation **(c)** WB analysis of tissue lysates from hURI-tetOFF^{hep} model, with and with out p53 inactivation **(d)** WB analysis of tissue lysates from hURI-tetOFF^{hep} model, fed with or with out doxycycline **(e)** WB analysis of tissue lysates from hURI-tetOFF^{hep} model, fed with or with out NR diet **(f)** IHC analysis of tissue lysates from hURI-tetOFF^{hep} model, fed with or with out NR diet, right histogram represents the quantification.

2.5 Ductal/LPCs expansion correlates with hURI induced inflammatory response.

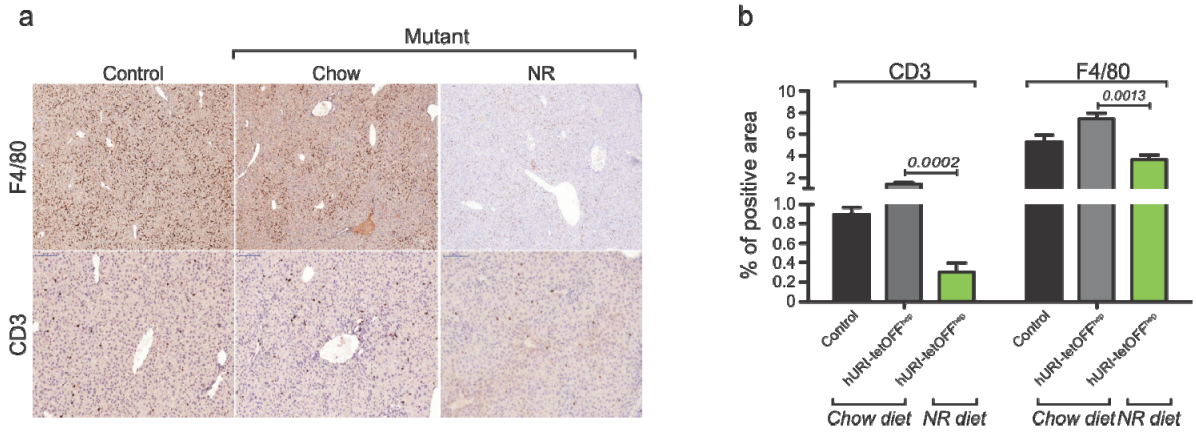

Figure 30 IHC analysis of inflammatory mediators upon NR diet (a) IHC staining of F4/80 and CD3 in 24-week old hURI-tetOFF^{hep} mice liver sections. **(b)** Quantification of (a).

LPC activation has been previosuly shown to be associated with fibrosis and inflammation. Elegant experiments have demonstrated that macrophage-derived Wnt opposes Notch signaling to specify hepatic progenitor cell fate in various mouse models of chronic liver disease. This is done either by secreting Wnt ligands direclty to drive the progenitor proliferation and differentiation towards hepatocyte lineage or stimulating fibroblasts to activate Notch pathway to drive their proliferation and differentiation towards bile duct lineage (Fig 25).

We checked whether LPC activation correlates with inflammation associated with URI induced liver damage. Feeding the mice with NR, not only inhibited DNA damage and LPC proliferation as shown before but also significantly reduced the numbers of F4/80 positive macrophages and CD3 positive T-cells (Fig 30a and 30b). The above data emphasize the possible role of inflammatory mediators in LPC activation.

Discussion

1 Hepatocarcinogenesis mediated by ectopic URI expression in hepatocytes

In this thesis, we demonstrated that URI is an oncogene in liver, which can induce spontaneous HCC when ectopically expressed in mouse hepatocytes. The hepatocarcinogenesis induced by URI expression resembles the human disease with dysplastic lesions accompanied with fibrosis. DNA damage was found as the early event in our model before increase in proliferation, dysplastic lesions and liver injury. DNA damage response (DDR) mediated by p53 effectively blocks the HCC formation, lack of which leads to less apoptosis, liver damage and rapid HCC formation.

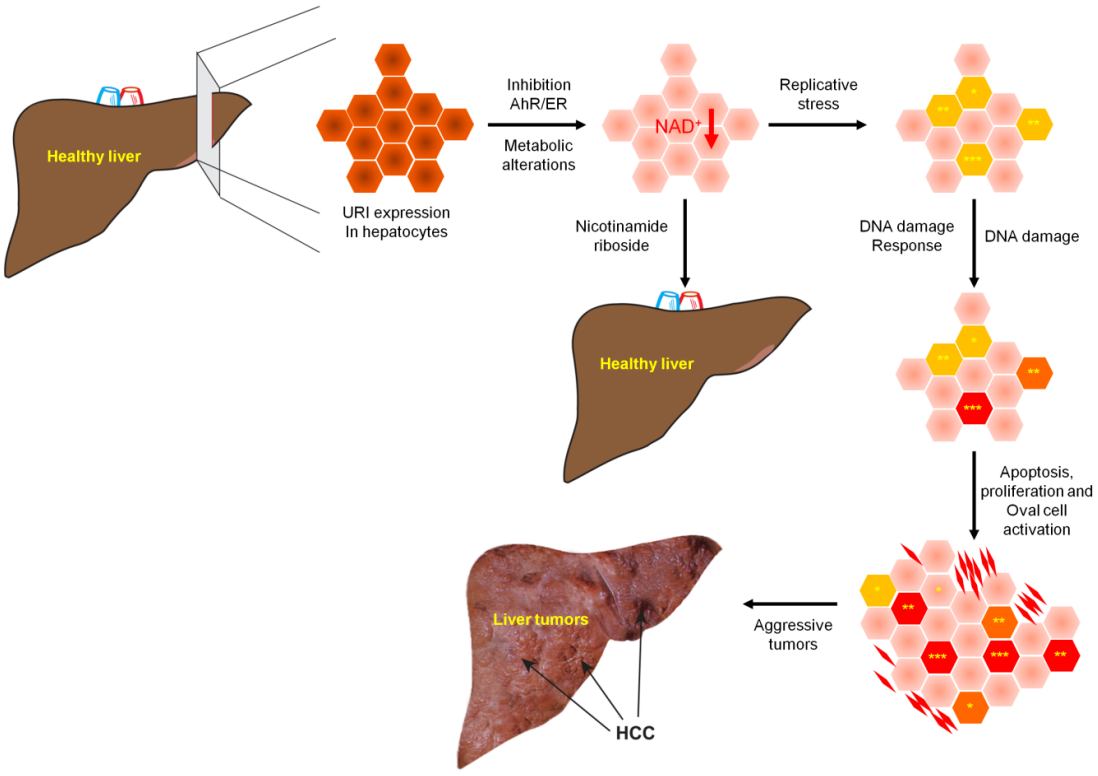

Figure 31 Schematic representation of different stages involved in URI mediated hepatocarcinogenesis

Mechanistically in a complex with HSP90, cytosolic URI inhibits the nuclear translocation of transcription factors (AhR and ER) regulating *de novo* NAD^+ synthesis leading to HCC. Deregulated *de novo* NAD^+ synthesis pathway, leading to the drop in NAD^+ levels is the cause of DNA damage and thus HCC. Supplementing diet with NAD^+ boosters (e.g. NR) prevents HCC. In addition, c-Myc induces DNA damage during asymptomatic stage of pancreas down-regulate *de novo* NAD^+ synthesis pathway, supplementation of NR boosters reduces the tumor development.

2 Oncogenic properties of URI

URI was previously demonstrated to be an "addicting" oncogene selectively required for the survival of ovarian cancer cells maintains the threshold of apoptosis in accordance of nutrients and growth factors availability (44). While, *URI* copy numbers were found to be increased in ovarian cancer cell lines and human cancer, in the analyzed cohort of human HCC samples, URI locus amplification was not detected (data not shown). Notably, RBP5-mediating protein (RMP), a URI isoform, was reported in tumor formation assays to promote HCC growth (93). We show that URI expression is significantly enriched in HBV- or HCV-associated HCC samples and implicates, in conjunction with HBV infection, an HBx-mediated transcriptional regulation program. Additional work is needed to determine whether URI is the molecular link in HBV-induced HCC.

URI expression in human HCC negatively correlates with the patient prognosis and *de novo* NAD^+ synthesis pathway. This is further supported by the fact that a comprehensive analysis comparing transcriptomic landscapes of the hURI GEMM and the HBV related-human HCC (85), showed a significant enrichment between both data sets, suggesting that the hURI-tetOFF^{hep} mouse displayed a HBV associated-human HCC signature. Although further studies are needed to know whether URI is the driving force for HCC development downstream of HBV and HCV viral infections, analysis of particular pathways deregulated in the hURI GEMM would be of relevance in human HCC.

3 Cause of HCC: Liver damage or genotoxicity

The presence of fibrosis/cirrhosis associated with chromosomal abnormalities is the most convincing clinical aspect of HCC. Despite detailed knowledge of its etiological and clinical features the molecular mechanisms and pathogenesis of HCC are poorly understood (94). While fibrosis predisposes to HCC development (95), our findings pinpoint to the initial and critical role of DNA damage in hepatocarcinogenesis. As determined by normal ALT levels in precancerous lesions, hepatic injury may not be sufficient to cause HCC in our model. Indeed, persistent normal ALT levels are not particularly reliable in most cases of chronic hepatitis B or C infected patients with mild to moderate histological liver damage (96) and ALT levels were not specifically associated with liver fibrosis or cirrhosis (97-99). Patients with chronic hepatitis B virus (HBV) infection and presenting normal ALT values still had a great incidence of HCC development (98,100)

Furthermore, we demonstrate that genotoxic stress-induced p53 is required for apoptosis. However, when p53 is inactivated and when hepatocyte death is reduced, carcinogenesis is accelerated, indicating that genotoxic stress, rather than high-grade apoptosis, initiates liver

tumorigenesis in our model. Interestingly complete URI loss dramatically increases ALT levels and livers show signs of massive apoptosis, whereas halving URI expression presents normal ALT levels in the DEN-induced carcinogenic model and thus, protects from liver injury. Further work is required to identify the cellular mechanisms of hepatic injury in URI$^{(\Delta/\Delta)hep}$ mice, in particular to determine whether apoptosis depends on PP1γ release (45) and whether these processes contribute to early mouse mortality.

4 Role of NAD$^+$ in carcinogenesis

NAD$^+$ is produced *de novo,* mainly in the liver from the L-tryptophan/kynurenine catabolism (33). Dietary tryptophan is converted to NAD$^+$ by key enzymes of the kynurenine pathway, the major route of tryptophan degradation in mammals. Alterations in enzyme activity or abundance may affect NAD$^+$ concentrations leading to the accumulation of tryptophan and its intermediate metabolites. Interestingly, increased tryptophan or other kynurenine metabolites has been suggested to play a role in several diseases, including cancer (81,101).

We therefore speculate that NR or other natural compound boosting NAD$^+$ levels containing the nicotinamide ring, such as vitamin B3, niacin or other derivatives (32) could be used as preventive treatment for HCC, in particular in patients with early signs of chronic liver damage and precancerous lesions. This is further supported by the fact that multiple epidemiologic studies reported the association between chronic tryptophan-poor diet and the incidence of certain types of cancers (102). Moreover, daily supplementation of niacin in a population with chronic nutritional deficiency was shown to decrease esophageal cancer incidence and mortality (102). In support of this, a human HCC genome-scale metabolic modeling using *in silico* and *in vivo* analyses identified metabolites from *de novo* NAD$^+$ synthesis which represent new potential drugs (103). However, further studies are still needed to determine whether long term boost of NAD$^+$ levels would not lead to accumulation of toxic tryptophan and other kynurenine metabolites.

Searching for new components that would directly elevate NAD$^+$ levels might therefore be a future strategy as a preventive therapy in liver cancer. To this end, similar to PARP inhibitors, AMPK activators such as metformin used in some cancer treatment were shown to increase NAD$^+$ levels (104,105). In contrast, Nampt inhibitors, which reduce salvage pathway-dependent NAD$^+$ pools, are currently used in several phase II clinical trials for cancer treatment (106). Based on our data, we cannot rule out that targeted therapies for inhibition of NAD$^+$ salvage pathway might be harmful for healthy cells that might generate genotoxic stress

Surprisingly, we observe that NR has therapeutic effects on fully developed liver tumors. Knowing that DNA damage-mediated chromosomal rearrangements is an irreversible feature of cancer cells, boosting NAD^+ levels may therefore activate the mitochondria SIRT3, recently shown to be a pro-apoptotic tumor suppressor enhancing BAK- and BAX-induced mitochondrial injury and cell death (107), enhancing cancer cell apoptosis and tumor regression. Interestingly, recent studies have shown that mitochondrial and metabolic dysfunctions either due to genetic abnormalities (Sco2 deletion) or aging respectively can be corrected by raising the NAD^+ levels, thus restoring the redox balance, mitochondrial activity through PGC1α and increased SIRT1/SIRT3 activity (49,108,109).

5 NAD^+ consuming enzymes in carcinogenesis

5.1 Role of PARP in carcinogenesis

PARPs (poly (ADP-ribose) polymerase) use NAD+ as a substrate to form poly(ADP-ribose) inresponse to DNA damage signaling. However, PARP activity has a profound effect on the intracellular NAD^+ levels and DNA damage response (110). PARP inhibitors are currently used in *BRACA* deficient cancer treatment and reportedly increase NAD^+ levels (104,105). *Parp1*$^{-/-}$ mice leads to spontaneous carcinogenesis (111) and *carcinogen*-induced tumorigenesis in the colon and in the liver is enhanced in *Parp1*$^{-/-}$ mice (112). Combinations of chemotherapies/genotoxic agents to kill cancer cells with NAD^+ boosters (e.g. NR) should prevent healthy cell transformation.

Interestingly, SIRT1-dependent deacetylation blocks PARP1 activity (30), indicating that NAD^+ deficits impact on the SIRT1-PARP axis. Because NAD^+ is a key hub that modulates various cellular metabolic responses and in particular is an essential cofactor in many metabolic pathways including dNTPs synthesis, we do not exclude that NAD^+ corruption may ultimately altered dNTPs synthesis essential in DNA integrity (113). However, further studies are needed to determine whether long term boost of NAD^+ levels would lead to accumulation of toxic tryptophan and other kynurenine metabolites

5.2 Role of Sirtulins (silent information regulator 2 (Sir2)) in carcinogenesis

Sirtulins are the intracellular NAD^+ sensors, uses NAD+ as a substrate and acetylate the lysine residues of the target proteins. Sirtulin family of proteins are multifaceted, implicated in different cellular processes like aging, apoptosis, inflammation and stress signalling. Cancer is considered as the disease of aging, as the cancer incidence increases with age. Mutations accumulated over

several patho-physiological insults increase the risk to develop cancer. SIRT1 levels increase in response to caloric restriction and the enzymatic activity is requiring for resistance to apoptosis induced by caloric restriction (114,115). For instance, SIRT1 localizes primarily to euchromatin, regulates the hepatic fatty acid oxidation and glucose homeostasis, which were reported to be the crucial process for the transformed cells. By activating critical transcription factors like PGC1α and Foxo1 SIRT1 modulates the glucose homeostasis via fatty acid oxidation and gluconeogenesis. SIRT1 limits the proliferation of human fibroblasts, where its depletion leads to increase in proliferation. The tumor suppressive activity of SIRT1 has been well documented in skin carcinogenesis models and drug resistance (116,117). Thus SIRT1 represents a viable chemotherapeutic targeted cancer therapy (118). Notably, DEN-treated SIRT1 transgenic mice present a significantly lower DNA damage, liver tumour incidence and tumor burden (29).

6 Role of HSP90 in carcinogenesis

We demonstrate that inhibition of AhR and ER transcriptional activity is mediated by hURI in a complex with HSP90 which represses their nuclear trafficking. In a non-ligand bound state, AhR and ER are retained in the cytoplasm as inactive proteins, in a complex including HSP90 and p23 co-chaperones (84,119). Upon ligand binding, AhR and ER dissociate from HSP90 and p23 and relocalize to the nucleus, thereby initiating gene transcription (84,119). The presence of hURI abolished the trafficking of AhR and ER receptors. The exact mechanism of how hURI modulates AhR and ER complex inhibition still remains to be understood. However, we can speculate that hURI might either stabilize the cytoplasmic complex containing HSP90, p23 and AhR or ER, thereby suppressing their translocation to the nucleus, or induce an allosteric conformational change of the AhR and ER active site, preventing ligand binding and nuclear targeting of AhR and ER.

We do not exclude that hURI might sterically hinder the AhR and ER ligand binding sites and abolish nuclear translocation. While inhibitors against HSP90 are currently used in clinical trials for cancer treatment, designing therapeutic strategies in either inhibiting HSP90 chaperone, scaffolding or cotranscriptional activities should be meticulously considered (Barrott and Haystead, 2013). Although mechanisms of downregulation of kynurenine pathway in pancreas by c-Myc expression still require elucidation, URI reduces *de novo* NAD^+ synthesis by inhibiting AhR and ER transcriptional activity in a complex with HSP90 (83,84). While HSP90 inhibitors are currently in clinical trials for cancer treatment designing therapeutic strategies based on inhibiting HSP90 chaperone, scaffolding or cotranscriptional activities should be carefully considered (120).

7 Role of Estrogen receptors in carcinogenesis

A protective effect of estrogens was therefore suggested in studies using DEN-induced HCC mouse model in which estrogens were shown to protect hepatocytes from malignant transformation via down-regulation of IL-6 release from kupffer cells (25). In contrast, since men have a higher incidence of HCC than women, several epidemiologic and in particular animal studies suggest that this gender disparity is due to the protective effects of estrogen (25,121-123). Additionally, the use of estrogen was reportedly effective in the treatment of traumatic liver injury (124), suggesting that ER inhibition may precede hepatocyte injury, in accordance to our model. The non gender disparity in HCC development in our hURI mouse model further supports the role of ER inhibition in HCC progression.

Not only because ERs are over-expressed in approximately 33% of HCC (125) but also estrogens have been reported to cause human hepatomas (126,127). Activating estrogen receptor may therefore be more beneficial in HCC, although a ddetrimental role of estrogens in HCC pathogenesis was suggested (126,127). Additionally, the use of tamoxifen, a potent antagonist of ERs was even proposed as a treatment in liver tumors (125), but the benefits were limited, if not inefficient and did not seem to be associated with the presence of ERs (125).

8 Role of AhR in carcinogenesis

AhR is also known to regulate xenobiotic-metabolizing enzymes and mediate toxic effects of dioxin-like compounds. Thus, reductions in its capacity to transcribe these enzymes may generate xenobiotic stress, which can accelerate liver tumorigenesis (128). Increases in liver tumor incidence in $AhR^{-/-}$ DEN treated mice indicate that AhR might function as tumor suppressors, which become silenced during tumor formation (129). While URI inhibition may represent a therapeutic option in early stages of liver tumorigenesis, combining therapies that synergistically activate AhR and ER should be further tested in pre-clinical models for HCC treatment, and may provide an elegant approach for targeted therapies in particular in patients with high URI expression.

9 HCC cancer cell of origin

Since the beginning of 19th century until the early 1980, many studies pointed out that cancers arose exclusively from dedifferentiation of mature hepatocytes (130). Appearance of altered hepatic foci and dysplastic nodules before HCC development suggested hepatocyte dedifferentiation. However, detailed morphologic and physiologic studies of AFP producing ductal/LPCs in different chemical induced HCC models and negatively correlating the AFP expression to the altered hepatic foci/dysplastic cells stemmed the notion of ductal/LPCs as the possible HCC cell of origin (131,132).

On the basis of low mitotic index, till 1980s liver was believed to lack any secondary stem cell pool. Either 70% partial hepatectomy and CCl4 treatment leads to the repair of liver by rapid hepatocyte proliferation, this has been confirmed later by several genetic fate tracing studies (9,133,134). However, contradicting evidence of adult hepatocytes originating from ductal/LPCs (Sox9 positive) put forward the continuous streaming hypothesis, which says that all adult hepatocytes are continuously deriving from the ductal/LPC cells (91). This was later challenged by several studies using different CRE-reporter lines and DNA sequencing analysis (135,136).

Recent study also demonstrated the isolation and characterization of HCC progenitor cells (HcPCs) in the preneoplastic collagenase-resistant nodules, which are enriched with LPCs/ductal markers in DEN induced carcinogenesis model (137). However, the tracing of LPCs/ductal cells in the context of tumorigenesis in vivo haven't been performed. Here in our study we showed that LPCs/ductal cells can contribute to the HCC formation, there is independent of p53/p19ARF dependent hepatocyte cell cycle arrest but rather on the continuous URI expression and decreased NAD^+ levels.

10 Summary

To summarize, this study reveals critical links between nutrient metabolism and genome integrity. While defects in metabolism and genomic instability are considered hallmarks of cancer, the above findings pinpoint the importance of therapeutic intervention on metabolic alterations prior to genomic instability, so as to prevent tumorigenesis. We show that ectopic URI expression decrease NAD^+ levels and induces DNA damage, dysplastic lesions and finally develop HCC. Moreover, decrease in NAD^+ levels also activate ductal/LPCs response via DNA damage, which develop into HCC in the due course. Therefore, development of more efficient and stable NAD^+ boosters could provide new innovative therapies to maintain human health and to prevent or cure cancers and various associated metabolic dysfunctions.

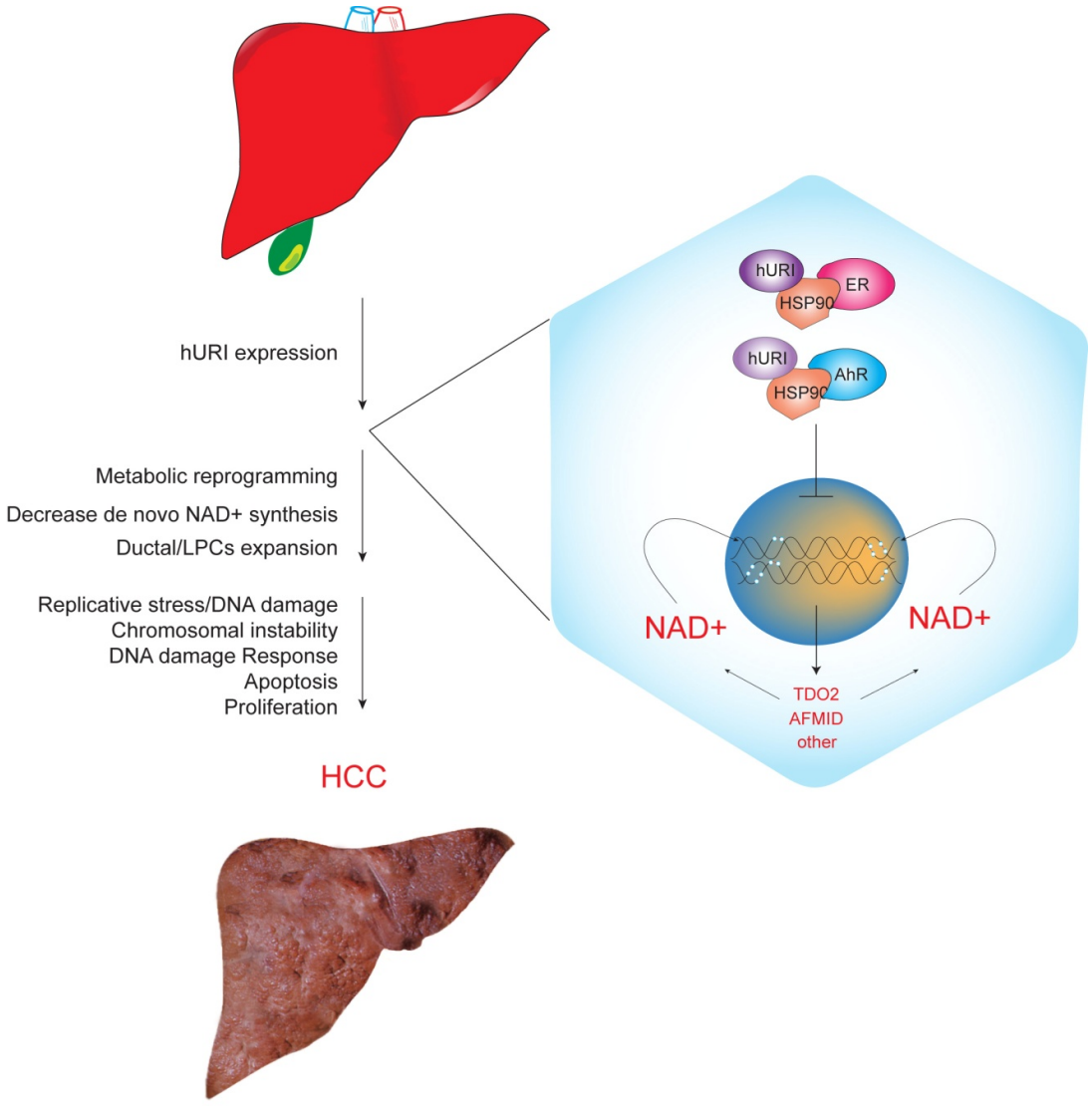

Figure 32 Scheme representing the molecular and cellular events of hepatocarcinogenesis induced by URI expression specifically in hepatocytes

Conclusions

1. Ectopic URI expression in mouse hepatocytes induces spontaneous HCC formation *in-vivo* mimicking distinct stages of human HCC development. Genetic reduction of mouse-URI expression confines protection to DEN induced hepatocarcinogenesis.

2. Before the premalignant lesion appearance, URI expression in mouse hepatocytes leads to DNA damage induced DNA damage response. In this context, inactivating p53 leads to the increase in tumorigenesis.

3. URI leads to the downregulation of L-tryptophan/kynurenine pathway in both asymptomatic and early stages of tumorigenesis pointed out by both transcript and proteomic analysis, and absolute NAD^+ levels. Downregulation of L-tryptophan/kynurenine pathway mimics the URI over expression; by reducing the total NAD^+ levels and increasing DNA damage formation.

4. Supplementation of nicotinamide riboside (NR) and thus increasing NAD^+ levels prevented DNA damage, preneoplastic lesion and tumor formation in HCC induced by URI expression and also have a therapeutic effect on the moderately developed tumors.

5. Mechanistically, URI down regulates L-tryptophan/kynurenine pathway by inhibiting the nuclear translocation of transcription factors Ahr and ER via HSP90 cytoplasmic interaction.

6. Oncogene-induced NAD^+ depletion and subsequent DNA damage is observed in Ela-1-myc model but not in similar $K\text{-}RAS^{G12V}$ mice model. In the Ela-1-myc model, short term NR supplementation doesn't affect the incidence of dysplastic lesions but abolishes carcinoma development and decrease dysplastic lesion development after long-term treatment.

7. URI expression is elevated in human HCC and associated with the poor prognosis of HCC patients. URI levels correlate with HBV and HCV infection in human HCC and are increased in human hepatitis and Con-A induced hepatitis mouse model. The HBx oncoprotein from HBV, transcriptionally upregulates URI expression. URI expression inversely correlates with NAD^+ levels and enzymes of *de-novo* NAD^+ synthesis and the decreased expression of enzymes from *de-novo* NAD^+ synthesis associated with the poor patient survival.

8. Ductal/LPCs cells are activated by non-cell-autonomous expression of URI in hepatocytes. Ductal/LPCs cell proliferation is independent of p19ARF and p53 mediated DNA damage response. Ductal/LPCs contribute to hepatocellular carcinoma (HCC) and hepatocellular adenoma (HCA) formation *in vivo*.

Conclusiones

1. La expresión ectópica de URI en los hepatocitos induce la formación espontánea de carcinomas hepatocelulares en el ratón que reflejan los distintos estadios de la progresión tumoral de carcinomas hepatocelulares humanos. La reducción a nivel genético de la expresión de URI tiene un efecto protector sobre el desarrollo de tumores hepáticos, inducidos por el carcinógeno DEN.

2. Previamente al desarrollo de las lesiones tumorales, la expresión de URI en los hepatocitos induce la activación de la respuesta al daño en el ADN. En este contexto, las mutaciones que inactivan p53 conducen a un aumento del desarrollo tumoral.

3. La expresión de la proteína URI conduce a una disminución de la vía molecular del L-triptófano/*kynurenine* en los estadios más tempranos de la progresión tumoral. Estos resultados fueron confirmados a nivel transcripcional, proteómico y mediante análisis de los niveles absolutos de NAD^+. Una disminución de la vía molecular del L-triptófano/*kynurenine in vivo* produce efectos equivalentes al aumento de la expresión de URI: una reducción de los niveles totales de NAD^+ y un aumento en el daño al ADN.

4. La adicción de nicotinamida ribósido (NR) en la dieta, y por lo tanto el aumento de los niveles de NAD^+, tiene un efector protector frente al año en el ADN, el desarrollo de lesiones preneoplásicas y la formación de carcinomas hepatocelulares como consecuencia del aumento de expresión de URI. Además, este tratamiento tiene un efecto terapéutico en los carcinomas hepatocelulares que presentan un desarrollo moderado.

5. A nivel mecanístico, URI disminuye la vía molecular del L-triptófano/*kynurenine* inhibiendo la translocación nuclear de los factores de transcripción Ahr and ER, a través de su interacción en el citoplasma con la proteína HSP90.

6. La disminución de los niveles de NAD^+ inducida por oncogenes y el consecuente daño al ADN se observa en el modelo tumoral Ela-1-myc pero no en el modelo K-RAS^{G12V}. En el modelo Ela-1-myc, la adicción por un corto periodo de tiempo de NR en la dieta no afecta al desarrollo de lesiones displásticas pero inhibe el desarrollo de carcinomas. Un tratamiento a largo plazo consigue la disminución del desarrollo de las lesiones displásticas.

7. Los niveles de expresión de URI están aumentados en carcinomas hepatocelulares humanos y se asocian con una peor prognosis para los pacientes. Los niveles de expresión de URI se correlacionan con la infección por el virus de la hepatitis B y el virus de la hepatitis C en carcinomas hepatocelulares humanos; aumentan en los casos de hepatitis en humanos y en los modelos murinos de hepatitis inducida por el tratamiento con Con-A. La oncoproteína HBx del virus de la hepatitis B, aumenta los niveles de expresión de URI a nivel transcripcional. La expresión de URI se

correlaciona negativamente con los niveles de NAD^+ y con las enzimas que sintentizan NAD^+ *de novo*. Además, los pacientes con niveles reducidos de dichas enzimas presentan una menor tasa de supervivencia.

8. Las células ductales/LPCs se activan como consecuencia de la expresión de URI en los hepatocitos. Las células ductales/LPCs contribuyen al desarrollo de carcinomas hepatocelulares y adenomas hepatocelulares *in vivo*.

References

1. Zaret, K. S. (2002) *Nat Rev Genet* **3**, 499-512
2. Beddington, R. S., and Robertson, E. J. (1998) *Trends Genet* **14**, 277-284
3. Jung, J., Zheng, M., Goldfarb, M., and Zaret, K. S. (1999) *Science* **284**, 1998-2003
4. Gualdi, R., Bossard, P., Zheng, M., Hamada, Y., Coleman, J. R., and Zaret, K. S. (1996) *Genes Dev* **10**, 1670-1682
5. Luedde, T., Kaplowitz, N., and Schwabe, R. F. *Gastroenterology*
6. Michalopoulos, G. K. *Am J Pathol* **176**, 2-13
7. Yamashita, T., and Wang, X. W. *J Clin Invest* **123**, 1911-1918
8. Malato, Y., Naqvi, S., Schurmann, N., Ng, R., Wang, B., Zape, J., Kay, M. A., Grimm, D., and Willenbring, H. *J Clin Invest* **121**, 4850-4860
9. Schaub, J. R., Malato, Y., Gormond, C., and Willenbring, H. *Cell Rep* **8**, 933-939
10. Holczbauer, A., Factor, V. M., Andersen, J. B., Marquardt, J. U., Kleiner, D. E., Raggi, C., Kitade, M., Seo, D., Akita, H., Durkin, M. E., and Thorgeirsson, S. S. *Gastroenterology* **145**, 221-231
11. Nyblom, H., Bjornsson, E., Simren, M., Aldenborg, F., Almer, S., and Olsson, R. (2006) *Liver Int* **26**, 840-845
12. McCullough, A. J. (2004) *Clin Liver Dis* **8**, 521-533, viii
13. Thoolen, B., Maronpot, R. R., Harada, T., Nyska, A., Rousseaux, C., Nolte, T., Malarkey, D. E., Kaufmann, W., Kuttler, K., Deschl, U., Nakae, D., Gregson, R., Vinlove, M. P., Brix, A. E., Singh, B., Belpoggi, F., and Ward, J. M. (2011) *Toxicol Pathol* **38**, 5S-81S
14. Spisni, R., Nervi, M., Matronola, M., Lijoi, C., Caldarelli, G. F., and Colizzi, C. (1988) *Minerva Chir* **43**, 821-824
15. Kurashina, M., Kozuka, S., Nakasima, N., Hirabayasi, N., and Ito, M. (1988) *Cancer* **61**, 2469-2474
16. Hickling, K. C., Hitchcock, J. M., Chipman, J. K., Hammond, T. G., and Evans, J. G. *Toxicol Pathol* **38**, 213-229
17. Jelnes, P., Santoni-Rugiu, E., Rasmussen, M., Friis, S. L., Nielsen, J. H., Tygstrup, N., and Bisgaard, H. C. (2007) *Hepatology* **45**, 1462-1470
18. Stinson, S. F., Hoover, K. L., and Ward, J. M. (1981) *Cancer Lett* **14**, 143-150
19. Jang, J. J., Weghorst, C. M., Henneman, J. R., Devor, D. E., and Ward, J. M. (1992) *Carcinogenesis* **13**, 1541-1547
20. Bugianesi, E. (2007) *Clin Liver Dis* **11**, 191-207, x-xi
21. Bosch, F. X., Ribes, J., Diaz, M., and Cleries, R. (2004) *Gastroenterology* **127**, S5-S16
22. Lencioni, R., Chen, X. P., Dagher, L., and Venook, A. P. *Oncologist* **15 Suppl 4**, 42-52
23. Llovet, J. M., Ricci, S., Mazzaferro, V., Hilgard, P., Gane, E., Blanc, J. F., de Oliveira, A. C., Santoro, A., Raoul, J. L., Forner, A., Schwartz, M., Porta, C., Zeuzem, S., Bolondi, L., Greten, T. F., Galle, P. R., Seitz, J. F., Borbath, I., Haussinger, D., Giannaris, T., Shan, M., Moscovici, M., Voliotis, D., and Bruix, J. (2008) *N Engl J Med* **359**, 378-390
24. Hallstrom, I. P., Liao, D. Z., Assefaw-Redda, Y., Ohlson, L. C., Sahlin, L., Eneroth, P., Eriksson, L. C., Gustafsson, J. A., and Blanck, A. (1996) *Hepatology* **24**, 849-854
25. Naugler, W. E., Sakurai, T., Kim, S., Maeda, S., Kim, K., Elsharkawy, A. M., and Karin, M. (2007) *Science* **317**, 121-124
26. Kang, T. W., Yevsa, T., Woller, N., Hoenicke, L., Wuestefeld, T., Dauch, D., Hohmeyer, A., Gereke, M., Rudalska, R., Potapova, A., Iken, M., Vucur, M., Weiss, S., Heikenwalder, M., Khan, S., Gil, J., Bruder, D., Manns, M., Schirmacher, P., Tacke, F., Ott, M., Luedde, T., Longerich, T., Kubicka, S., and Zender, L. (2011) *Nature* **479**, 547-551
27. Burrell, R. A., McClelland, S. E., Endesfelder, D., Groth, P., Weller, M. C., Shaikh, N., Domingo, E., Kanu, N., Dewhurst, S. M., Gronroos, E., Chew, S. K., Rowan, A. J., Schenk, A., Sheffer, M., Howell, M., Kschischo, M., Behrens, A., Helleday, T., Bartek, J., Tomlinson, I. P., and Swanton, C. (2013) *Nature* **494**, 492-496

28. Negrini, S., Gorgoulis, V. G., and Halazonetis, T. D. (2010) *Nat Rev Mol Cell Biol* **11**, 220-228
29. Herranz, D., Munoz-Martin, M., Canamero, M., Mulero, F., Martinez-Pastor, B., Fernandez-Capetillo, O., and Serrano, M. (2010) *Nat Commun* **1**, 3
30. Rajamohan, S. B., Pillai, V. B., Gupta, M., Sundaresan, N. R., Birukov, K. G., Samant, S., Hottiger, M. O., and Gupta, M. P. (2009) *Mol Cell Biol* **29**, 4116-4129
31. Rongvaux, A., Andris, F., Van Gool, F., and Leo, O. (2003) *Bioessays* **25**, 683-690
32. Bogan, K. L., and Brenner, C. (2008) *Annu Rev Nutr* **28**, 115-130
33. Houtkooper, R. H., Canto, C., Wanders, R. J., and Auwerx, J. (2009) *Endocr Rev* **31**, 194-223
34. Canto, C., and Auwerx, J. (2012) *Cold Spring Harb Symp Quant Biol* **76**, 291-298
35. Collins, P. B., and Chaykin, S. (1972) *J Biol Chem* **247**, 778-783
36. Eferl, R., and Wagner, E. F. (2003) *Nat Rev Cancer* **3**, 859-868
37. Min, L., Ji, Y., Bakiri, L., Qiu, Z., Cen, J., Chen, X., Chen, L., Scheuch, H., Zheng, H., Qin, L., Zatloukal, K., Hui, L., and Wagner, E. F. *Nat Cell Biol* **14**, 1203-1211
38. Boulon, S., Pradet-Balade, B., Verheggen, C., Molle, D., Boireau, S., Georgieva, M., Azzag, K., Robert, M. C., Ahmad, Y., Neel, H., Lamond, A. I., and Bertrand, E. (2010) *Mol Cell* **39**, 912-924
39. Dorjsuren, D., Lin, Y., Wei, W., Yamashita, T., Nomura, T., Hayashi, N., and Murakami, S. (1998) *Mol Cell Biol* **18**, 7546-7555.
40. Delgermaa, L., Hayashi, N., Dorjsuren, D., Nomura, T., Thuy le, T. T., and Murakami, S. (2004) *Mol Cell Biol* **24**, 8556-8566
41. Kanemaki, M., Makino, Y., Yoshida, T., Kishimoto, T., Koga, A., Yamamoto, K., Yamamoto, M., Moncollin, V., Egly, J. M., Muramatsu, M., and Tamura, T. (1997) *Biochem Biophys Res Commun* **235**, 64-68
42. Gstaiger, M., Luke, B., Hess, D., Oakeley, E. J., Wirbelauer, C., Blondel, M., Vigneron, M., Peter, M., and Krek, W. (2003) *Science* **302**, 1208-1212
43. Gimeno, C. J., Ljungdahl, P. O., Styles, C. A., and Fink, G. R. (1992) *Cell* **68**, 1077-1090
44. Theurillat, J. P., Metzler, S. C., Henzi, N., Djouder, N., Helbling, M., Zimmermann, A. K., Jacob, F., Soltermann, A., Caduff, R., Heinzelmann-Schwarz, V., Moch, H., and Krek, W. (2011) *Cancer Cell* **19**, 317-332
45. Djouder, N., Metzler, S. C., Schmidt, A., Wirbelauer, C., Gstaiger, M., Aebersold, R., Hess, D., and Krek, W. (2007) *Mol Cell* **28**, 28-40
46. Menon, S., Yecies, J. L., Zhang, H. H., Howell, J. J., Nicholatos, J., Harputlugil, E., Bronson, R. T., Kwiatkowski, D. J., and Manning, B. D. (2012) *Sci Signal* **5**, ra24
47. Beard, C., Hochedlinger, K., Plath, K., Wutz, A., and Jaenisch, R. (2006) *Genesis* **44**, 23-28
48. Kistner, A., Gossen, M., Zimmermann, F., Jerecic, J., Ullmer, C., Lubbert, H., and Bujard, H. (1996) *Proc Natl Acad Sci U S A* **93**, 10933-10938
49. Canto, C., Houtkooper, R. H., Pirinen, E., Youn, D. Y., Oosterveer, M. H., Cen, Y., Fernandez-Marcos, P. J., Yamamoto, H., Andreux, P. A., Cettour-Rose, P., Gademann, K., Rinsch, C., Schoonjans, K., Sauve, A. A., and Auwerx, J. (2012) *Cell Metab* **15**, 838-847
50. Vesselinovitch, S. D., and Mihailovich, N. (1983) *Cancer Res* **43**, 4253-4259
51. Livak, K. J., and Schmittgen, T. D. (2001) *Methods* **25**, 402-408
52. Kline, K. G., Frewen, B., Bristow, M. R., Maccoss, M. J., and Wu, C. C. (2008) *J Proteome Res* **7**, 5055-5061
53. Wisniewski, J. R., Zougman, A., Nagaraj, N., and Mann, M. (2009) *Nature methods* **6**, 359-362
54. Ernoult, E., Gamelin, E., and Guette, C. (2008) *Proteome Sci* **6**, 27
55. Rappsilber, J., Ishihama, Y., and Mann, M. (2003) *Anal Chem* **75**, 663-670
56. Olsen, J. V., de Godoy, L. M., Li, G., Macek, B., Mortensen, P., Pesch, R., Makarov, A., Lange, O., Horning, S., and Mann, M. (2005) *Mol Cell Proteomics* **4**, 2010-2021
57. Perkins, D. N., Pappin, D. J., Creasy, D. M., and Cottrell, J. S. (1999) *Electrophoresis* **20**, 3551-3567

58. Chen, Y., Choong, L. Y., Lin, Q., Philp, R., Wong, C. H., Ang, B. K., Tan, Y. L., Loh, M. C., Hew, C. L., Shah, N., Druker, B. J., Chong, P. K., and Lim, Y. P. (2007) *Mol Cell Proteomics* **6**, 2072-2087
59. Gan, C. S., Chong, P. K., Pham, T. K., and Wright, P. C. (2007) *J Proteome Res* **6**, 821-827
60. Ho, J., Kong, J. W., Choong, L. Y., Loh, M. C., Toy, W., Chong, P. K., Wong, C. H., Wong, C. Y., Shah, N., and Lim, Y. P. (2009) *J Proteome Res* **8**, 583-594
61. Trapnell, C., Roberts, A., Goff, L., Pertea, G., Kim, D., Kelley, D. R., Pimentel, H., Salzberg, S. L., Rinn, J. L., and Pachter, L. (2012) *Nat Protoc* **7**, 562-578
62. Langmead, B., Trapnell, C., Pop, M., and Salzberg, S. L. (2009) *Genome Biol* **10**, R25
63. Li, H., Handsaker, B., Wysoker, A., Fennell, T., Ruan, J., Homer, N., Marth, G., Abecasis, G., and Durbin, R. (2009) *Bioinformatics* **25**, 2078-2079
64. Trapnell, C., Roberts, A., Goff, L., Pertea, G., Kim, D., Kelley, D. R., Pimentel, H., Salzberg, S. L., Rinn, J. L., and Pachter, L. *Nat Protoc* **7**, 562-578
65. Carpenter, B., Lin, Y., Stoll, S., Raffai, R. L., McCuskey, R., and Wang, R. (2005) *Development* **132**, 3293-3303
66. Libbrecht, L., Craninx, M., Nevens, F., Desmet, V., and Roskams, T. (2001) *Histopathology* **39**, 66-73
67. He, G., Dhar, D., Nakagawa, H., Font-Burgada, J., Ogata, H., Jiang, Y., Shalapour, S., Seki, E., Yost, S. E., Jepsen, K., Frazer, K. A., Harismendy, O., Hatziapostolou, M., Iliopoulos, D., Suetsugu, A., Hoffman, R. M., Tateishi, R., Koike, K., and Karin, M. (2013) *Cell* **155**, 384-396
68. Schuler, M., Dierich, A., Chambon, P., and Metzger, D. (2004) *Genesis* **39**, 167-172
69. Maeda, S., Kamata, H., Luo, J. L., Leffert, H., and Karin, M. (2005) *Cell* **121**, 977-990
70. Reinhardt, H. C., and Schumacher, B. (2012) *Trends Genet* **28**, 128-136
71. Sotillo, R., Hernando, E., Diaz-Rodriguez, E., Teruya-Feldstein, J., Cordon-Cardo, C., Lowe, S. W., and Benezra, R. (2007) *Cancer Cell* **11**, 9-23
72. Christophorou, M. A., Martin-Zanca, D., Soucek, L., Lawlor, E. R., Brown-Swigart, L., Verschuren, E. W., and Evan, G. I. (2005) *Nat Genet* **37**, 718-726
73. Subramanian, A., Tamayo, P., Mootha, V. K., Mukherjee, S., Ebert, B. L., Gillette, M. A., Paulovich, A., Pomeroy, S. L., Golub, T. R., Lander, E. S., and Mesirov, J. P. (2005) *Proceedings of the National Academy of Sciences of the United States of America* **102**, 15545-15550
74. Merdanovic, M., Sauer, E., and Reidl, J. (2005) *J Bacteriol* **187**, 4410-4420
75. Jain, M., Nilsson, R., Sharma, S., Madhusudhan, N., Kitami, T., Souza, A. L., Kafri, R., Kirschner, M. W., Clish, C. B., and Mootha, V. K. (2012) *Science* **336**, 1040-1044
76. Son, J., Lyssiotis, C. A., Ying, H., Wang, X., Hua, S., Ligorio, M., Perera, R. M., Ferrone, C. R., Mullarky, E., Shyh-Chang, N., Kang, Y., Fleming, J. B., Bardeesy, N., Asara, J. M., Haigis, M. C., DePinho, R. A., Cantley, L. C., and Kimmelman, A. C. (2013) *Nature* **496**, 101-105
77. Zwilling, D., Huang, S. Y., Sathyasaikumar, K. V., Notarangelo, F. M., Guidetti, P., Wu, H. Q., Lee, J., Truong, J., Andrews-Zwilling, Y., Hsieh, E. W., Louie, J. Y., Wu, T., Scearce-Levie, K., Patrick, C., Adame, A., Giorgini, F., Moussaoui, S., Laue, G., Rassoulpour, A., Flik, G., Huang, Y., Muchowski, J. M., Masliah, E., Schwarcz, R., and Muchowski, P. J. (2011) *Cell* **145**, 863-874
78. Murga, M., Campaner, S., Lopez-Contreras, A. J., Toledo, L. I., Soria, R., Montana, M. F., D'Artista, L., Schleker, T., Guerra, C., Garcia, E., Barbacid, M., Hidalgo, M., Amati, B., and Fernandez-Capetillo, O. (2011) *Nat Struct Mol Biol* **18**, 1331-1335
79. Tijet, N., Boutros, P. C., Moffat, I. D., Okey, A. B., Tuomisto, J., and Pohjanvirta, R. (2006) *Mol Pharmacol* **69**, 140-153
80. Matic, M., Bryzgalova, G., Gao, H., Antonson, P., Humire, P., Omoto, Y., Portwood, N., Pramfalk, C., Efendic, S., Berggren, P. O., Gustafsson, J. A., and Dahlman-Wright, K. (2013) *PLoS One* **8**, e57458
81. Stone, T. W., and Darlington, L. G. (2002) *Nat Rev Drug Discov* **1**, 609-620

82. Liao, Y. J., Liu, S. P., Lee, C. M., Yen, C. H., Chuang, P. C., Chen, C. Y., Tsai, T. F., Huang, S. F., Lee, Y. H., and Chen, Y. M. (2009) *Int J Cancer* **124**, 816-826
83. Perdew, G. H. (1988) *J Biol Chem* **263**, 13802-13805
84. Knoblauch, R., and Garabedian, M. J. (1999) *Mol Cell Biol* **19**, 3748-3759
85. Huang, Q., Lin, B., Liu, H., Ma, X., Mo, F., Yu, W., Li, L., Li, H., Tian, T., Wu, D., Shen, F., Xing, J., and Chen, Z. N. (2011) *PLoS One* **6**, e26168
86. Wurmbach, E., Chen, Y. B., Khitrov, G., Zhang, W., Roayaie, S., Schwartz, M., Fiel, I., Thung, S., Mazzaferro, V., Bruix, J., Bottinger, E., Friedman, S., Waxman, S., and Llovet, J. M. (2007) *Hepatology* **45**, 938-947
87. Roessler, S., Jia, H. L., Budhu, A., Forgues, M., Ye, Q. H., Lee, J. S., Thorgeirsson, S. S., Sun, Z., Tang, Z. Y., Qin, L. X., and Wang, X. W. (2010) *Cancer Res* **70**, 10202-10212
88. Evarts, R. P., Nagy, P., Marsden, E., and Thorgeirsson, S. S. (1987) *Carcinogenesis* **8**, 1737-1740
89. Preisegger, K. H., Factor, V. M., Fuchsbichler, A., Stumptner, C., Denk, H., and Thorgeirsson, S. S. (1999) *Lab Invest* **79**, 103-109
90. Akhurst, B., Croager, E. J., Farley-Roche, C. A., Ong, J. K., Dumble, M. L., Knight, B., and Yeoh, G. C. (2001) *Hepatology* **34**, 519-522
91. Furuyama, K., Kawaguchi, Y., Akiyama, H., Horiguchi, M., Kodama, S., Kuhara, T., Hosokawa, S., Elbahrawy, A., Soeda, T., Koizumi, M., Masui, T., Kawaguchi, M., Takaori, K., Doi, R., Nishi, E., Kakinoki, R., Deng, J. M., Behringer, R. R., Nakamura, T., and Uemoto, S. *Nat Genet* **43**, 34-41
92. Srinivas, S., Watanabe, T., Lin, C. S., William, C. M., Tanabe, Y., Jessell, T. M., and Costantini, F. (2001) *BMC Dev Biol* **1**, 4
93. Yang, H., Gu, J., Zheng, Q., Li, M., Lian, X., Miao, J., Jiang, J., and Wei, W. (2011) *J Biol Chem* **286**, 11865-11874
94. Teoh, N. C., Dan, Y. Y., Swisshelm, K., Lehman, S., Wright, J. H., Haque, J., Gu, Y., and Fausto, N. (2008) *Hepatology* **47**, 2078-2088
95. Malhi, H., and Gores, G. J. (2008) *Gastroenterology* **134**, 1641-1654
96. Kumar, M., Sarin, S. K., Hissar, S., Pande, C., Sakhuja, P., Sharma, B. C., Chauhan, R., and Bose, S. (2008) *Gastroenterology* **134**, 1376-1384
97. Seto, W. K., Lai, C. L., Ip, P. P., Fung, J., Wong, D. K., Yuen, J. C., Hung, I. F., and Yuen, M. F. (2012) *PLoS One* **7**, e32622
98. Nunnari, G., Pinzone, M. R., and Cacopardo, B. (2013) *J Viral Hepat* **20**, e131-137
99. Wong, G. L., Chan, H. L., Yu, Z., Chan, H. Y., Tse, C. H., and Wong, V. W. (2013) *J Gastroenterol Hepatol* **28**, 1762-1769
100. Kumada, T., Toyoda, H., Kiriyama, S., Sone, Y., Tanikawa, M., Hisanaga, Y., Kanamori, A., Atsumi, H., Takagi, M., Arakawa, T., and Fujimori, M. (2010) *J Med Virol* **82**, 539-545
101. Chung, K. T., and Gadupudi, G. S. (2010) *Environ Mol Mutagen* **52**, 81-104
102. Surjana, D., Halliday, G. M., and Damian, D. L. (2010) *J Nucleic Acids* **2010**
103. Agren, R., Mardinoglu, A., Asplund, A., Kampf, C., Uhlen, M., and Nielsen, J. (2014) *Mol Syst Biol* **10**, 721
104. Quinn, B. J., Kitagawa, H., Memmott, R. M., Gills, J. J., and Dennis, P. A. (2013) *Trends Endocrinol Metab*
105. Canto, C., Gerhart-Hines, Z., Feige, J. N., Lagouge, M., Noriega, L., Milne, J. C., Elliott, P. J., Puigserver, P., and Auwerx, J. (2009) *Nature* **458**, 1056-1060
106. Jieyu, H., Chao, T., Mengjun, L., Shalong, W., Xiaomei, G., Jianfeng, L., and Zhihong, L. (2012) *Curr Pharm Des* **18**, 6123-6132
107. Verma, M., Shulga, N., and Pastorino, J. G. (2013) *J Cell Sci* **126**, 274-288
108. Gomes, A. P., Price, N. L., Ling, A. J., Moslehi, J. J., Montgomery, M. K., Rajman, L., White, J. P., Teodoro, J. S., Wrann, C. D., Hubbard, B. P., Mercken, E. M., Palmeira, C. M., de Cabo, R., Rolo, A. P., Turner, N., Bell, E. L., and Sinclair, D. A. *Cell* **155**, 1624-1638

109. Cerutti, R., Pirinen, E., Lamperti, C., Marchet, S., Sauve, A. A., Li, W., Leoni, V., Schon, E. A., Dantzer, F., Auwerx, J., Viscomi, C., and Zeviani, M. *Cell Metab* **19**, 1042-1049
110. Skidmore, C. J., Davies, M. I., Goodwin, P. M., Halldorsson, H., Lewis, P. J., Shall, S., and Zia'ee, A. A. (1979) *Eur J Biochem* **101**, 135-142
111. Piskunova, T. S., Yurova, M. N., Ovsyannikov, A. I., Semenchenko, A. V., Zabezhinski, M. A., Popovich, I. G., Wang, Z. Q., and Anisimov, V. N. (2008) *Curr Gerontol Geriatr Res*, 754190
112. Nozaki, T., Fujihara, H., Watanabe, M., Tsutsumi, M., Nakamoto, K., Kusuoka, O., Kamada, N., Suzuki, H., Nakagama, H., Sugimura, T., and Masutani, M. (2003) *Cancer Sci* **94**, 497-500
113. Bester, A. C., Roniger, M., Oren, Y. S., Im, M. M., Sarni, D., Chaoat, M., Bensimon, A., Zamir, G., Shewach, D. S., and Kerem, B. (2011) *Cell* **145**, 435-446
114. Nemoto, S., Fergusson, M. M., and Finkel, T. (2004) *Science* **306**, 2105-2108
115. Cohen, H. Y., Miller, C., Bitterman, K. J., Wall, N. R., Hekking, B., Kessler, B., Howitz, K. T., Gorospe, M., de Cabo, R., and Sinclair, D. A. (2004) *Science* **305**, 390-392
116. Hida, Y., Kubo, Y., Murao, K., and Arase, S. (2007) *Arch Dermatol Res* **299**, 103-106
117. Chu, F., Chou, P. M., Zheng, X., Mirkin, B. L., and Rebbaa, A. (2005) *Cancer Res* **65**, 10183-10187
118. Wang, C., Chen, L., Hou, X., Li, Z., Kabra, N., Ma, Y., Nemoto, S., Finkel, T., Gu, W., Cress, W. D., and Chen, J. (2006) *Nat Cell Biol* **8**, 1025-1031
119. Kazlauskas, A., Sundstrom, S., Poellinger, L., and Pongratz, I. (2001) *Molecular and cellular biology* **21**, 2594-2607
120. Barrott, J. J., and Haystead, T. A. (2013) *FEBS J* **280**, 1381-1396
121. Yang, W., Lu, Y., Xu, Y., Xu, L., Zheng, W., Wu, Y., Li, L., and Shen, P. (2012) *J Biol Chem* **287**, 40140-40149
122. Yang, W., Lu, Y., Xu, Y., Xu, L., Zheng, W., Wu, Y., Li, L., and Shen, P. *The Journal of biological chemistry* **287**, 40140-40149
123. Shi, L., Feng, Y., Lin, H., Ma, R., and Cai, X. (2014) *J Transl Med* **12**, 93
124. Hsieh, Y. C., Yu, H. P., Frink, M., Suzuki, T., Choudhry, M. A., Schwacha, M. G., and Chaudry, I. H. (2007) *The American journal of pathology* **170**, 1210-1218
125. Garcia-Leiva, J., Gamboa-Dominguez, A., Ceron-Lizarraga, T., Morales-Espinosa, D., Meza-Junco, J., and Arrieta, O. (2006) *Ann Hepatol* **5**, 263-267
126. Kalra, M., Mayes, J., Assefa, S., Kaul, A. K., and Kaul, R. (2008) *World J Gastroenterol* **14**, 5945-5961
127. Villa, E. (2008) *Womens Health (Lond Engl)* **4**, 41-50
128. Walisser, J. A., Glover, E., Pande, K., Liss, A. L., and Bradfield, C. A. (2005) *Proc Natl Acad Sci U S A* **102**, 17858-17863
129. Fan, Y., Boivin, G. P., Knudsen, E. S., Nebert, D. W., Xia, Y., and Puga, A. (2009) *Cancer Res* **70**, 212-220
130. Sell, S., and Pierce, G. B. (1994) *Lab Invest* **70**, 6-22
131. Sell, S., and Leffert, H. L. (1982) *Hepatology* **2**, 77-86
132. Marquardt, J. U., and Thorgeirsson, S. S. *Semin Liver Dis* **30**, 26-34
133. Espanol-Suner, R., Carpentier, R., Van Hul, N., Legry, V., Achouri, Y., Cordi, S., Jacquemin, P., Lemaigre, F., and Leclercq, I. A. *Gastroenterology* **143**, 1564-1575 e1567
134. Yanger, K., Knigin, D., Zong, Y., Maggs, L., Gu, G., Akiyama, H., Pikarsky, E., and Stanger, B. Z. *Cell Stem Cell*
135. Fellous, T. G., Islam, S., Tadrous, P. J., Elia, G., Kocher, H. M., Bhattacharya, S., Mears, L., Turnbull, D. M., Taylor, R. W., Greaves, L. C., Chinnery, P. F., Taylor, G., McDonald, S. A., Wright, N. A., and Alison, M. R. (2009) *Hepatology* **49**, 1655-1663
136. Dorrell, C., Erker, L., Schug, J., Kopp, J. L., Canaday, P. S., Fox, A. J., Smirnova, O., Duncan, A. W., Finegold, M. J., Sander, M., Kaestner, K. H., and Grompe, M. *Genes Dev* **25**, 1193-1203

137. He, G., Dhar, D., Nakagawa, H., Font-Burgada, J., Ogata, H., Jiang, Y., Shalapour, S., Seki, E., Yost, S. E., Jepsen, K., Frazer, K. A., Harismendy, O., Hatziapostolou, M., Iliopoulos, D., Suetsugu, A., Hoffman, R. M., Tateishi, R., Koike, K., and Karin, M. *Cell* **155**, 384-396